Climate Change Projection and Time-varying Multi-dimensional Risk Analysis

by

Ali Sarhadi

A thesis
presented to the University of Waterloo
in fulfillment of the
thesis requirement for the degree of
Doctor of Philosophy
in
Civil Engineering

Waterloo, Ontario, Canada, 2016

AUTHOR'S DECLARATION

This thesis consists of material all of which I authored or co-authored: see Statement of Contributions included in the thesis. This is a true copy of the thesis, including any required final revisions, as accepted by my examiners.

I understand that my thesis may be made electronically available to the public.

Statement of Contributions

This thesis is partially the product of collaborative research and co-authored publications as follows:

Chapter 2:

- Sarhadi, A., D. H. Burn, G. Yang, and A. Ghodsi (2016), Advances in Projection of Climate Change Impacts Using Supervised Nonlinear Dimensionality Reduction Techniques, Climate Dynamics, DOI: 10.1007/s00382-016-3145-0.

Chapter 3:

- Sarhadi, A., D. H. Burn, F. Johnson, R. Mehrotra, and A. Sharma (2016), Water resources climate change projections using supervised nonlinear and multivariate soft computing techniques, Journal of Hydrology, 536, 119-132.

Chapter 4:

- Sarhadi, A., D. H. Burn, M. Concepción Ausín, and M. P. Wiper (2016), Time varying nonstationary multivariate risk analysis using a dynamic Bayesian copula, Water Resources Research, 52(3), 2327-2349.

- Sarhadi, A., M. C. Ausín, and P. M. Wiper (2016), A New Time-varying Concept of Risk in a Changing Climate, Scientific Reports, Submitted.

Abstract

In recent decades, population growth and global warming consequent to greenhouse gas emissions because of human activities, has changed the atmospheric composition leading to intensifying extreme climate phenomena and overall increase of extreme events. These extreme events have caused human suffering and devastating effects in recent record-breaking warming years. To mitigate adverse consequences arising from global warming, the best strategy is to project the future probabilistic behavior of extreme climate phenomena under changing environment.

The first contribution of this research is to improve the predictive power of regression-based statistical downscaling processes to accurately project the future behavior of extreme climate phenomena. First, a supervised dimensionality reduction algorithm is proposed for the statistical downscaling to derive a low-dimensional manifold representing climate change signals encoding of high-dimensional atmospheric variables. Such an algorithm is novel in climate change studies as past literature has focused on deriving low-dimensional principal components from large-scale atmospheric projectors without taking into account the target hydro-climate variables. The new algorithm called Supervised Principal Component analysis (Supervised PCA) outperforms all of the existing state-of-the-art dimensionality reduction algorithms. The model improves the performance of the statistical downscaling modelling through deriving subspaces that have maximum dependency with the target hydro-climate variables. A kernel version of Supervised PCA is also introduced to reduce nonlinear dimensionality and capture all of the nonlinear and complex variabilities between hydro-climate response variable and atmospheric projectors.

To address the biases arising from difference between observed and simulated large-scale atmospheric projectors, and to represent anomalies of low frequency variability of teleconnections in General Circulation Models (GCMs), a Multivariate Recursive Nesting Bias Correction (MRNBC) is proposed to the regression-based statistical downscaling. The proposed method is able to use multiple variables in multiple locations to simultaneously correct temporal and spatial biases in cross dependent multi-projectors. To reduce another source of uncertainty arising from complexity and nonlinearity in quantitative empirical relationships in the statistical downscaling, the results demonstrate the superiority of a Bayesian machine-learning algorithm. The predictive power of the statistical downscaling is therefore improved through addressing the aforementioned sources of uncertainty. This results in improvement of the projection of the global warming impacts on the

probabilistic behavior of hydro-climate variables using future multi-model ensemble GCMs under forcing climate change scenarios. The results of two Design-of-Experiments also reveal that the proposed comprehensive statistical downscaling is credible and adjustable to the changes under non-stationary conditions arising from climate change.

Under the impact of climate change arising from anthropogenic global warming, it is demonstrated that the nature and the risk of extreme climate phenomena are changed over time. It is also well known that the extreme climate processes are multi-dimensional by their very nature characterized by multi-dimensions that are highly dependent. Accordingly, to strength the reliability of infrastructure designs and the management of water systems in the changing climate, it is of crucial importance to update the risk concept to a new adaptive multi-dimensional time-varying one to integrate anomalies of dynamic anthropogenically forced environments. The main contribution of this research is to develop a new generation of multivariate time-varying risk concept for an adaptive design framework in non-stationary conditions arising from climate change. This research develops a Bayesian, dynamic conditional copula model describing time-varying dependence structure between mixed continuous and discrete marginals of extreme multi-dimensional climate phenomena. The framework is able to integrate any anomalies in extreme multi-dimensional events in non-stationary conditions arising from climate change. It generates iterative samples using a Markov Chain Monte Carlo (MCMC) method from the full conditional marginals and joint distribution in a fully likelihood-based Bayesian inference. The framework also introduces a fully Bayesian, time-varying Joint Return Period (JRP) concept to quantify the extent of changes in the nature and the risk of extreme multi-dimensional events over time under the impact of climate change. The proposed generalized time-dependent risk framework can be applied to all stochastic multi-dimensional climate systems that are under the influence of changing environments.

Acknowledgements

First and foremost, I would like to express my sincere appreciation to my advisor Prof. Don Burn. I have been amazingly fortunate to have an advisor who gave me the freedom to explore on my own. A distinguished supervisor whose academic advice, encouragement, and unconditional support helped me step forward throughout my PhD. I appreciate all his contributions of time, inspiring suggestions, and funding to make my PhD experience productive and stimulating.

I wish to express my sincere gratitude to Prof. Concepcion Ausin and Prof. Michael Peter Wiper for their wonderful advice, support, and friendship, both academically and personally during my stay in Madrid, Spain. I would also like to thank Prof. Ali Ghodsi, Prof. Ashish Sharma, Prof. Fiona Johnson, and Prof. Raj Mehrotra for their collaboration and helpful advice that improved my research.

It is my pleasure to thank my defense committee members, Prof. Fateh Chebana from the Institut National de Recherche Scientifique (INRS-ETE), University of Québec, Prof. Claude Duguay, Prof. Mahesh Pandey, and Prof. Bryan Tolson from the University of Waterloo.

The majority of the thesis contents were peer-reviewed in the form of technical journal papers before thesis submission. I would like to thank Prof. Ben Kirtman the executive editor of *Climate Dynamics* and the anonymous reviewer who reviewed the paper associated with Chapter 2. Prof. Andras Bardossy, editor-in-chief of *Journal of Hydrology*, associate editor, Prof. Fi-John Chang, and two anonymous reviewers that improved the paper associated with Chapter 3. I also acknowledge Prof. Alberto Montanari, editor-in-chief of *Water Resources Research* journal, associate editor Prof. Alberto Viglione, and three anonymous reviewers whose suggestions helped improve the paper associated with Chapter 4.

During my PhD I received a PhD Thesis Completion Award, Dr. T.E. Unny Memorial Award, and six University of Waterloo Graduate Merit Scholarships, which are hereby acknowledged.

My gratitude goes to all my dearest friends in Waterloo without whom my PhD's journey would not have been filled with the wonderful times and enjoyable moments that we shared together. Last, but not least, my warmest gratitude goes to my family, and in particular to my parents. I would not be anywhere near where I am today without their love, support, sacrifice, guidance, and the opportunities they provided for me throughout my life.

Table of Contents

List of Figures

List of Tables

Chapter 1
Introduction

1.1 Problem Statement

Global warming is recognized as one of the major threats to the planet in the 21st century. Anthropogenic greenhouse gas emissions are changing atmospheric composition leading to climate change. According to the Intergovernmental Panel on Climate Change (IPCC) fifth Assessment Report (IPCC, 2014), it is "extremely likely" that observed surface and atmospheric warming in recent decades since the mid-twentieth century is due to the increase in anthropogenic greenhouse gas emissions. There is a strong relationship between climate and hydrological systems. Subsequent increased temperature as a consequence of global warming enhances atmosphere water vapor—as the main greenhouse gas—which adversely influences hydro-climatic processes, leading to an overall increase of extreme events (Cheng and AghaKouchak, 2014). Global warming is thus directly increasing the risk of extreme climate events that are becoming more severe and frequent (Cheng and AghaKouchak, 2014; Karl and Trenberth, 2003) and threatening water resources in the future in different parts of the world. These extreme events have caused major human suffering and economic damages all around the world in recent record-breaking warmer years (Coumou and Rahmstorf, 2012). Global changing climate raises the question of how reliable are our water resources planning and infrastructure designs to deal with these changing extreme disasters.

Water professionals struggle to develop approaches that account for the impact of climate change on hydrological designs to reduce associated risks. Traditional, risk-based decision-making principles in water resources planning are based on the fundamental assumption of statistical stationarity. Under stationarity, it is assumed that the probabilistic characteristics of hydro-meteorological processes will not change over time, and that future water resources planning can be designed with past records in mind. Milly et al. (2008; 2015) argued that the fundamental assumption of stationarity has been influenced by climate change and anthropogenic effects, and therefore it is no longer applicable for water resources risk assessment and planning. Accordingly, water planners must revise current planning and analytic strategies to develop non-stationary probabilistic models based on the anomalies of the changing environment arising from climate change (Read and Vogel, 2015; Salas and Obeysekera, 2013). Therefore, in the changing environment an effective and flexible time-varying design approach must be adopted for risk-based decision-making.

Univariate non-stationarity modelling in hydrological risk assessment has drawn a great deal of attention in hydrological science in recent years (Rosner et al., 2014; Salas and Obeysekera, 2013; Westra et al., 2014). It is well known that natural stochastic hydro-climate processes are, however, multivariate phenomena and by their very nature characterized by multi-dimensional properties that are statistically dependent. Accordingly, univariate risk analysis methods even under non-stationary conditions cannot fully characterize the properties of hydro-climate processes that are highly correlated. This inability may lead to high uncertainty for infrastructure designs, and destructive consequences in water resources systems. It is hence of crucial importance that water associated communities change from a univariate to a non-stationary multivariate perspective. Substituting this perspective in risk analyses leads to changing probabilistic behavior of each variable in multi-dimensional hydro-climate processes. In a changing climate, a generalized fully time-varying multivariate risk framework should be designed to allow each dimension (marginal) and dependence structure between multi-dimensions (copula) to evolve simultaneously through time under non-stationary conditions. In this time-dependent framework, the effect of non-stationarity will thus be integrated and probabilistic parameters of marginals and copula are allowed to change over time. The currently-used multivariate static (time-independent) risk analysis should thus be updated and substituted with the new multivariate time-varying risk concept for long-term decision making in water resources planning and infrastructure designs under changing environments arising from human-induced climate change.

To develop a long-term risk-based water resources plan in a non-stationary condition, the limitations of the relatively short historical hydro-climate records, and the uncertainties associated with future climate model projections, are considered major restrictions. To address these limitations, a time varying stochastic model can be developed by synthetizing historical observed records and future climate model projections using multiple climate forcing scenarios (Borgomeo et al., 2014; Milly et al., 2008). Future climate change information is derived from simulated large-scale atmospheric processes developed based on General Circulation Models (GCMs). GCMs simulate future climate at coarse spatial scales, and are unable to provide information that can be directly used at the finer scales of interest to hydrologists (Bennett et al., 2012; Dingbao Wang, 2013). This inadequacy has been the reason for developing dynamical and statistical downscaling techniques to transfer large-scale global atmospheric variables (provided by GCMs) to regional and local hydro-climate information for use in climate change impact studies. One option for this is dynamical downscaling approaches, which are based on obtaining finer scale information from Regional Climate

Models (RCMs) driven by boundary conditions simulated using GCMs (Najafi and Moradkhani, 2015). The limitation of these approaches is that they require expensive and complicated computations and use biased lateral boundary inputs as the basis of their simulations (Rocheta et al., 2014a) that cannot be easily bias corrected for use. Statistical downscaling approaches rely on developing a statistical and quantitive relationship between large-scale atmospheric variables and fine scale variables at a particular site and have gained popularity among hydrologists wanting to predict climate change impacts on hydro-climate variables. The most popular methods in statistical downscaling are regression-based ones, which are preferred over other methods (weather typing and transfer function, and weather generation) because they have low computation requirements and are relatively straightforward to apply (Tofiq and Guven, 2014; Wilby et al., 2004). These transfer function methods involve developing direct quantitive relationships between predictands and predictors through different forms of regression (Dibike and Coulibaly, 2005a).

Due to the complexity of climate-associated processes, the three main challenges in developing the stochastic regression-based statistical downscaling approaches that need to be addressed in climate change impact assessments are: (i) development of the right quantitative functional relationship for capturing the complex nonlinearity between target hydro-climate variables and atmospheric simulated predictors; (ii) identification of predictor variables from high dimensional atmospheric predictors conveying climate change information with respect to the hydro-climate variable of interest; and iii) correction of biases in raw GCMs to represent interannual and interdecadal fluctuation of climate.

It is well known that due to the complex nonlinear relationship existing between target hydro-climate variables and large-scale atmospheric variables, standard linear methods fail to capture the nonlinear functional relationship. To address the first challenge in developing a statistical downscaling model, attention should be paid to nonlinear-based soft computing data-driven regression models. From these techniques, Bayesian-based machine-learning methods have become very popular as they can improve projections of climate change impacts in terms of performance accuracy through avoiding over-fitting.

In terms of the second challenge, projecting a dependent hydro-climate variable from high-dimensional large-scale atmospheric variables leads to inadequate results in terms of performance accuracy, due to the curse of dimensionality. The number of potentially important input variables may be large and the existence of correlation among data may subsequently induce redundancy and collinearity. To complicate matters further, the inherent complexity, nonlinearity, and

interdependency among explanatory large-scale atmospheric parameters give rise to unsatisfactory predictive performance of data-driven models in statistical downscaling. Despite its critical importance in climate change studies, the second challenge has so far gained only limited attention. Developing supervised learning-based dimensionality reduction methods, which take into account the dependence between target hydro-climate variable and atmospheric predictors, may thus lead to improvement of the predictive power of the statistical downscaling process.

Bias correction as the third challenge in statistical downscaling has been shown to improve the quality of GCMs for use in projecting hydro-climate variables under different climate change scenarios of the future (Mehrotra and Sharma, 2012; Ojha et al., 2013). In the statistical downscaling processes, therefore, an initial post-processing correction must be carried out on GCM outputs to represent the current climate. In this procedure, based on the statistical characteristics of observations, the differences between observed and simulated large-scale atmospheric variables are removed. In addition, interannual and interdecadal variability in the large-scale climate modes are often not well represented in GCM simulations (Rocheta et al., 2014b) resulting in uncertainty and biases in projections of hydro-climate variables relating to the future. Thus, raw data from GCMs must also be corrected to capture the effect of low frequency variability of teleconnections on large-scale atmospheric variables (Mehrotra and Sharma, 2012).

Reducing different sources of uncertainty is hence crucial in statistical downscaling as it enhances the quality of the hydro-climate variable projections in the future. Multi-model ensemble future projections derived from the statistical downscaling process can subsequently be combined with historical records to quantify probabilistic behavior of multivariate hydro-climate processes. Relying on the synthetized information as inputs, decision makers are able to effectively develop an adaptive time-varying risk framework to improve the reliability of infrastructure designs and the management of water systems under non-stationary conditions.

1.2 Research Outline

The objectives of this thesis are: (i) to enhance the reliability of future projections to be synthetized with recorded observations as inputs of the adaptive multivariate risk framework. For this purpose, this research attempts to address all the aforementioned challenges in the regression-based statistical downscaling processes; (ii) to update currently-used stationary multivariate risk concepts to develop new generation of the adaptive multivariate non-stationary-based methodologies for future risk-based

water system designs under changing environments arising from climate change. These general research objectives are elaborated on as follows.

Due to the complexity of climate-associated processes, identification of predictor variables from high dimensional atmospheric variables is considered a key factor for improvement of climate change projections in statistical downscaling approaches. To address the curse of dimensionality, this thesis aims to adopt a new approach of supervised learning dimensionality reduction to regression-based statistical downscaling. The proposed technique enhances the performance accuracy of the downscaling as it takes into account the target response variable and extracts principal components in which the dependency between response hydro-climate variable and large-scale atmospheric projectors is maximized. Moreover, two soft-computing nonlinear machine-learning methods are employed in the modelling procedure to capture non-linearity between the predictand and dimension-reduced predictors.

One of the main post-processing analyses in statistical downscaling approaches that improves the quality of raw data from GCMs in projecting target hydro-climate variables under future climate changes scenarios is bias correction. The main drawback of many bias correction methods is that they only take into account biases in the distribution of GCM simulations rather than biases in the representation of persistence and variability in simulations. To address this source of uncertainty and to represent interannual and interdecadal fluctuation of climate in raw GCM outputs, this thesis develops an adaptation of the Multivariate Recursive Nesting Bias Correction (MRNBC) approach to the regression-based statistical downscaling. Using this method, one is able to correct biases in the spatial cross dependence statistical attributes over multiple time scales in GCM predictors.

Under non-stationary conditions arising from climate change, the behavior of extreme hydro-climate processes changes and their probabilistic parameters may no longer be constant. In this condition, alternative approaches should be developed in which the effect of non-stationarity is integrated and probabilistic parameters are allowed to change over time in risk assessment studies. This concept has been studied in terms of non-stationarity modelling in the univariate context in recent years. Due to unavailability of robust methodology and complexity of theoretical concepts, however, the notion of time-varying non-stationary risk is relatively new in the multivariate context and scarcely investigated in the water resources area. This thesis argues that the risk concept should be updated to a flexible time-varying multivariate one to model dependent time-varying multi-dimensions under non-stationarity conditions generated by climate change. The main goal of this

research is to introduce a new time-varying non-stationary multivariate risk framework by developing a Bayesian, dynamic copula. In the proposed methodology, the effect of non-stationarity is integrated and probabilistic parameters of marginals and the dependence structure between multi-dimensions (copula) are allowed to change over time. Doing so, water resources authorities will be able to compute time-varying risk of extreme multi-dimensional hydro-climatic events in a changing climate.

1.3 Thesis Structure and Research Contributions

This thesis is structured around published and submitted manuscripts. Chapter 2 is based on a manuscript published by (Sarhadi et al., 2016d) in the Climate Dynamics journal. Chapter 3 corresponds to a published paper by Sarhadi et al. (2016c) in the Journal of Hydrology. Chapter 4 corresponds closely to a published paper by Sarhadi et al. (2016b) in the Water Resources Research journal and a submitted manuscript in the journal of Scientific Reports by (Sarhadi et al., 2016a).

The main contributions that this research has made to hydrological modelling in climate change impact assessment and multivariate risk studies are summarized as follows:

- A Supervised Principal Component Analysis (Supervised PCA) is adopted to regression-based statistical downscaling for identification of influential atmospheric predictors. Supervised PCA method is a generalization of PCA that explores subspaces along which the dependency between target hydro-climate variable and large-scale atmospheric projectors is maximized. This procedure improves the performance and the predictive power of regression-based statistical downscaling processes with high-dimensional input data. To capture the complexity and nonlinear variability between hydro-climatic response variables and projectors, a kernelized version of Supervised PCA is also presented for nonlinear data transformation. Details about Supervised PCA algorithms and results are presented in Chapter 2.
- The development of a comprehensive regression-based statistical downscaling approach using nonlinear and multivariate soft-computing techniques to reduce different sources of uncertainty and enhance the quality of hydro-climate projections. The approach captures complex and nonlinear relationships between large-scale atmospheric processes and target hydro-climate variable. The approach also proposes a framework to address bias correction using multiple locations to include spatial as well as temporal dependence in GCM simulations. In Chapter 3, the comprehensive statistical downscaling approach and its successful application in projection of an illustrative example are presented.

- The development of a generalized time-varying multivariate risk framework evolving through time under non-stationary conditions. This concept is developed by introducing a Bayesian, dynamic conditional copula to model the time-varying dependence structure between mixed continuous and discrete multi-dimensional hydro-climate phenomena. The research also improves the concept of Joint Return Period (JRP) in stationary multivariate risk studies to a fully time-varying JRP concept to compute time-dependent risk of extreme multi-dimensional hydro-climatic events in a changing climate. Details about this contribution are presented in Chapter 4. Moreover, an uncertainty analysis is run on currently-used time-independent (static) and the proposed time-dependent multivariate risk. The results demonstrate that multivariate stationary risk analysis is no longer applicable to projecting probabilistic behavior of changing multi-dimensional extreme events, and this may lead to increases in the risk of failure for water systems under non-stationary conditions arising from climate change. More details and results are reported in Chapter 4.

The following flowchart shows the aims and the inter-connections among different chapters in this study.

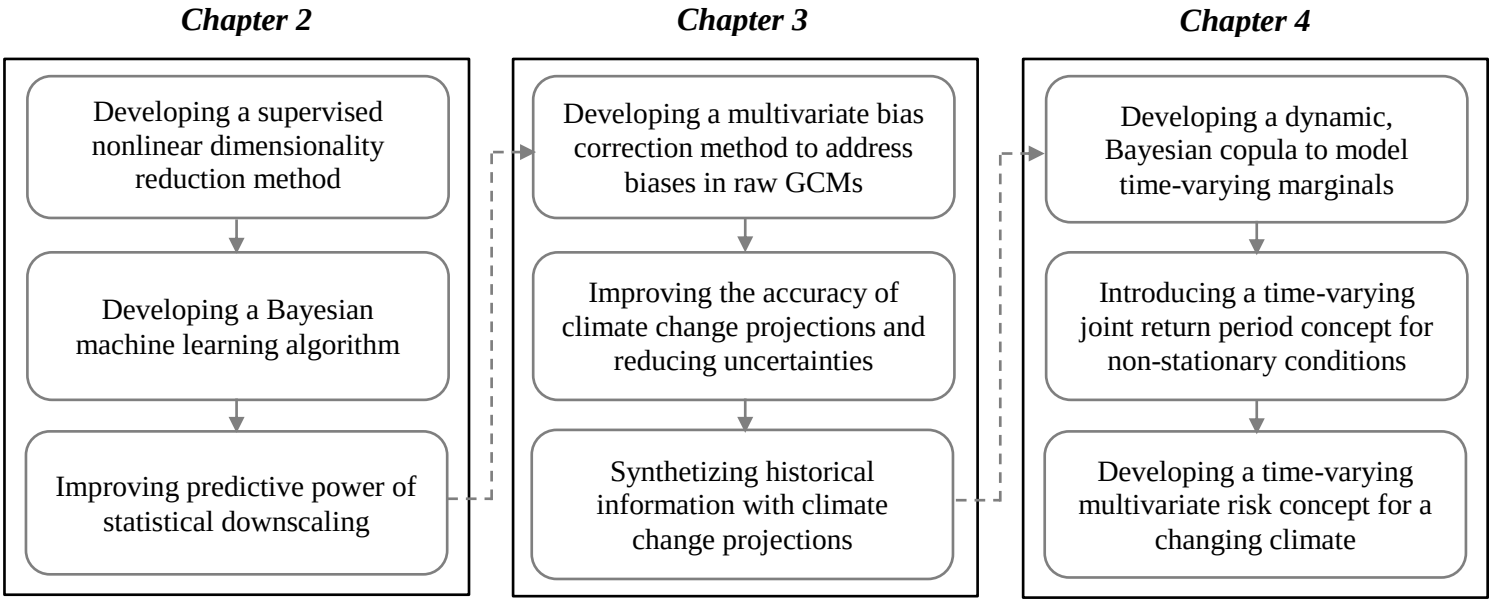

Figure 1-1. Schematic flowchart of the main contributions in each chapter

Chapter 2

Advances in Projection of Climate Change Impacts Using Supervised Nonlinear Dimensionality Reduction Techniques

This chapter is based on the following published article with the same title in the Climate Dynamics journal. Minor changes are made on some parts of the article to be more consistent with the body of the thesis. Thus, the content of this chapter is not exactly the same as the paper. There are also minor changes in response to comments from the examining committee.

Sarhadi, A., D. H. Burn, G. Yang, and A. Ghodsi (2016d), Advances in Projection of Climate Change Impacts Using Supervised Nonlinear Dimensionality Reduction Techniques, *Climate Dynamics*, DOI: 10.1007/s00382-016-3145-0.

Summary

One of the main challenges in climate change studies is accurate projection of the global warming impacts on the probabilistic behavior of hydro-climate processes. Due to the complexity of climate-associated processes, identification of predictor variables from high dimensional atmospheric variables is considered a key factor for improvement of climate change projections in statistical downscaling approaches. For this purpose, the present paper adopts a new approach of supervised dimensionality reduction, which is called "Supervised Principal Component Analysis (Supervised PCA)" to regression-based statistical downscaling. This method is a generalization of PCA, extracting a sequence of principal components of atmospheric variables that have maximal dependence on the response hydro-climate variable. To capture the nonlinear variability between hydro-climatic response variables and projectors, a kernelized version of Supervised PCA is also applied for nonlinear dimensionality reduction. The effectiveness of the Supervised PCA methods in comparison with some state-of-the-art algorithms for dimensionality reduction is evaluated in relation to the statistical downscaling process of precipitation in a specific site using two soft computing nonlinear machine learning methods, Support Vector Regression (SVR) and Relevance Vector Machine (RVM). The results demonstrate a significant improvement over Supervised PCA methods in terms of performance accuracy.

2.1 Introduction

Climate change is recognized as one of the major threats to the planet in the 21st century. According to the Intergovernmental Panel on Climate Change (IPCC) fifth Assessment Report (IPCC, 2013), it is "extremely likely" that observed surface and atmospheric warming in the decades since the mid-twentieth century is due to the increase in anthropogenic greenhouse gas emissions. Since a strong interrelation exists between climate and hydrological systems, it is expected that hydrological processes will be adversely affected as a consequence of global warming, leading to the overall increase of extreme events, and subsequently threatened water resources in the future. Therefore, to better plan and adapt water resource systems for mitigation of associated adverse consequences, it is necessary to understand the effect of future climate change on the availability of surface water resources.

Future climate changes are modelled under several simulated scenarios developed based on outputs from physically-based General Circulation Models (GCM), which are mechanistic models representing the large scale atmospheric processes (Tisseuil et al., 2010). However, inconsistency in the spatial scales is considered to be a key challenge in the application of GCMs. GCM outputs providing simulation of atmospheric variables at a coarse global resolution cannot capture hydrological changes in the finer local and regional resolutions that are of interest to hydrologists and decision makers. Consequently, the results of GCMs cannot be directly used at the finer scales for assessing how possible climate-change impacts on surface water availability may affect water supply (Bennett et al., 2012; Dingbao Wang, 2013). To overcome this problem, interest has increased in bridging global and regional climate data by developing and using a technique called "downscaling". Two types of downscaling—dynamic and statistical—are most commonly used techniques in transferring large-scale global atmospheric variables (provided by GCMs) to regional and local hydro-climate information for use in climate change impact studies. Dynamical downscaling approaches are based on obtaining finer scale information from Regional Climate Models (RCMs) driven by boundary conditions simulated using GCMs (Najafi and Moradkhani, 2015). The limitation of these approaches is that they require expensive and complicated computations and use biased lateral boundary inputs as the basis of their simulations (Rocheta et al., 2014a), inputs that cannot be easily bias corrected for use. Hence, the statistical downscaling approaches relying on developing empirical and quantitative relationships between large-scale atmospheric variables and fine scale variables at a particular site have gained more popularity among hydrologists wanting to predict

climate change impacts on hydro-climate variables. The most popular methods in statistical downscaling are regression-based ones, which are preferred over other methods (weather typing and transfer function, and weather generation) because they have low computation requirements and are relatively straightforward to apply (Tofiq and Guven, 2014; Wilby et al., 2004). These transfer function methods involve developing direct quantitative relationships between predictands and predictors through different forms of regression (Dibike and Coulibaly, 2005b).

The regression-based statistical downscaling is carried out in two main steps: i) deriving statistical relationships from historical climate information and hydro-climate variables of interest (developing a statistical model step); and ii) using these models to project hydro-climate variables in the future, relying on the assumption that current empirical models are applicable to GCM simulations of the future (a projection step). Due to the complexity of climate-associated processes, the two main challenges in the first step of the procedure (developing statistical model step) are: i) identification of the large-scale atmospheric predictors conveying relevant climate change information; and ii) development of the right quantitative functional relationship for capturing the complex nonlinearity between target hydro-climate variables and atmospheric simulated predictors. While the first of these problems is partly due to the high dimensionality of the climate processes that lead to inadequate results in projection of hydro-climate variables, the second is due to poor characterisation of the functional form. This chapter attempts to address both these limitations in the regression-based statistical downscaling as discussed below.

In statistical downscaling processes, projecting a dependent hydro-climate variable from high-dimensional large-scale atmospheric variables leads to inadequate results in terms of performance accuracy, due to the curse of dimensionality. The number of potentially important input variables may be large, and the existence of correlation among data may subsequently induce redundancy and collinearity. To complicate matters further, the inherent complexity, nonlinearity, and interdependency among explanatory large-scale atmospheric parameters give rise to unsatisfactory predictive performance of data-driven models in statistical downscaling. Despite its critical importance in climate change studies, this challenge has so far gained only limited attention. The majority of attempts to reduce dimensionality's impacts, and thus improve the performance of models in statistical downscaling, have used conventional methods. Principal Component Analysis (PCA) (Shashikanth et al., 2014; Tripathi et al., 2006b), Canonical Correlation Analysis (CCA) (Joshi et al., 2013; Wójcik, 2014), Correlation Analysis (CA) (Chen et al., 2010), Multivariate Sequential

(forward, backward, and stepwise) Regression Models (Hessami et al., 2008; Joshi et al., 2013), and different types of clustering (Ghosh and Mujumdar, 2008b; Tisseuil et al., 2010; Wójcik, 2015) are the most commonly used dimensionality reduction techniques in downscaling processes. A few attempts have also been made to select effective variables from high dimensional atmospheric predictor variables, using a combination of Gamma test (GT) and entropy methods (Ahmadi et al., 2014), Bayesian Model Averaging (BMA) (Tareghian and Rasmussen, 2013), Mutual Information (Nasseri et al., 2013), the Least Absolute Shrinkage and Selection Operator (LASSO) (Hammami et al., 2012), and Independent Component Analysis (ICA) (Moradkhani and Meier, 2010; Najafi et al., 2011).

The prominent dimensionality reduction techniques are unsupervised, ignore the response variable, and seek a sequence of directions capturing the maximum variability and modelling the covariance structure of data. However, in regression-based statistical downscaling, projecting atmospheric predictor variables along directions that are related to the response variable is of particular interest. Moreover, the recent variable selection-based approaches also select a limited number of predictors, which do not adequately encompass the properties of the explanatory data, leading to insufficient performance of statistical downscaling models. For example, the relevance between each potential predictor and target variable is considered separately, ignoring the interactions within the input dataset. Consequently, an irrelevant individual predictor may be discarded, even though its combination with other atmospheric predictors would make it a very relevant variable (Galelli et al., 2014; Saeys et al., 2007). These methods are also inappropriate for dimension reduction purposes for nonlinear predictors. The other drawback is that some feature selection-based methods utilize optimization algorithms as a part of the input variable selection procedure, resulting in computationally expensive analyses (Galelli et al., 2014).

To address the abovementioned drawbacks of the dimensionality reduction in the statistical downscaling processes, this study presents a new approach of supervised dimensionality reduction: "Supervised Principal Component Analysis (Supervised PCA)". This method, proposed by Barshan et al. (2011), is a generalization of PCA, extracting the principal components of explanatory variables that have maximal dependency on the response variable. The Supervised PCA technique explores subspaces along which the dependency between target hydro-climate variable and large-scale atmospheric projectors is maximized. To capture the nonlinear variability between hydro-climatic

response variables and projectors, a kernel version of Supervised PCA is also presented for nonlinear data transformation.

Due to the complex nonlinear relationship existing between target hydro-climate variables and large-scale atmospheric variables, standard linear methods fail to capture the nonlinear functional relationship. To address the second challenge in developing a statistical modelling step, considerable attention has also been paid in the last few years to nonlinear-based soft computing data-driven regression models. Machine-learning methods have gained more popularity for statistical downscaling modelling. Among machine learning methods, Support Vector Regression (SVR) has been widely employed in hydrology for nonlinear stochastic modelling of different hydro-climatic variables (Chen et al., 2010; 2012; Nasseri et al., 2013). In recent years, however, a fully probabilistic Bayesian framework of the SVR known as Relevance Vector Machine (RVM) has gained more popularity in regression-based statistical modelling. Ghosh and Mujumdar (2008a) compared the results obtained from the SVR and RVM models for projection of streamflow in a statistical downscaling process. They presented the advantages of the RVM over the SVR to improve the model performance. In another attempt, the authors also employed the RVM model with a fuzzy clustering method to downscale GCM outputs for monsoon streamflow projections (Mujumdar and Ghosh, 2008). Joshi et al. (2013) analyzed the performance of two statistical downscaling frameworks to characterize the low-flow regime of three rivers in eastern Canada. They also mentioned the superiority of the RVM model to the Automated Statistical Downscaling (ASD) method in terms of performance criteria. Other studies such as Bai et al. (2014), Khalil et al. (2005), and Okkan and Inan (2014) have also discussed the power of the RVM model compared with other learning algorithms in capturing the nonlinearity and improving the performance accuracy of different water resources associated projections.

The remainder of this chapter is organized as follows: Section 2.2 provides a mathematical background of dimensionality reduction methods in two different categories, unsupervised and supervised. In the unsupervised category, PCA and CCA methods are described, with particular focus on the drawbacks of these currently used dimension-reduction techniques. In the supervised category, the dependence measurement criterion on which the supervised dimensionality reduction methods is based on is described. The Supervised PCA, its extensions, and the connection to the conventional PCA are next presented. Section 2.3 presents the performance evaluation procedure for the dimensionality reduction methods of the two different categories in relation to statistical downscaling

using two machine-learning methods (SVR and RVM). Section 2.4 describes the data used for statistical downscaling in this study. The effectiveness of the supervised methods is then examined for the statistical downscaling of precipitation for a specific site and compared with other dimensionality reduction methods in section 2.5. Conclusions are given in section 2.6.

Figure 2-1 depicts a flowchart of different methods and procedures applied in this chapter.

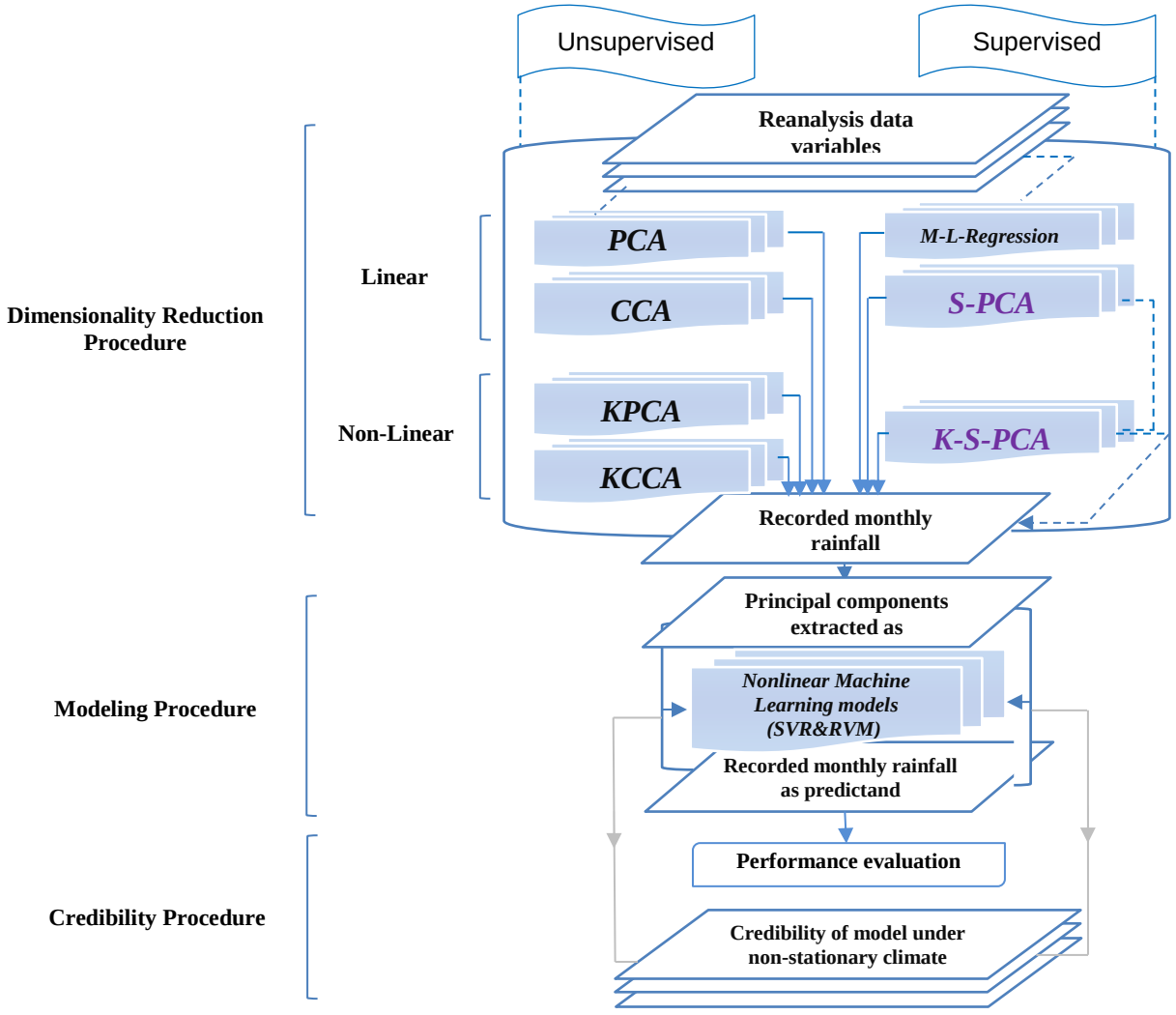

Figure 2-1. Summarized methodology used in the current chapter

2.2 Dimensionality Reduction Methods

In a given high-dimensional data set, consider projecting a response stochastic variable using a set of independent high-dimensional explanatory random variables. Using conventional regression methods, projecting the target variable leads to unsatisfactory results in terms of performance accuracy, simply due to the "curse of dimensionality" (Ahmadi et al., 2014; Barshan et al., 2011; Najafi et al., 2011). In addition, the number of observations required for learning is exponentially increased with the dimensionality of the data set. A preprocessing step deriving an appropriate low-dimensional manifold encoding of a high-dimension data set is thus crucial to reaching the best performance on learning. This step forms the dimensionality reduction procedure.

The following subsections describe the mathematical framework of the dimensionality reduction methods applied in this study.

2.2.1 Unsupervised Methods

2.2.1.1 Linear and Nonlinear Principal Component Analysis

Principal Component Analysis (PCA) is a technique currently popular for dimensionality reduction in different climate-related disciplines, especially for statistical downscaling processes in climate change studies. PCA is a classical and prominent data analysis method providing a reduced sequence of linear subspaces from a high-dimensional data set, capturing maximum variability, and modelling the covariance structure of the explanatory data.

The specified linear subspaces projected by d orthogonal vectors in a new coordinate system are called 'principal components'. In a given data set of vectors x_i, $i \in 1 \dots p$, the d principal components are defined as orthonormal transformations onto which the variance retained under projection is maximal (Hotelling, 1993).

Suppose all centered observations are stacked into matrix X, which has dimension of $p \times n$, where p corresponds to p-dimensional columns with n observations. To capture the maximum variability, let the first principal component denoted by U_1, be a combination of X defined by combinations (weights) $w = [w_1, w_2, \dots, w_n]$. Then the first principal component will be

$$U_1 = w^T X \qquad (2.1)$$

and

$$var(U_1) = var(w^T X) = w^T S w \qquad (2.2)$$

where S is the $n \times n$ sample covariance matrix of X. The objective is maximization of $\mathrm{var}(U_1)$, while that can be increased arbitrarily by increasing the magnitude of w. Hence, constraining w to having unit length, w is chosen to maximize $w^T S w$. Therefore, the objective will be:

$$\max w^T S w \qquad (2.3)$$

$$\text{subject to } w^T w = 1$$

The first d principal components are determined using the d dominant eigenvectors of covariance matrix S.

A kernel PCA (Schölkopf et al., 1998) can be defined by performing nonlinear transformation of data to find the principal components associated with the input (explanatory) data. Given the set of centred observations x_i, PCA diagonalizes the covariance matrix $S = \frac{1}{t}\sum_{j=1}^{t} x_j x_j^T$ by solving the eigenvalue problem $\lambda v = Sv$. Using kernels (which are methods of implicitly mapping data into a higher dimension feature space) the same computation can be performed in a dot product space $\mathcal{H}$ by a nonlinear mapping of input data $\Phi: x \to \mathcal{H}$, $x \to \Phi(x)$, so that the covariance matrix can be re-written as:

$$\hat{S} = \frac{1}{t}\sum_{j=1}^{t} \Phi(x_j)\Phi(x_j)^T \qquad (2.4)$$

The kernel principal components are then extracted by computing projections onto the eigenvectors of the centred kernel matrix $K_{ij} = \langle \Phi(x_j), \Phi(x_j) \rangle$.

2.2.1.2 Linear and Nonlinear Canonical Correlation Analysis

Canonical Correlation Analysis (CCA) (Hotelling, 1936) is a dominant technique that can be applied in modelling the association between two variables. The CCA method seeks two sets of basis vectors for two blocks of variables, so that the correlation between the projections of variables onto these basis vectors is maximized.

Suppose n observations from explanatory variable $\mathcal{X} \epsilon \mathbb{R}^{\mathrm{p}}$ and response variable $\mathcal{Y} \epsilon \mathbb{R}^{\mathrm{l}}$, are stacked in zero-mean matrices $X_{p \times n}$ and $Y_{l \times n}$. Then CCA searches for linear transformation of matrices W_x and W_y to maximize the correlation between the two vectors as follows:

$$\rho = \frac{Cov\,(W_x^T X, W_y^T Y)}{\sqrt{Var(W_x^T X) Var(W_y^T Y)}} = \frac{W_x^T X Y^T W_y}{\sqrt{(W_x^T X X^T W_x)(W_y^T Y Y^T W_y}} \tag{2.5}$$

Equation 2.5 equivalents to the following optimization problem:

$$\begin{aligned} &\underset{W_x, W_y}{\text{argmax}} \quad W_x^T \mathrm{X} Y^T W_y \\ &subject\ to: \quad W_x^T X X^T W_x = I \\ &\qquad\qquad W_y^T Y Y^T W_y = I \end{aligned} \tag{2.6}$$

The optimum value of W_x is therefore obtained by first solving for generalized eigenvectors of the form (Hardoon et al., 2004):

$$X Y^T (Y Y^T)^{-1} Y X^T W_x = \lambda^2 X X^T W_x \tag{2.7}$$

and then the corresponding W_y is found as $W_y = (Y Y^T)^{-1} Y X^T W_x / \lambda$.

CCA may not extract useful descriptors of data due to the existence of the dependence in nonlinear relationships. In this case, kernel CCA addresses this drawback by projecting data into a higher dimensional feature space, and then preforming CCA in the new feature space. If kernel matrices K_x and K_y contain inner products of Φ_x and Ψ_y as the new projection of data, then W_x and W_y can be re-written as $W_x = \Phi(X)\alpha$ and $W_y = \Psi(Y)\beta$. Replacing the inner products as $K_x = \Phi(X)^T \Phi(X)$ and $K_y = \Psi(Y)^T \Psi(Y)$, equation 2.6 becomes:

$$\begin{aligned} &\underset{\alpha, \beta}{\text{argmax}} \quad \alpha^T K_x K_y \beta \\ &subject\ to: \quad \alpha^T K_x^2 \alpha = I \\ &\qquad\qquad \beta^T K_y^2 \beta = I \end{aligned} \tag{2.8}$$

Therefore, after implementing the kernel process, CCA can be applied in the mapping space. It should be noted that other nonlinear methods such as nonlinear CCA using neural networks (CCA-NN) (Ouali et al., 2016) can be applied in the same context for nonlinear data transformation.

In spite of being the most popular methods in dimensionality reduction, PCA and CCA suffer from several drawbacks. PCA's effectiveness is influenced by its linearity and unsupervised problems. PCA method projects a sequence of linear subspaces (manifolds) corresponding to the maximum

variation of the covariate explanatory data without taking into account the response variable. CCA is also unable to capture nonlinearity between data. In statistical downscaling, certain modes of variability that are dependent on the response variable are of particular interest. Thus, projection of the explanatory variables along directions that are associated with the response variable is preferable, but is not achieved by deriving subspaces that have maximum variation or correlation.

To overcome this drawback, supervised dimensionality reduction methods seek subspaces in which the dependency between response variable and explanatory variables (predictors) is maximized.

2.2.2 Supervised Methods

2.2.2.1 Supervised Principal Component Analysis (Supervised PCA)

The supervised dimensionality reduction method proposed by Barshan et al. (2011) is based on extracting the principal components of predictors that have maximal dependency on the response variable. This method relies on Hilbert-Schmidt Independence Criterion (HSIC), measuring the dependence between response variable and predictors. According to the HSIC, two random variables, $\mathcal{X}$ and $\mathcal{Y}$, are statistically independent if and only if any bounded continuous function of the variables is uncorrelated. Consider $\mathcal{F}$ and $\mathcal{G}$ as the separable Reproducing Kernel Hilbert Spaces (RKHS) containing bounded real-valued functions of *x* from $\mathcal{X}$ to $\mathbb{R}$, and *y* from $\mathcal{Y}$ to $\mathbb{R}$, respectively. In this case, the HSIC can be expressed in terms of kernel functions as

$$\begin{aligned} HSIC(P_{\mathcal{X},\mathcal{Y}}, \mathcal{F}, \mathcal{G}) \\ &= E_{x,x',y,y'}[k(x,x')l(y,y')] + E_{x,x'}[k(x,x')E_{y,y'}[l(y,y')] \\ &- 2E_{x,y}\left[E_{x'}[k(x,x')]E_{y'}[l(y,y')]\right] \end{aligned} \qquad (2.9)$$

where $E_{x,x',y,y'}$ is the expectation over both pairs of (x, y) and (x', y') drawn independently from $P_{\mathcal{X},\mathcal{Y}}$ (the joint probability distribution of random variables $\mathcal{X}$ and $\mathcal{Y}$). Here k and l are the associated kernels of $\mathcal{F}$ and $\mathcal{G}$, respectively. To use HSIC as a practical test for dependency testing, it is necessary to approximate HSIC $(p_{\mathcal{X},\mathcal{Y}}, \mathcal{F}, \mathcal{G})$, given a finite number of observations. Let $\mathcal{Z} \coloneqq \{x_1, y_1), \dots, (x_n, y_n)\} \subseteq \mathcal{X} \times \mathcal{Y}$ be a series of *n* independent observations drawn from $P_{\mathcal{X},\mathcal{Y}}$. An empirical estimate of HSIC is:

$$HSIC(\mathcal{Z}, \mathcal{F}, \mathcal{G}) \coloneqq (n-1)^2 tr(KHLH) \qquad (2.10)$$

where $H, K, L \in \mathbb{R}^{n \times n}$, $k_{ij} \coloneqq k(x_i, x_j)$, $L_{ij} \coloneqq l(y_i, y_j)$, and $H_{ij} \coloneqq I - n^{-1}ee^T$ (the centering matrix, 'e' is a vector of all ones). Thus, it can be concluded that to maximize the dependence between two kernels, it is necessary to increase the value of the empirical estimate, i.e., $tr\,(KHLH)$. It should be noted that if one of the kernel matrices (*K* or *L*) is already centered, for example *L* (i.e., *HLH=L*), then the objective function no longer includes the centering matrix *H*, and it will be addressed as $tr\,(KL)$. Likewise, if *HKH=K*, then the objective function will be $tr\,(KHLH) = tr(HKHL)$ with the same identical results (Barshan et al., 2011).

After defining HSIC as a measure for determining dependency between random variables, Supervised PCA is developed. Suppose for explanatory variables, there is a set of *n* data points $\{X_i\}_{i=1}^{n}$with p features, stacked in the $p \times n$ matrix X. The target variable is also Y in the $l \times n$ matrix. The goal is finding the subspace in which the dependency between the projected data $U^T X$ and the target variable is maximized. According to the empirical HSIC, the objective function can be formulated to maximize $tr(HKHL)$, such that:

$$tr(HKHL) = tr(HX^T UU^T XHL) \qquad (2.11)$$
$$= tr(U^T XHLHX^T U)$$

where *K* is the kernel of $U^T X$ (e.g., $X^T UU^T X$), *L* is the kernel of target variable *Y* (e.g., $Y^T Y$), and $H_{ij} \coloneqq I - n^{-1}ee^T$.

As an orthogonal transformation matrix U mapping a data set into a space in which the features are uncorrelated, the optimization problem is constrained and can be written as:

$$\underset{U}{\text{argmax}} \quad tr(U^T XHLHX^T U)$$
$$\text{subject to} \quad U^T U = I \qquad (2.12)$$

If the symmetric and real matrix denotes $Q = XHLHX^T$, the optimal solution will be $U = [u_1, u_i, \ldots, u_d]$, where u_i is the corresponding eigenvector to the *i*-th largest eigenvalue. Supervised PCA also has a closed-form in dual formulation that is described in Barshan et al. (2011).

The procedure of the Supervised PCA is summarized in Algorithm 1.

Algorithm 1 (Supervised PCA)

Input: Matrix of training data, ***X***, testing data example, ***x***, kernel matrix of target variable, ***L***, and training data size, ***n***.

Output: Dimension reduced training and testing data, $\boldsymbol{Z}$, and $\boldsymbol{z}$.

1: $H \leftarrow I - n^{-1}\boldsymbol{e}\boldsymbol{e}^T$

2: $Q \leftarrow XHLHX^T$

3: **Compute basis**: $U \leftarrow$ eigenvectors of Q corresponding to the top d eigenvalues.

4: **Encode training data**: $Z \leftarrow U^T X$

5: **Encode test example**: $\boldsymbol{z} \leftarrow U^T \boldsymbol{x}$

2.2.2.2 Kernel Supervised Principal Component Analysis

Supervised PCA and PCA are designed to find linear subspaces of high-dimensional data, with and without taking into account the response variable, respectively, such that a data set can be represented with a minimal loss of variance. This approach allows the detection of linear patterns (Jackson, 1991), and cannot model the variability of data correctly. However, high-dimensional hydro-climatic variables have a nonlinear nature (Raghavendra and Deka, 2014), and therefore linear models cannot capture their variabilities. In this case, nonlinear transformation of the variables is required to successfully apply learning algorithms for dimensionality reduction. One efficient method that can address the problem of nonlinear dimensionality reduction is to use kernels, computing the similarity measure between any two data points. This section presents how, through the use of a kernel, Supervised PCA can be extended to nonlinear mapping of data to compute principal components efficiently in high-dimensional feature spaces.

The nonlinear mapping function maps the feature matrix *x*, from $x \rightarrow \Phi(x)$. Thus, the non-linear kernel is $K = \Phi(x)^T \Phi(x)$. Accordingly, Supervised PCA objective can be formulated as:

$$\underset{U}{\text{argmax}} \quad tr(U^T \Phi(x) HLH \Phi(X)^T U)$$

$$\text{subject to } U^T U = I \qquad (2.13)$$

It should be noted that the matrix $K = \Phi(x)^T \Phi(x)$ can be efficiently computed, without computing $\Phi(x)$ explicitly. The transformation matrix, U, can be further represented as a linear combination of the projected dataset $U = \Phi(X)\beta$. Thus, the objective function is rewritten as

$$tr(U^T \Phi(x) HLH \Phi(X)^T U) = tr(\beta^T \Phi(X)^T \Phi(X) HLH \Phi(X)^T \Phi(X) \beta)$$

$$= tr(\beta^T KHLHK\beta) \qquad (2.14)$$

the constraint is:

$$U^T U = \beta^T \Phi(X)^T \Phi(X) \beta$$

$$= \beta^T K \beta \qquad (2.15)$$

where K is a kernel function. After defining a new objective function and constraint in terms of inner products between data points that are computed via the kernel, a new optimization problem can be formulated as

$$\underset{U}{\text{argmax}} \quad tr(\beta^T KHLHK\beta) \qquad (2.16)$$

$$\text{subject to} \quad \beta^T K \beta = I$$

This is considered to be a generalized eigenvector problem. Here β can be computed as the top d generalized eigenvectors of $(KHLHK, K)$ (Barshan et al., 2011). Kernel Supervised PCA is summarized in Algorithm 2.

Algorithm 2 (Kernel Supervised PCA)

Input: Kernel matrix of training data, $\boldsymbol{K}$, kernel matrix of testing data, $\boldsymbol{K}_{test}$, kernel matrix of target variable, $\boldsymbol{L}$, testing data example, $\boldsymbol{x}$, training data size, $\boldsymbol{n}$.

Output: Dimension reduced training and testing data, $\boldsymbol{Z}$ and $\boldsymbol{z}$.

1. $H \leftarrow I - n^{-1}\boldsymbol{e}\boldsymbol{e}^T$
2. $Q \leftarrow KHLHK$
3. **Compute basis**: $\beta \leftarrow$ generalized eigenvectors of (Q, K) corresponding to the top d eigenvalues.
4. **Encode training data**: $Z \leftarrow \beta^T[\Phi(X)^T \Phi(X)] = \beta^T K$
5. **Encode test example**: $\boldsymbol{z} \leftarrow \beta^T[\Phi(X)^T \Phi(\boldsymbol{x})] = \beta^T K_{test}$

In addition to the aforementioned methods for dimensionality reduction, three common backward, forward, and stepwise multivariate linear regression methods are also considered to provide a basis (as feature selection-based methods) for comparison of the performance accuracy of the different supervised dimensionality reduction methods.

2.3 Evaluation of Dimensionality Reduction Approaches

The presented Supervised PCA method's effectiveness in comparison to that of some of the state-of-the-art algorithms for dimensionality reduction is evaluated under a statistical downscaling

procedure. For this purpose, the performances of Supervised PCA and Kernel Supervised PCA are compared with those of conventional and feature selection-based linear dimensionality reduction approaches on a target predictand variable and a set of predictor variables. A random section of a 75% training set and 25% testing set is performed on the input dataset. Note that the input features of both training and testing dataset are provided at learning time for conventional and feature selection-based dimensionality reduction approaches. Before that, all the input features are normalized and the kernel parameter is obtained using 10-fold cross-validation in Supervised PCA approaches.

For each method, after estimating the transformation matrix (using the training set for Supervised PCA approaches) a regression model is fitted to the response variable Y and the dimension-reduced explanatory data Z. Since the relationship between climate variables and transformed explanatory atmospheric projectors is still complex and nonlinear, two soft computing nonlinear machine learning methods Support Vector Regression (SVR), and Relevance Vector Machine (RVM) are employed to capture the nonlinearity and evaluate different dimensionality reduction methods in terms of response variable projection performance.

2.3.1 Nonlinear Support Vector Regression (SVR)

Unlike most traditional Artificial Neural Network (ANN) models, which use empirical risk minimization, SVR implements Structural Risk Minimization (SRM) principles. The concept of SRM is to minimize an upper bound on the generalization error rather than to minimize the training error. This principal helps the SVR to achieve an optimum network structure (Lin et al., 2006). This superior feature has made the SVR popular for generalization purposes in statistical modelling and led to its wide application in pattern recognition.

Given an input dataset as predictors and a target variable as a predictand, a function $f(X)$ should be developed to describe the inherent nonlinear relationship between the dataset and predictand. This function can be used later to project the target variable from generated new input data (here principal components extracted by Supervised PCA techniques). The standard nonlinear function in the SVR is formulated as

$$\hat{y} = f(X) = \sum_{i=1}^{n} w_i K(X_k . X) + b \qquad (2.17)$$

where $K(X_k.X)$ is a kernel function, based on which basis functions are defined in the training dataset. A detailed introduction to the SVR method may be found in Dibike et al. (2001) and Vapnik (1998).

In spite of its many advantages in modelling, the SVR suffers from practical drawbacks. SVR makes unnecessary liberal use of basis functions while the training dataset size grows, leading to complexity in computation and over-fitting in prediction, which are addressed in the Sparse Bayesian Learning (SBL) algorithm known as Relevance Vector Machine (RVM) (Tipping, 2001).

2.3.2 Relevance Vector Machine (RVM)

In the SVR, predictions are not probabilistic and the model outputs a point estimate and a 'hard' binary decision in classification, whereas the conditional distribution $p(Y|X)$ is desired to capture uncertainty in predictions (Ghosh and Mujumdar, 2008b). There is also a need to estimate the "nuisance" parameter of C and the insensitivity parameter 'ε', which is wasteful in both data and computation. The kernel function $K(X, X_i)$ must also satisfy Mercer's condition (for a continuous symmetric kernel of a positive operator). To cover these limitations, Tipping (2001) developed a Sparse Bayesian Learning (SBL) algorithm.

The RVM is a Bayesian treatment of equation 2.17, which covers all limitations of the SVR. The RVM proposes a fully probabilistic framework and introduces prior information over the model weights governed by a set of hyper-parameters that are iteratively estimated from the data. In practice, the posterior distribution of the majority of weights peaks sharply around zero. A few training vectors associated with the remaining non-zero weights are called relevant vectors. While RVM is capable of generalization performance in comparison to the SVR, its most compelling feature is that it utilizes fewer kernel functions, thus avoiding over-fitting (Khalil et al., 2006; Tipping, 2001). A detailed mathematical background of the SBL algorithm for regression modelling is found in Tipping (2001).

Once the two methods (SVR and RVM) are applied in the downscaling procedure based on transformed projector components, the validation of the model performances is evaluated for each dimensionality reduction method. A two-fold cross-validation procedure is used for training and testing. In this procedure, the datasets (including inputs and the target datasets) are randomly split into two non-overlapping subsets (a shuffling is implemented on the data array and then the dataset is split into two training and testing subsets). Each of the nonlinear regression models is then trained based on training subset. The validation of the model is then examined based on testing subset assumed as

unobserved data points (validation). A sampling 10-fold cross validation method is used for tuning of the machine-learning parameters (gamma, cost, and error in SVR and kernel width in RVM). The training and testing process is carried out based on a chosen kernel. Gaussian (radial basis), Polynomial, and Laplacian kernel functions are used as nonlinear functions in both SVR and RVM models in this study. In the validation process, the consistency of input features, division into two training datasets and testing datasets remains the same in the Supervised PCA methods, as a random selection (of a 75% training set and 25% testing set) is performed on the input features in other dimensionality reduction methods.

To increase the predictive performance for low and high magnitudes of the target variable, a unique clustering method is employed. First a threshold is tuned on the precipitation values to partition the training data points into two classes, high and low. Since the high and the low data points are from two different distributions, it is possible to separate them and develop two different regression models for them. In the training step, after the partitioning, the low class and high class are fitted separately with two different SVR and RVM models. Now given the two classes of training data, i.e., high and low, support vector machine (classification) is used to find the margin of these two classes. In the testing step, it is first classified whether the given test data point belongs to high or low class and then the SVR and RVM models are applied correspondingly.

To evaluate the goodness of fit of the two machine learning models, in terms of the agreement between observed and model-predicted target variable for the testing dataset, and to assess the performance of the dimensionality reduction methods, the following criteria are used in this study:

I: *Correlation coefficient* between observed and predicted series.

II: *Nash-Sutcliffe Model Efficiency* (*E*):

The model efficiency criterion, proposed by Nash and Sutcliffe (1970), for model evaluation is:

$$E = 1 - \frac{\sum(O_i - F_i)^2}{\sum(O_i - \bar{Q})^2} \qquad (2.18)$$

where E is the coefficient of efficiency, O_i is the observations of the target variable, F_{i} is the predicted target variable, and $\bar{Q}$ is the average of the observed time series. A value of 1 represents a perfect model and for a value of $E<0$, the model predictions are worse than those from the reference model.

III: *Root Mean Squared Error (RMSE)*:

$$RMSE = \left(\frac{\sum_{i=1}^{n}(F_i - O_i)^2}{n}\right)^{0.5} \quad (2.19)$$

IV: *Mean Absolute Error (MAE)*

The mean absolute error is used to measure how close predictions and observations of the target variables are to each other. This criterion is given by:

$$MAE = \frac{1}{n}\sum_{i=1}^{n}|F_i - O_i| \quad (2.20)$$

The parameters are defined as in the preceding equations.

V: *Mean Bias Error (MBE)*

The mean bias error is usually intended to indicate model average 'bias'. The criterion measures average over or under-prediction of a model. MBE formula can be written as:

$$MBE = \frac{1}{n}\sum_{i=1}^{n} e_i = \overline{F_i} - \overline{O_i} \quad (2.21)$$

The parameters are the same as in the aforementioned equations.

Considering the above criteria, the best dimensionality reduction method is then determined in terms of the best performance accuracy using machine-learning methods. Subsequently, the best reduction method is employed for transformation of the same explanatory variables from different climate change scenarios to project the potential impact of climate change on the target variable for the upcoming decades.

2.4 Study Area and Data Set

2.4.1 Study area

The domain of interest in this study is the capital of Iran, Tehran. This megacity, with a population surpassing 14 million, is the largest and the most-populated city in Iran and in western Asia. The consistent rapid expansion of the city and population has led to several environmental issues, particularly surface water resources shortages. Additionally, the occurrence of severe dry spells and mismanagement of surface water resources in recent years have made this shortage much more complicated, so that water authorities are obliged to ration water. Therefore, it is essential to have a

plan for better management of water resources in relation to the future likelihood of extreme hydrological events, which could lead to dry spells and increase the water shortage in this city. The present study thus investigates the impact of future climate change on the availability of surface water resources for different purposes, especially the water supply in this megacity.

2.4.2 Observations

To better understand the impact of climate change on the availability of surface water resources for various purposes, especially for water supply, a meteorological station (Mehrabad) has been selected to project the future behavior of precipitation in this city. Launched by the Iran Meteorological Organization (IRIMO), Mehrabad synoptic station, with its mean annual rainfall of 235 mm, represents the semi-arid climate condition of the Tehran city. The recorded monthly-based precipitation time series applied in the current study, span from 1951 to 2011 (60 years) at the site. Tehran's climate is largely influenced by its geographical location, surrounded by Alborz Mountains in the north and the central flat plains in the south. Seasonal precipitation is varied in this city and influenced by the monsoon phenomenon, so that summer and winter are characterized as dry seasons, while spring and fall are almost lush, with the main precipitation occurring in these seasons. Figure 2-2 illustrates the location of the study site.

National Center for Environmental Prediction/National Center for Atmospheric Research (NCEP/NCAR) reanalysis data are employed as a proxy of observed large-scale atmospheric predictors. The NCEP/NCAR dataset comprised of outputs of a high-resolution atmosphere model, reproduced through assimilated data from surface observations, upper air stations, and a satellite-observing platform (Kalnay et al., 1996) are typically viewed on a regular grid with a spatial resolution of $2.5^{\circ} \times 2.5^{\circ}$ (approximately $250\ \text{km} \times 250\ \text{km}$). Reanalysis NCEP/NCAR datasets are available from 1948 to present. In the pre-processing phase of the statistical downscaling procedure, NCEP/NCAR data are considered as observations and are employed as a benchmark for correcting systematic biases in the different GCMs. In the next phase, variables from the NCEP/NCAR dataset act as atmospheric predictors for developing the empirical model, which forms a basis for projecting the hydro-climate predictand of interest (precipitation here) for the following decades.

Since the downscaling model is sensitive to the choice of predictor variables (Shashikanth et al., 2014), the selection of reanalysis variables that are highly associated and show meaningful relationships with the precipitation data is of crucial importance.

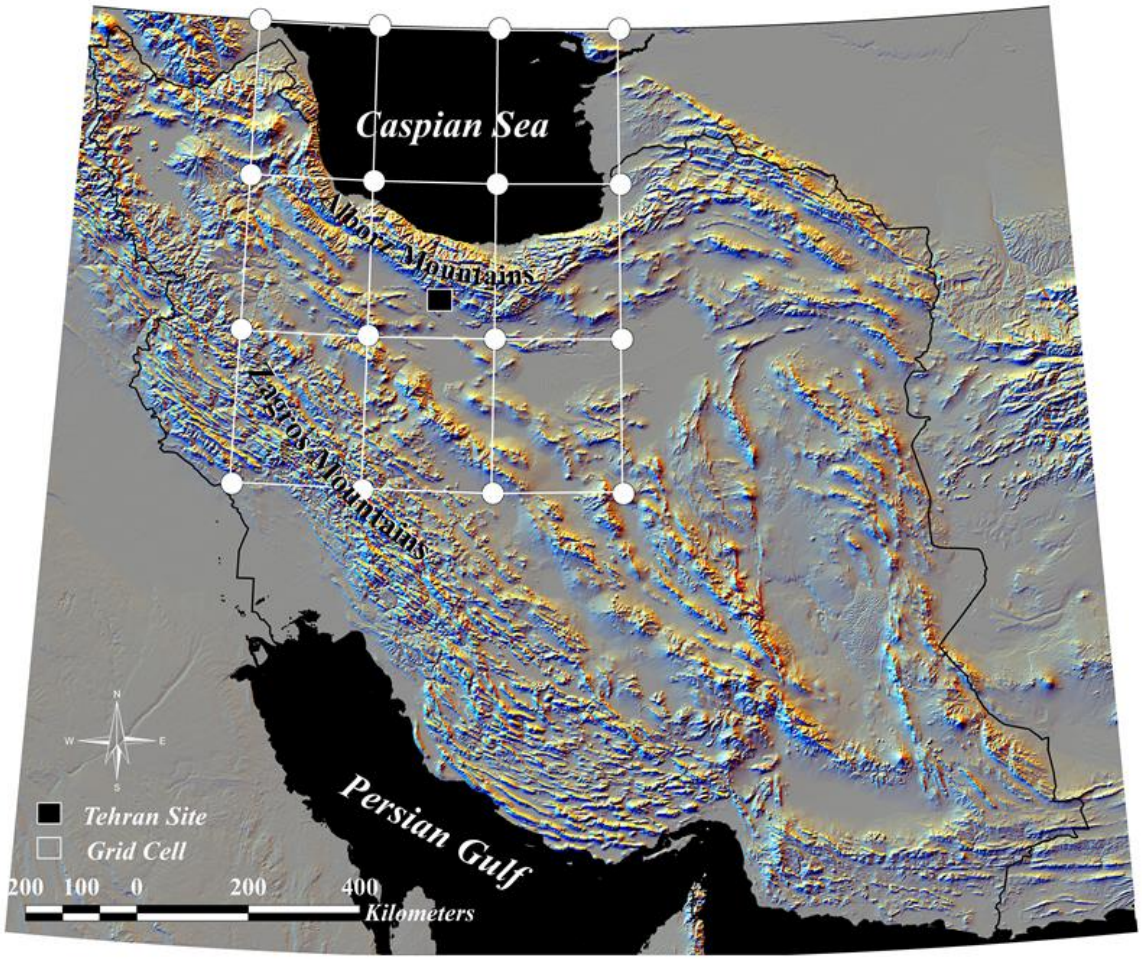

Figure 2-2. Study area and grids surrounding the study site

The criteria that the selection of predictors are based on are that: (i) predictors should be physically relevant to the host GCMs; (ii) predictors can be realistically simulated by GCMs; and (iii) selected predictors are able to represent climate change signals (Hewitson and Crane, 2012). Considering these criteria, the main predictors identified are precipitation (PRECFLUX), surface, maximum, and minimum air temperature variables (AIR, TMAX, and TMIN), which explain soil moisture and precipitation feedback (Dery and Wood, 2005; Nasseri et al., 2013). Mean sea level pressure (SLP) is also included, as it provides a basis for other variables such as surface vorticity, airflow strength, meridional and zonal wind flow components, and divergence (Kannan and Ghosh, 2013; Wilby and Wigley, 2000). Surface specific and relative humidity variables (SHUM and RHUM) are chosen because of their importance to GCM precipitation schemes (Hennessy et al., 1997; Kannan and

Ghosh, 2013). Geopotential height (HGT) at three pressure levels (1000, 500, 250 hPa) are also selected as predictors for precipitation in this study (Ahmadi et al., 2014; Nasseri et al., 2013). All the predictors are extracted in a monthly based temporal resolution (from 1948 to present) from the NCEP/NCAR reanalysis data for nine grid cells surrounding the Tehran meteorological site. These cells lie between latitude 32.5°N-37.5°N and longitude 37.5°E-52.5°E (illustrated in Figure 2-2). The monthly-recorded precipitation time series at the Tehran site is used as predictand and the overlapped time period with NCEP/NCAR data (1951-2011) is selected as a baseline for developing downscaling modelling. Therefore, in the study site a matrix with dimension 1×732 as predictand and 72×732 as predictors (here 732 is the number of recorded monthly observations in the study site and 72 is the number of predictors) is considered as the input dataset for different dimensionality reduction methods.

2.4.3 CMIP5 Climate Models

For future projection, outputs of the Coupled Model Intercomparison Project Phase 5 (CMIP5) multi-model dataset are used. The World Climate Research Program (WCRP) initiated the intercomparison project, CMIP5, to provide the most recent generation of GCMs in the Intergovernmental Panel on Climate Change (IPCC) fifth assessment report (Taylor et al., 2012a). In this study, 15 GCMs of CMIP5 multi-model ensemble are employed. Table 2-1 shows the list of the selected GCM models of CMIP5 covering the whole time period of 2015-2100, and also encompassing the same projector variables selected from NCEP/NCAR reanalysis data.

To compare the projection results, all the GCM models are re-gridded by bilinear interpolation method to match the resolution of the NCEP/NCAR reanalysis data ($2.5^{\circ} \times 2.5^{\circ}$). The CMIP5 provides future projection simulations with specified concentrations referred to as "representative concentration pathways" (RCPs), which are forced by anthropogenic influences on the atmospheric composition and land cover. The CMIP5 projections of future climate change underlying the RCPs provide a consistent combination of future population growth, technological advances, and socioeconomic parameters (Taylor et al., 2012a). Three RCPs employed in this study provide a rough estimate range of the radiative forcing in the 21st century. RCP2.6 radiative forcing increases to about 3 W/m^2 near the middle of the 21st century, before decreasing to nominal level of 2.6 W/m^2 by 2100. RCP2.6 is also called a peak-decline scenario in which 2° C global warming is satisfied. In intermediate RCP4.5, by the end of 21st century the radiative forcing reaches about 4.5 W/m^2. The

radiative forcing increases fast throughout the 21st century before reaching the level of 8.5 W/m^2 at the end of the century in RCP8.5 (Gräler et al., 2013; Taylor et al., 2012a).

Table 2-1. List of CMIP5 models evaluated in the present study

				Data Duration			
Number	**Model**	**Modelling center**	**Spatial Resolution**	**Historical**	**RCP2.6**	**RCP4.5**	**RCP8.5**
1	BCC-CSM1.1	BCC (China)	1° × 1.33°	1948-2014	2006-2100	2006-2100	2006-2100
2	CanESM2	CCCMA (Canada)	2.8° × 2.8°	1948-2014	-	2006-2100	-
3	CCSM4	NCAR (USA)	0.9° × 1.25°	1948-2014	2006-2100	2006-2100	-
4	CNRM-CM5	CNRM-CERFACS (France)	1.5° × 1.5°	1948-2014	2006-2100	-	-
5	CSIRO-Mk3.6.0	CSIRO-QCCCE (Australia)	1.875° × 1.875°	1948-2014	2006-2100	-	-
6	GFDL-ESM2M	NOAA GFDL (USA)	2° × 2.5°	1948-2014	-	2006-2100	2006-2100
7	GISS-E2-R	NASA GISS (USA)	2° × 2.5°	1948-2014	2006-2100	2006-2100	2006-2100
8	HadGEM2-ES	MOHC (UK)	1.25° × 1.875°	1948-2014	2006-2100	-	-
9	INM-CM4	INM (Russia)	1.5° × 2.0°	1948-2014	-	2006-2100	2006-2100
10	IPSL-CM5A-MR	IPSL (France)	1.25° × 2.5°	1948-2014	2006-2100	2006-2100	2006-2100
11	MIROC5	MIROC (Japan)	2.8° × 2.8°	1948-2014	2006-2100	2006-2100	2006-2100
12	MIROC-ESM	MIROC (Japan)	2.8° × 2.8°	1948-2014	2006-2100	2006-2100	2006-2100
13	MIROC-ESM-CHEM	MIROC (Japan)	2.8° × 2.8°	1948-2014	2006-2100	2006-2100	2006-2100
14	MRI-CGCM3	MRI (Japan)	1.125° × 1.125°	1948-2014	2006-2100	2006-2100	2006-2100
15	NorESM1-M	NCC (Norway)	1.875° × 2.5°	1948-2014	2006-2100	2006-2100	2006-2100

2.5 Results and Discussion

2.5.1 Dimensionality Reduction Performances

To better evaluate the effectiveness of the dimensionality reduction methods in the downscaling process, they are first classified into different categories. All of the dimensionality reduction methods in this study can be categorized under two main approaches: unsupervised and supervised methods. According to the type of data transformation in a learning algorithm, each of the main approaches is placed in either the linear or nonlinear group. Therefore, PCA and CCA are considered to be linear unsupervised methods, and KPCA and KCCA are located in the nonlinear unsupervised group. The same subdivision can be recognized for the supervised category, where the three feature selection-

based multivariate regression methods (Backward, Forward, and Stepwise) accompanying Supervised PCA are studied as supervised linear methods, while Kernel Supervised PCA method is a supervised nonlinear method.

In the category of the unsupervised methods, the input dataset encompasses the large-scale atmospheric variables (predictors), while for the supervised ones, the precipitation time series (as the response variable) is also added to the dataset. The results of both Pearson's and Spearman's rank correlation analyses show that all of the projectors are significantly correlated with the target precipitation variable at the 1% significance level. All observations in the unsupervised category and also feature selection-based multivariate regression methods are provided in the learning algorithms, whereas in the Supervised PCA and Kernel Supervised PCA, 75% random splits of observations are employed as a training set for calculation of the transformation matrix. It should be noted that the projection of datasets in nonlinear unsupervised and supervised methods is carried out using an RBF kernel. After computing the low dimensional projection of the data, the performance of the different dimensionality reduction methods is evaluated through two nonlinear SVR and RVM machine learning-based methods for 25% of the sample testing dataset. Doing so requires many steps to obtain optimum results. For each dimensionality reduction method output, a K-fold cross validation (K=10) procedure is applied on the testing dataset to choose the best tuning parameters for the SVR and RVM methods. Based on the choice of parameters, goodness of fit is then assessed for the different methods. Prior to that the clustering method is carried out on both training and testing datasets to improve the performance of the precipitation predictability for extreme minimum and maximum values. Table 2-2 provides the results of the performance criteria for different projections of the dimensionality reduction methods with the best selected kernels.

As these results show, in the unsupervised approach category, the nonlinear methods perform better than the linear ones in terms of the performance criteria in both SVR and RVM methods. The KPCA outperforms both linear methods (including PCA and CCA), and also nonlinear KCCA, indicating the existence of nonlinear relationships in the atmospheric predictor variables and the ability of KPCA to capture the nonlinear dependence among the predictors. The transformation of a nonlinear atmospheric dataset into a higher dimension feature space to capture the maximum variation leads to a more well-posed objective function in comparison with maximizing the correlation coefficient. Compared with the linear supervised multivariate regression methods using the same atmospheric projectors, the KPCA still yields a better embedding in terms of performance, because KPCA

Table 2-2. Results of the performance criteria obtained for different dimensionality reduction methods with the best selected kernels using SVR and RVM on testing dataset

Approach	Transfer Function	Dimensionality Reduction Method	Machine Learning Method	Kernel Function	No of vectors	R^2	RMSE	NSE	MAE	MBE
Unsupervised	Linear	PCA	SVR	RBF	384	0.38	18.05	0.37	11.94	-2.43
			RVM	Laplacian	47	0.39	17.46	0.38	12.17	-0.64
		CCA	SVR	RBF	365	0.34	18.30	0.33	12.65	-2.57
			RVM	RBF	28	0.36	17.86	0.35	12.45	-1.20
	Nonlinear	KPCA	SVR	RBF	336	0.49	16.14	0.47	10.67	1.32
			RVM	RBF	**69**	**0.57**	**14.37**	**0.55**	**9.21**	**0.55**
		KCCA	SVR	RBF	372	0.43	16.85	0.42	11.72	-1.48
			RVM	RBF	28	0.53	17.42	0.51	10.7	-0.69
Supervised	Linear	Backward	SVR	RBF	344	0.56	14.66	0.54	9.61	-1.37
			RVM	Laplacian	42	0.55	14.76	0.53	9.87	-0.61
		Forward	SVR	RBF	309	0.53	15.38	0.51	10.22	-3.62
			RVM	RBF	49	0.55	15.01	0.52	10.13	-2.48
		Stepwise	SVR	RBF	338	0.52	15.6	0.50	10.31	-3.21
			RVM	RBF	30	0.54	14.8	0.52	9.96	-2.32
		S-PCA	SVR	RBF	188	0.65	2.95	0.61	2.37	-0.87
			RVM	Laplacian	37	0.68	2.66	0.63	2.33	-0.23
	Nonlinear	K-S-PCA	SVR	RBF	135	0.76	1.45	0.75	1.32	-0.12
			RVM	RBF	**12**	**0.79**	**1.39**	**0.78**	**1.27**	**-0.02**

* Bold signifies preferred (optimal) result in each category.

provides a nonlinear projection while the linear feature selection-based multivariate regression (backward, forward, and stepwise) methods, can only produce linear embedding based on linear dependence between the target variable and the projectors.

Comparison of the methods in the supervised linear group shows that Supervised PCA significantly improves the prediction performance of the testing data. The multivariate feature selection-based regression methods are only able to detect linear dependence between precipitation and large-scale atmospheric predictors, while Supervised PCA is potentially capable of capturing any kind of dependence (linear and nonlinear) (Barshan et al., 2011). Although application of a linear kernel for response variable results in capturing the linear dependence between the target variable and projectors, other kernels can be also employed, leading to the capture of nonlinear dependence.

Accordingly, Supervised PCA with an RBF kernel to the target variable not only performs as the best in the supervised linear group, but also outperforms the best selected nonlinear KPCA method in the unsupervised category. By using Kernel Supervised PCA in the next step, significant progress can be achieved in comparison with even Supervised PCA in terms of the performance criteria. This improvement indicates the benefit of nonlinear transformation of the data into a higher dimensional space in capturing the nonlinear dependence between the target precipitation and the projector variables. As can be seen, close competition occurs amongst the unsupervised methods and feature selection-based methods in the supervised category, while using Supervised PCA (linear and nonlinear) methods leads to significant improvement in the goodness of fit. Moreover, Kernel Supervised PCA outperforms all of the other linear and nonlinear methods and remains superior in terms of dimensionality reduction. Figure 2-3 shows how Kernel Supervised PCA method can reduce the nonlinearity and complexity in the atmospheric predictors (from NCEP/NCAR dataset), and extract components that are highly dependent on the target variable.

It is worth noting that in all of the dimensionality reduction methods in the present study, the RVM method using very few relevant vectors compared with the number of support vectors in SVR outperforms the SVR method in the regression-based statistical downscaling in terms of goodness of fit. This superiority indicates the probabilistic reasoning of this method, which leads to minimizing the possibility of overfitting and reducing computational time as well.

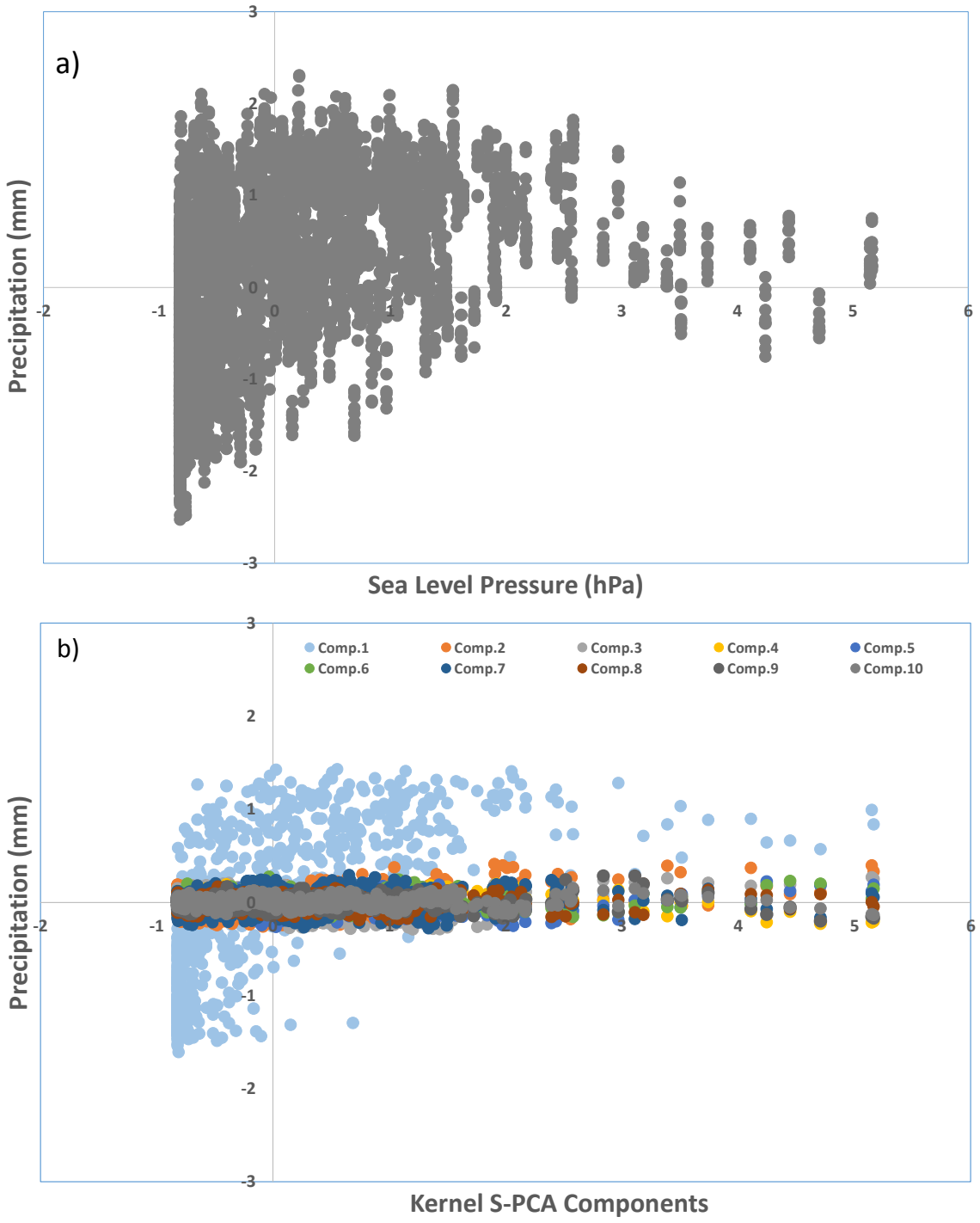

Figure 2-3. a) Nonlinear and complex relationship between one of the atmospheric predictors (SLP) and the target variable before using dimensionality reduction, and b) Relationship between reduced-dimension atmospheric predictors (components) extracted from Kernel Supervised PCA and the target variable. All the variables have already been standardized

Figure 2-4 illustrates the observed and predicted precipitation time series and the scatter plot between them derived from the Kernel Supervised PCA and the RVM method for validation period (testing data) at the Tehran station. The figure indicates a good agreement between observed and predicted precipitation time series. Therefore, the combination of the Kernel Supervised PCA and the RVM method performs best in the modelling section of the statistical downscaling process. Although the presented model is able to capture extreme minimum and maximum precipitation events, in very rare cases, it cannot completely mimic extreme recorded monthly precipitation events. The reason might be related to the essence of regression based statistical downscaling models that cannot explain entire variance of the downscaled response variable (Ghosh and Mujumdar, 2008a; Tripathi et al., 2006a).

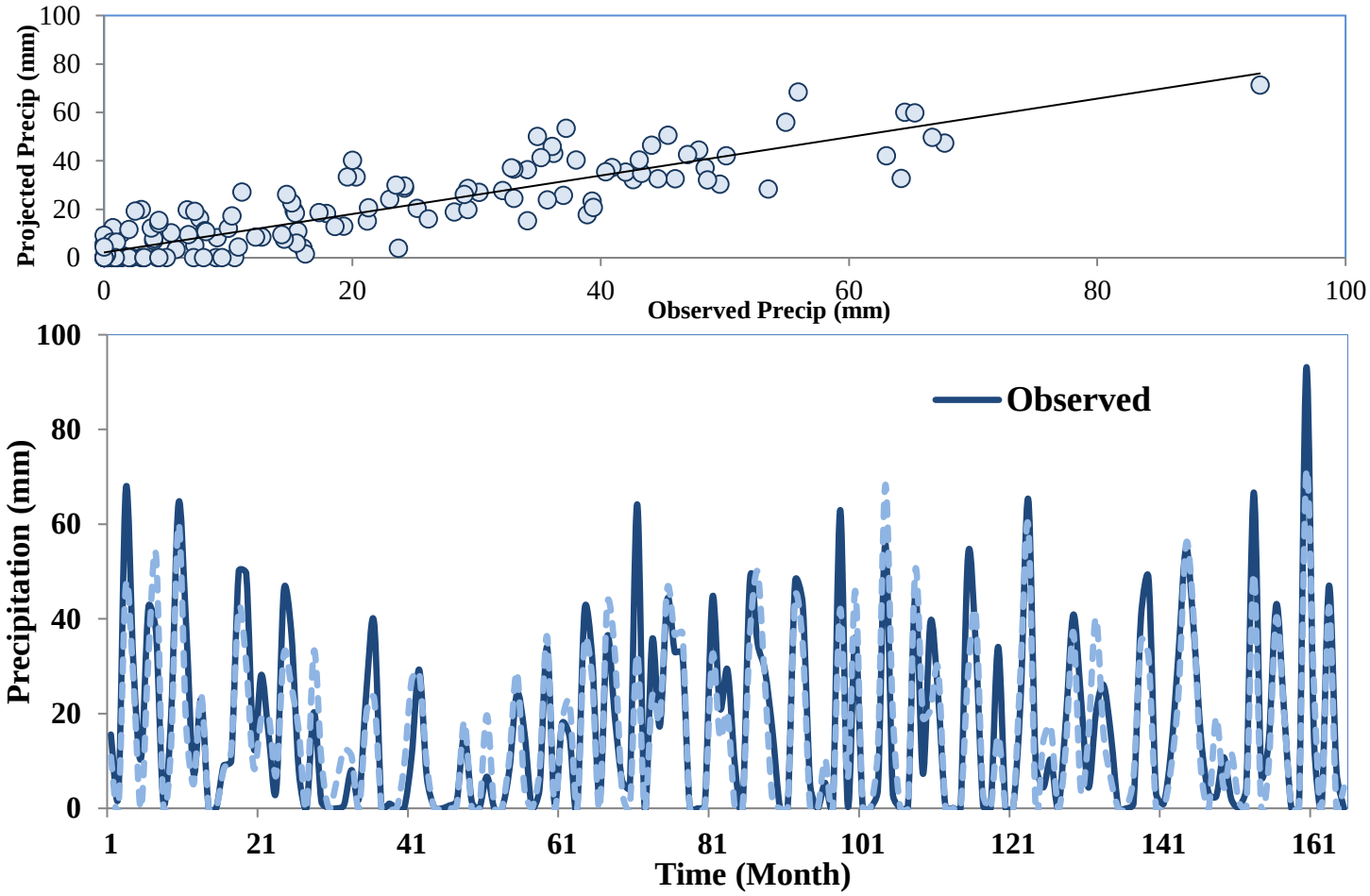

Figure 2-4. Observed and predicted precipitation time series derived from combination of the Kernel Supervised PCA and the RVM method

2.5.2 Predictor Domain

There is no priori predictor domain for any region and hydro-climate variables (Spak et al., 2007). Predictor domains in terms of spatial extent and geographical location may contain different potential relevant information for the predictand. To address the concern of whether other projector domains could improve the performance accuracy of the best-selected model, the model's sensitivity to predictor domains is quantified based on the NCEP/NCAR dataset using the same downscaling procedure on the six states of projector domains illustrated in Figure 2-5. Doing so, the best-selected models (Kernel Supervised PCA and RVM) are employed on the different dimension-size of the atmospheric projectors formed based on the six predictor domain states to compare the model performances over the study area. Following the procedure used in the previous section, the optimum transformed-dimension is computed using the Kernel Supervised PCA method. The performance results are then derived based on the transformed low-dimension projectors using the RVM model. Figure 2-5 shows the results of performance accuracy in terms of the NSE coefficient for the six projector domains based on the testing dataset. The results indicate that relying on only the center host grid-cell with the same atmospheric projectors leads to the least performance accuracy. Adding the neighbor grid-cells and increasing the domain size from one to five results in better performance accuracy, with NSEs of 0.67 and 0.64 for state 2 and state 3, respectively. Compared with the other states with fewer local predictors, taking into account the nine surrounding grid-cells in state 4 improves the accuracy of downscaled time series and leads to the highest performance accuracy. Enlarging the domain size by adding more surrounding grid-cells (states 5 and state 6) results in less performance accuracy compared with state 4. The reason is that in comparison with state 4 adding more predictor from surrounding zones leads to a nonhomogeneous region in terms of effective synoptic circulation patterns. The study area is surrounded by the Alborz Mountains in the north, the Zagros Mountains in the west, and the central flat plains in the south (Figure 2-2). The high mountains form an orographic barrier and divert the northern hemisphere westerlies carrying moisture sources from the Mediterranean, Black, and Caspian Seas to the study area (Ballato et al., 2010). This blockage creates different nonhomogeneous zones in terms of climate, so that the northern parts (of the study region) are dominated with a different Mediterranean climate and dense forests, while the southern parts (central Iran) are characterized with arid climate and almost flat deserts. Including different irrelevant zones of predictors from nonhomogeneous climates in state 5 and state 6, the results of the models demonstrate that the new spatial extent of predictors contain unrepresentative synoptic scale circulation patterns influencing precipitation process in the study area.

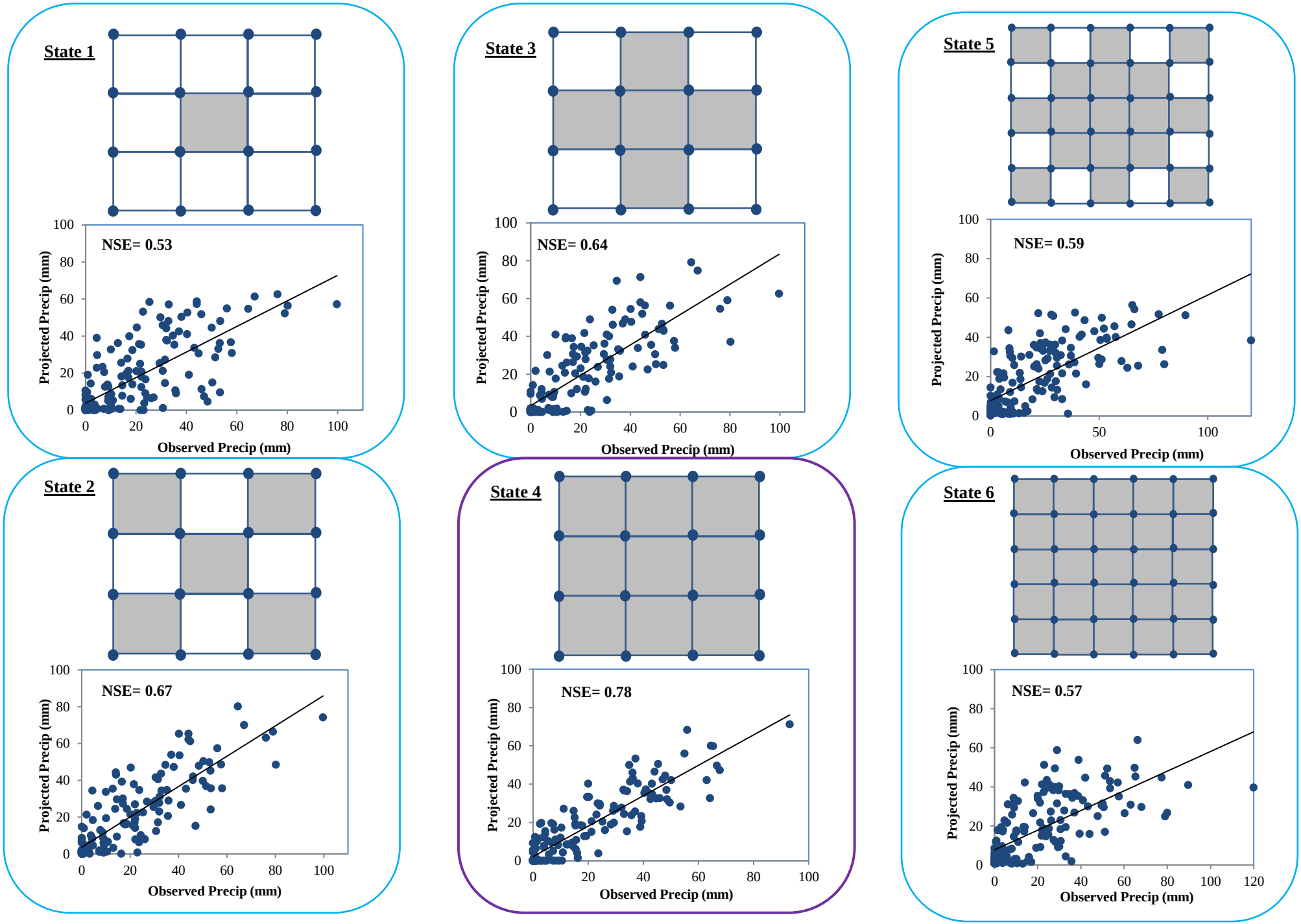

Figure 2-5. Sensitivity analysis on the predictor domains

Therefore, analyzing the sensitivities of the predictor domains demonstrates that including atmospheric subspaces from nine-surrounding-grid cells is much more informative, and the projector interactions of the subspaces play an important role in enhancing the modelling performance. Furthermore, the results emphasize that predictor domain size is an important factor in the regression statistical downscaling procedure, and the Kernel Supervised PCA method has high efficiency in capturing spatial patterns of the projector behaviours at the different spatial scales by taking into account the linkage and the dependency between the predictand and the atmospheric characteristics.

After selecting the best dimensionality reduction method and demonstrating the sensitivities and corresponding sources of uncertainty in terms of predictor sets, the best combination of the Kernel Supervised PCA and the RVM model formed based on the nine surrounding-grid-cells is employed for projecting precipitation time series for the upcoming decades.

2.5.3 Future Precipitation Projection

To project the impact of climate change on future precipitation, 15 GCMs of the CMIP5 multi-model ensemble are used under three forcing emission scenarios. After extracting the same atmospheric projectors for each model and rescaling them, different models are used as input for the best selected dimensionality reduction method (Kernel Supervised PCA). Using the same tuned Kernel Supervised PCA model in the modelling section, the derived transformed atmospheric projectors for the upcoming decades based on different scenarios (in the same reduced-dimension extracted in the modelling) are employed for precipitation projection using the best selected RVM data-mining method.

To better understand whether the supervised dimensionality reduction method acts differently from the commonly-used standard PCA method over different climate change scenarios (RCPs), the representations of precipitation are projected through the standard PCA method under three forcing scenarios as well. Figure 2-6 illustrates the results of precipitation reproduced based on the best-selected Kernel Supervised PCA and the standard PCA in the form of empirical cumulative distributions under the three RCPs scenarios. The behavior of precipitation projected through the two dimensionality methods is completely different under the three climate-change scenarios. The difference is obvious across the different exceedance probabilities, especially in the extreme high and low-magnitude observations. In Figure 2-6, the standard PCA cannot capture low magnitude observations and over-estimates the low-value observations in the lower tails, while in the upper tails, it under-estimates observations and cannot capture extreme high-magnitude events for future decades.

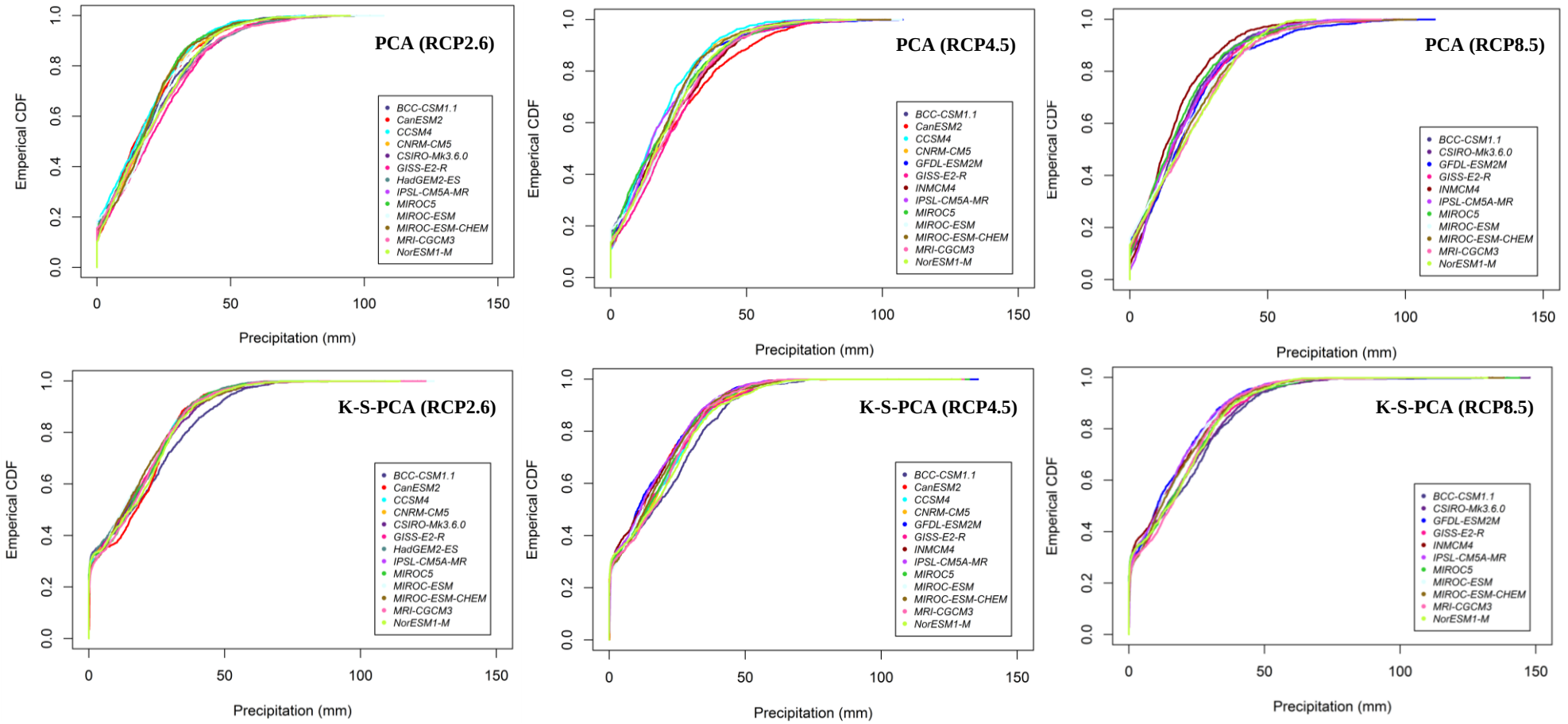

Figure 2-6. Empirical cumulative distribution of reproduced precipitation based on two kernel supervised PCA and standard-PCA models under three different forcing scenarios for the future decades

In contrast, Kernel Supervised PCA is not only able to project the majority of the dry-spells in the lower tails across the different GCMs, but also projects the rare-frequent observations in the upper tails under different forcing scenarios, quite similar to the values for the historical time period. The reason is due to exploring subspaces through orthogonal transformations (using nonlinear kernel functions) onto which the dependency (between precipitation and the atmospheric predictors) and the variance retained under projection in the Kernel Supervised PCA are maximal. Using these reduced sequences of nonlinear subspaces (manifolds) in the downscaling model leads to capturing extreme observations in all GCMs and reducing uncertainty.

Thus, applying the standard PCA as a dimensionality reduction may result in entirely different RCP projections for future time periods and is considered a main source of uncertainty in terms of projecting extreme values in the statistical downscaling. Using a supervised dimensionality reduction model leads to reducing this source of uncertainty and to the projection of extreme observations based on different GCM models under different climate change scenarios for the upcoming decades.

To better explain the differences arising from the two dimensionality reduction methods and to understand how each can influence future precipitation behavior, the linear trends of the projected precipitation using a simple linear regression are calculated based on the annual mean under the different scenarios. The difference between precipitation amount at the beginning and the end of the 21st century is calculated as an index to show the increase or reduction of precipitation over future time periods. The projection of precipitation based on CMIP5's models is provided in two time scales, near-term (2015-2040) and long-term (2015-2100), under three scenarios RCP2.6, RCP4.5, and RCP8.5 (Table 2-3).

In the 15 CMIP5 multi-model ensemble data employed in the present study, there are 13 models available in RCP2.6, 13 in RCP4.5, and 11 in RCP8.5 scenarios, respectively. The missing models in each scenario are due to the unavailability of some large-scale atmospheric variables in the models at the time of this manuscript's preparation. According to the results in Table 2-3, the precipitation linear trend fluctuates in both methods in all three scenarios for the near-term and the long-term scales. However, the majority of the models indicate different trends in terms of both the magnitude and the direction, based on the Kernel Supervised PCA and the standard-PCA under the different scenarios in both the future time periods. Although both the dimensionality reduction methods lead to precipitation reduction on average compared with the historical records (1951-2011) showing an increasing trend of 7.29 mm $(10yr)^{-1}$, the magnitude of reduction varies based on each method for different GCM models under the forcing scenarios.

Table 2-3. Linear trends for projected precipitation (mm $(10yr)^{-1}$) in near-term (2015-2040) and long-term (2015-2100) temporal scale under different climate change scenarios

	RCP2.6				**RCP4.5**				**RCP8.5**			
	Near-Term		Long-Term		Near-Term		Long-Term		Near-Term		Long-Term	
Model	PCA	S-PCA	PCA	S-PCA	PCA	S-PCA	PCA	S-PCA	PCA	S-PCA	PCA	S-PCA
BCC-CSM1.1	3.32	-8.69	-3.90	-1.07	1.89	-9.61	-0.93	-4.80	-33.75	-25.63	-23.27	-6.41
CanESM2	-12.72	-1.11	0.23	-0.07	2.64	-9.24	-0.44	-3.58	-	-	-	-
CCSM4	-1.91	0.12	1.42	-1.85	-15.77	0.58	-0.95	-0.17	-	-	-	-
CNRM-CM5	4.74	6.76	-4.22	1.38	-12.78	12.31	-5.64	0.92	-	-	-	-
CSIRO-Mk3.6.0	-15.48	-19.40	-0.87	-0.25	-	-	-	-	17.79	-2.34	0.11	-2.80
GFDL-ESM2M	-	-	-	-	-7.15	-19.98	-0.64	-6.25	13.94	4.46	-1.52	-3.90
GISS-E2-R	-10.53	-4.09	1.64	-0.82	-2.53	19.49	4.14	-1.69	3.41	3.46	3.61	-1.39
HadGEM2-ES	11.93	10.11	-1.70	2.57	-	-	-		-	-	-	-
INM-CM4	-	-	-	-	20.85	-6.03	4.39	-4.63	-4.60	1.25	-0.76	-3.80
IPSL-CM5A-MR	19.13	4.72	1.36	2.26	-18.85	-7.29	-3.30	-0.14	-0.64	7.90	0.75	-6.60
MIROC5	9.45	-3.43	0.42	-3.15	-11.35	-13.72	-0.55	-1.92	-12.16	6.49	-12.50	-5.76
MIROC-ESM	-6.09	-22.05	-0.63	-3.72	-6.09	-10.34	-0.63	-8.56	2.95	3.84	-4.35	-9.23
MIROC-ESM-CHEM	-22.31	-8.51	-0.80	-3.34	2.23	10.38	-6.21	-4.78	-2.15	-26.45	-9.65	-5.52
MRI-CGCM3	8.63	4.88	-1.06	1.80	-29.30	-1.05	-1.45	-0.74	-41.51	-2.84	-17.89	-1.48
NorESM1-M	-5.82	-2.09	-2.56	-2.25	-19.32	-12.16	3.60	-4.95	-1.65	-2.20	-13.74	-8.94
Average	-1.35	-3.29	-0.82	-0.66	-7.34	-3.59	-0.66	-3.18	-5.31	-2.92	-7.20	-5.08
Variance	124.99	79.76	3.18	4.09	147.45	114.64	9.35	7.94	238.78	104.22	65.49	10.52
No. of negative models	7/15	8/15	8/15	9/15	9/15	9/15	10/15	12/15	7/15	5/15	8/15	11/15

* It should be noted that the precipitation linear trend analysis for the historical records (1951-2011) shows an increasing trend of 7.29 mm $(10yr)^{-1}$.

A variance comparison of the magnitude of linear trends across different ensemble GCM models reveals that a difference exists between the standard-PCA and the Kernel Supervised PCA linear trend results. For the various RCP scenarios, the difference is much greater in the near time period, ranging from 124.9 to 238.78 mm $(10yr)^{-1}$ based on the PCA's results, and much less, ranging from 79.76 to 114.64 mm $(10yr)^{-1}$, based on the Kernel Supervised's ones. In contrast, the variance magnitude of linear trends derived from the two dimensionality reduction methods is less for the long-term period, varying from 3.18 to 4.09 mm $(10yr)^{-1}$ in RCP2.6, from 9.35 to 7.97 mm $(10yr)^{-1}$ in RCP4.5, and from 65.4 to 10.52 mm $(10yr)^{-1}$ in RCP8.5 based on the PCA and Kernel Supervised PCA results, respectively. However, the difference between the variances of the two methods in RCP8.5 is still significant in comparison with the other two scenarios.

Therefore, it can be concluded that in statistical downscaling the commonly used standard PCA is not only unable to project extreme precipitation values, but also leads to different trends in terms of near-term and long-term precipitation projection. Consequently, compared with the PCA method, using Kernel Supervised PCA method and extracting a sequence of principal component of the projector variables, which have maximum dependency on the predictand, can better explain projector interactions and improve future projections of precipitation in a nonlinear downscaling.

2.5.4 Seasonal projection

In some water resources applications, projecting precipitation changes in different seasons is more important than projecting the changes in annual-based temporal scale. Relying on the Kernel Supervised PCA, seasonal precipitation changes are projected at the study site based on this dimensionality reduction method. Figure 2-7 shows seasonal changes in projected precipitation based on different emission scenarios for the near-term and long-term periods. Without taking into account post-processing analyses on projected precipitation (bias corrections), all of the scenarios indicate an increase of precipitation for spring and fall, and a significant reduction in winter and summer precipitation in both future temporal scales relative to the historical time period. The mean reduction of projected precipitation in winter ranges from -26.31% under RCP8.5 in the near-term to -31.72% under RCP2.6 in the long-term compared with the historical period based on the existing GCM models. Spring precipitation is projected to increase, but not significantly. The largest dispersion of 8.76% is expected to occur in RCP8.5 in the near-term, and the least dispersion of 0.85% occurs in RCP8.5 in the long-term. Although precipitation reduction is highest in the summer, it is not significant in terms of precipitation magnitude. Consistent with that of spring, fall precipitation also tends to increase based on the ensemble averages in both near and long term periods, with larger intermodel variability than in

other seasons in different scenarios. Although different scenarios demonstrate an increase in total precipitation for some of the seasons in the study site, two other characteristics - distribution and intensity of rainfall through the seasons - may potentially be significantly impacted by climate change. It is thus important to consider them as well.

Overall, comparing the annual linear trend results with the seasonal ones based on the Kernel Supervised PCA method, it is clear that precipitation reduction in winter has an important role in the occurrence of negative annual trends in the near and long-term periods. Therefore, to better manage future near and long-term surface water resources for various purposes, especially drinking water use, authorities must be ready to mitigate adverse effects of rainfall shortage and surface water reduction under the impact of climate change.

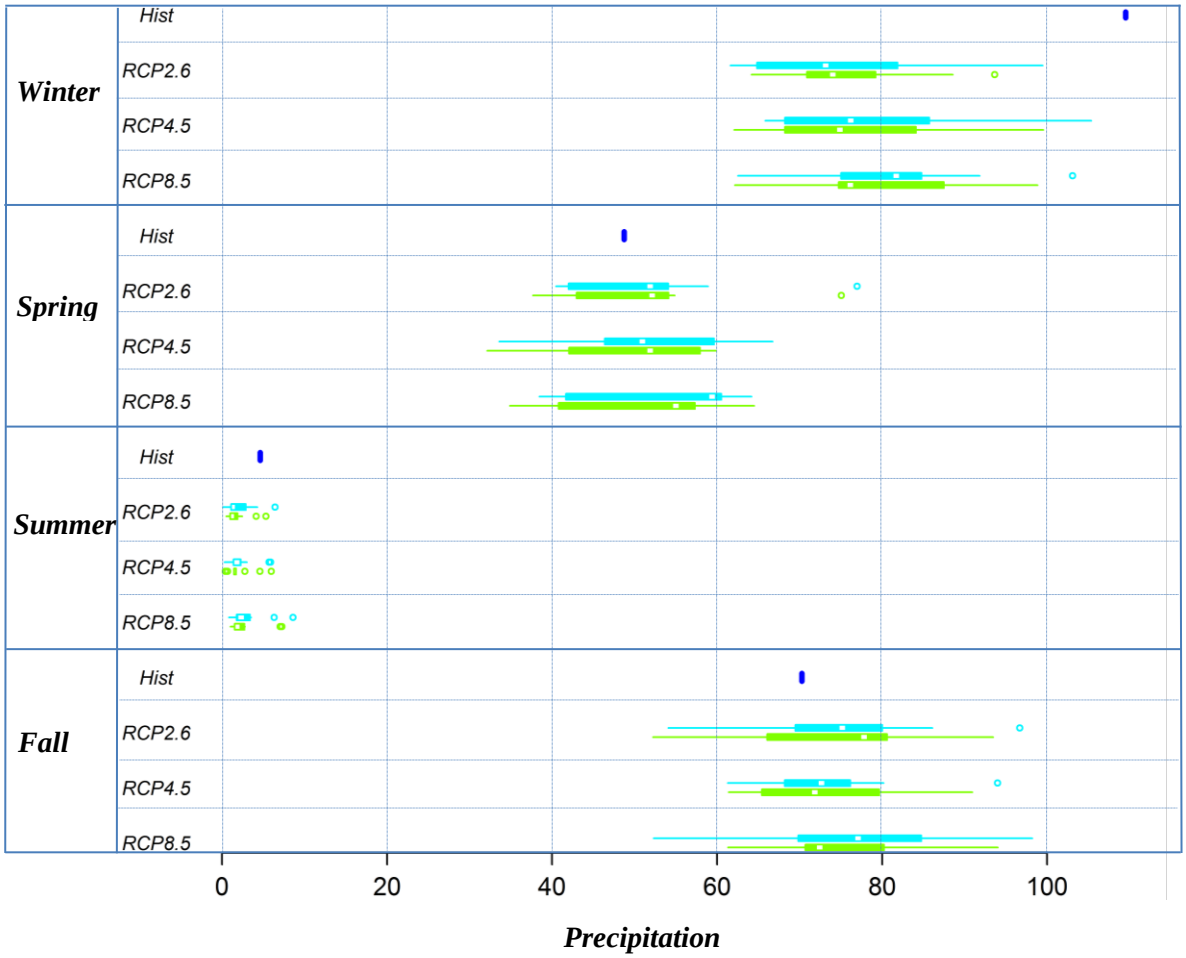

Figure 2-7. Seasonal changes of projected precipitation under different emission scenarios relative to the historical (1951-2011) mean for that season. The near-term time periods are depicted in green color and the long-term ones are in blue.

2.6 Conclusions

To improve the performance and the predictive power of the statistical downscaling processes with high-dimensional input data, this study has presented a supervised nonlinear dimensionality reduction technique–Supervised PCA–for extracting principal components in which the dependency between the response hydro-climate variable and large-scale atmospheric projectors is maximized. Due to the complexity and nonlinearity of climate associated processes, and the existence of nonlinear interdependency within atmospheric projectors, a kernelized form of supervised dimensionality reduction is able to efficiently model the nonlinear variability of the data.

The results demonstrate the high efficiency of the Supervised PCA techniques in enhancing performance accuracy of the precipitation downscaling using two machine learning methods, SVR and RVM methods, so that the Supervised PCA methods outperform all of the existing state-of-the-art dimensionality reduction techniques. The Supervised PCA method is able to capture the complex nonlinear dependency between target precipitation variable and the atmospheric projectors.

The proposed methodology can be used for other hydro-climate variables and also other regression-based statistical downscaling processes to improve the projection accuracy of target hydro-climate variables in the future. Hence, the application of the presented methodology in climate change studies will result in more-accurate projections for future proactive strategies, by which decision makers will be able to develop effective and long-term policies to be adopted in response to potential future changes and to mitigate adverse consequences of severe hydro-climate processes.

Since GCM simulations of precipitation for the current climate should be consistent with observed data, future work will focus on application of newly developed analyses for bias correction of projected precipitation time series for the upcoming decades.

Chapter 3

Water Resources Climate Change Projections Using Supervised Nonlinear and Multivariate Soft Computing Techniques

This chapter is a mirror of the following published paper with the same title in Journal of Hydrology. Only minor changes are made to the paper to be consistent in the thesis format.

Sarhadi, A., D. H. Burn, F. Johnson, R. Mehrotra, and A. Sharma (2016c), Water resources climate change projections using supervised nonlinear and multivariate soft computing techniques, *Journal of Hydrology, 536,* 119-132.

Summary

Accurate projection of global warming on the future probabilistic behavior of hydro-climate variables is one of the main challenges in climate change impact assessment studies. Due to the complexity of climate-associated processes, different sources of uncertainty influence the projected behavior of hydro-climate variables in regression-based statistical downscaling procedures. The current study presents a comprehensive methodology to improve the predictive power of the procedure to provide improved future projections. It does this by minimizing the uncertainty sources arising from the biases that exist in climate model simulations. To correct the spatial and temporal biases over multiple time scales in the GCM predictands, the Multivariate Recursive Nesting Bias Correction (MRNBC) approach is proposed for the regression-based statistical downscaling. The results demonstrate that this approach significantly improves the downscaling procedure in terms of future precipitation projection.

3.1 Introduction

Bias correction has been shown to improve the quality of GCMs for use in projecting hydro-climate variables under different climate change scenarios of the future (Mehrotra and Sharma, 2012; Ojha et al., 2013). Regarding the projection step of the statistical downscaling, the accuracy of climate change simulations is influenced by the similarity in the relationship between actual atmospheric variables and observed rainfall, as compared to simulated variables and the presumed projected rainfall. This similarity is expected to be influenced by the biases that characterise the raw GCM fields. Therefore, in the statistical downscaling processes an initial

post-processing correction must be carried out on GCM outputs representing the current climate, based on the statistical characteristics of observations, to remove the difference between observed and simulated large-scale atmospheric variables. The bias correction model over a historical time period is assumed to be the same in the future and can thus be employed on future GCM simulations (Johnson and Sharma, 2015). In addition, anomalous atmospheric circulation patterns influence the hydrological cycle and large-scale atmospheric variables. Interannual and interdecadal variability in the large-scale climate modes are often not well represented in GCM simulations (Rocheta et al., 2014b), resulting in uncertainty and biases in projections of hydro-climate variables relating to the future. Thus, raw data from GCMs must also be corrected to capture the effect of low frequency variability of teleconnections on large-scale atmospheric variables (Mehrotra and Sharma, 2012).

It is therefore critical to identify the nature of these biases and develop methods to address these sources of uncertainty. Several bias correction approaches have been developed to quantify the difference between observed (or reanalysis) data and large-scale GCM-simulated variables and form the basis on which to correct biases in both current and future atmospheric GCM simulations. Commonly used bias correction procedures can be classified into two main categories. The first relies on delta change and scaling approaches, including quantile mapping, scaling, correction factor, and transfer functions (a detailed review of the various methods can be found in Johnson and Sharma (2012) and Fowler et al. (2007)). All the methods in this category can be applied for post-processing either on GCM variables or outputs of downscaling models. Their main drawback is that they only take into account biases in the distribution of GCM simulations rather than biases in the representation of persistence and variability in simulations. Current climate variability is thus assumed to remain the same in the future. The second category involves approaches relying on statistical bias correction. Simple techniques in this category such as Monthly Bias Correction (MBC) (Ojha et al., 2013) correct only systematic biases in the mean and variance of GCM-simulated variables or output of downscaled processes in an independent time scale, ignoring the influence of regional and global teleconnection signals. However, the impact of teleconnections on hydro-climate variable behaviour in large scales makes it important to properly represent the interannual and interdecadal fluctuation of climate in the raw GCM outputs. To do so, Johnson and Sharma (2012) developed a bias correction methodology by adding lag-1 correlation to the procedure to correct the representation of low frequency variability between GCM simulations and observed data. The approach corrects the distributional and persistence GCM biases from fine to progressively longer time series and is called Nested Bias Correction (NBC). An extension of NBC was proposed by Mehrotra and Sharma (2012) to

enhance the representation of variability at multiple time series by reducing biases through repeating the nesting process several times (Recursive Nesting Bias Correction, RNBC method).

One of the criticisms of bias correction is that the statistical corrections do not maintain the physical relationships between different climate variables (Ehret et al., 2012; Haerter et al., 2011; Rocheta et al., 2014a). To overcome this problem Mehrotra and Sharma (2015) developed a bias correction method that can consider multiple variables and correct the cross correlations between them over a range of time scales. The Multivariate Recursive Nesting Bias Correction (MRNBC) extends the previous nesting bias correction approaches (Johnson and Sharma, 2012) and has been shown to be effective at correcting predictors for statistical downscaling leading to improved downscaled simulations. An alternative implementation could include using multiple locations rather than multiple variables in statistical downscaling to correct spatial as well as temporal dependence in the GCM simulations.

Reducing different sources of uncertainty is crucial in statistical downscaling as it enhances the quality of the hydro-climate variable projections. Consequently, these accurate projections help hydrological and water resources studies better assess the impact of climate change on the availability and allocation of water resources for various sectors, especially drinking water supply. While the uncertainty sources, including the complex and nonlinear relationship between large-scale atmospheric processes and hydro-climate variables are discussed in the previous chapter, the present chapter focuses on the multivariate bias correction methods to address the uncertainty arising from GCM simulations. Figure 3-1 depicts a flowchart of the applied procedures and their relationships in the present study.

The rest of the paper is organized as follows: Section 3.2 explains the mathematical background of the methodologies used in the regression-based statistical downscaling, namely bias correction of multivariate atmospheric projectors. The study is completed with the presentation of the results and discussion on the bias correction findings in Section 3.3. The credibility of the statistical downscaling model under non-stationary conditions is also examined in the same section. The conclusions are given in Section 3.4.

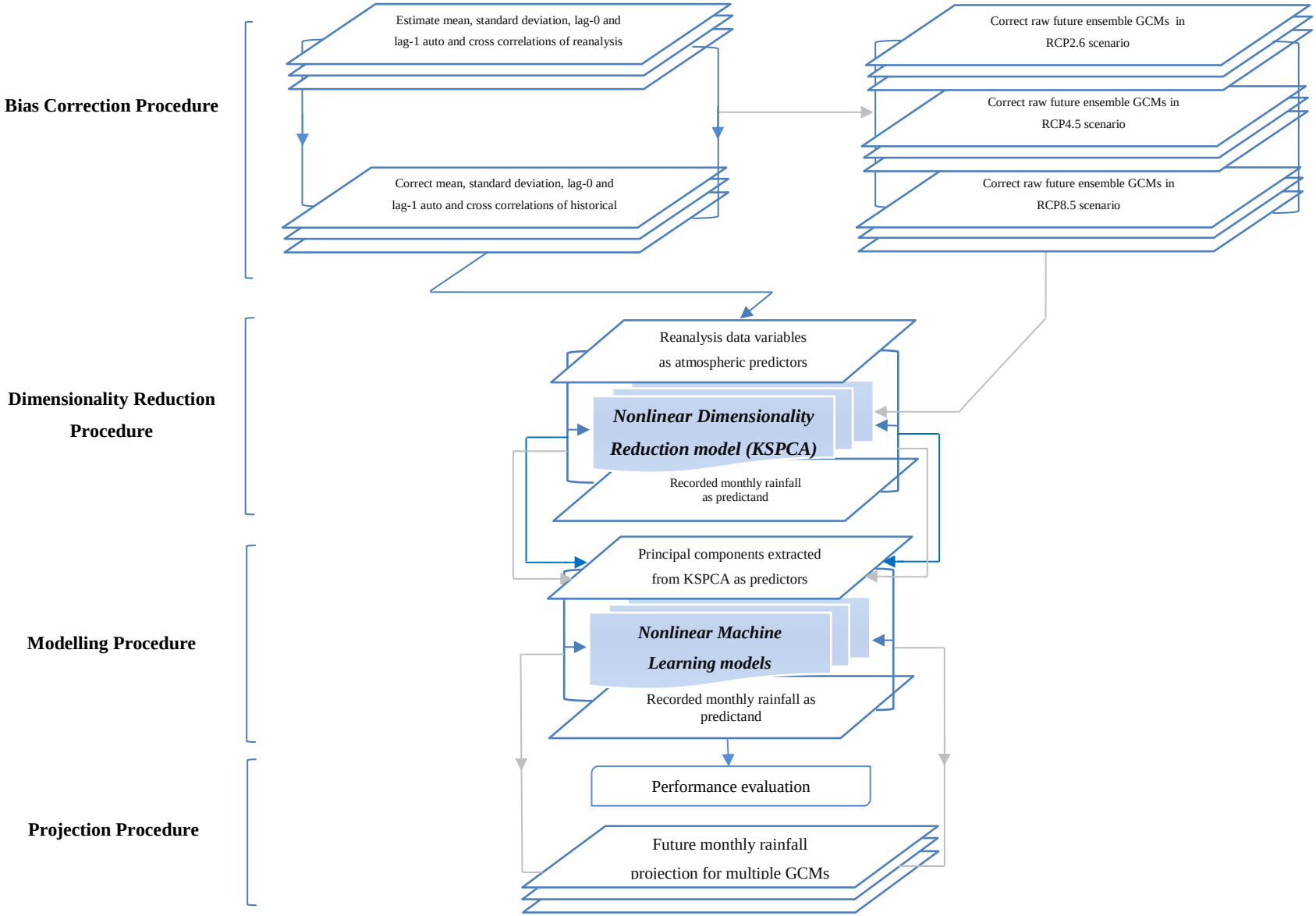

Figure 3-1. Schematic flowchart of the methodology

3.2 Methodology

3.2.1 Bias correction

A brief description of the logic of the multivariate bias correction is provided with readers referred to Mehrotra and Sharma (2015) for the full derivation. The MRNBC is based on a Multivariate Autoregressive order 1 model (MAR1) (Salas, 1980) that is used to represent both the observed data and the GCM simulations. The general idea is that for all time scales of interest the GCM simulations are nested into the observed time series. In this case the observed data are the chosen atmospheric predictors from the reanalysis data set as described in Chapter 2. To achieve the nesting, both time series are standardized to have zero mean and standard deviation of one. Then the lag one autocorrelations and lag one and lag zero cross correlations in the GCM simulations can be corrected to match the observed correlations in time and space. Although this study uses only an MAR1 model, the possibility of correlations in higher order lags can also be checked (Molina et al., 2013).

Let $\mathbf{X}$ be a p x n matrix of p predictor variables with n time steps at a single location. $\mathbf{X}^{h}$ is used to denote the observations and $\mathbf{X}^{\mathbf{m}}$ the GCM variables. For the monthly correction, the parameters are allowed to vary seasonally so for month i, the data to be corrected is $\mathbf{X}^{\mathbf{m}}_{\mathbf{i}}$ for all years of data. The data are first standardized to form a periodic time series $\breve{\mathbf{X}}_i^m$ and $\breve{\mathbf{X}}_i^h$ for the observations.

In general the MAR1 model describes each data set as:

$$\breve{\mathbf{X}}_i^h = \mathbf{C}\breve{\mathbf{X}}_{i-1}^h + \mathbf{D}\varepsilon_i \text{ and } \breve{\mathbf{X}}_i^m = \mathbf{E}\breve{\mathbf{X}}_{i-1}^m + \mathbf{F}\varepsilon_i \quad (3.1)$$

where $\mathbf{C}$ and $\mathbf{D}$ are the lag zero and lag one auto and cross correlations from the observations, $\mathbf{E}$ and $\mathbf{F}$ are calculated in the same way for the standardized GCM simulations and ε_i is a vector of p independent random variates having zero mean and the identity covariance matrix.

To obtain the corrected data for any particular year t the model for correction is:

$$\mathbf{X}'^m_{t,i} = \mathbf{C}_i\mathbf{X}'^m_{t,i-1} + \mathbf{D}_i\mathbf{F}_i^{-1}\breve{\mathbf{X}}^m_{t,i} - \mathbf{D}_i\mathbf{F}_i^{-1}\mathbf{E}_i\breve{\mathbf{X}}^m_{t,i-1} \quad (3.2)$$

where $\mathbf{X}'^m_{t,i-1}$ is the value in the corrected time series from the previous month in year t. After correction the time series $\mathbf{X}'^m$ is rescaled by the observed mean and standard deviation to give the final corrected time series $\overline{\mathbf{X}}^m$. Details on solving for the matrices $\mathbf{C}$, $\mathbf{D}$, $\mathbf{E}$ and $\mathbf{F}$ are provided by Mehrotra and Sharma (2015) based on Srikanthan and Pegram (2009) and Matalas (1967).

Following the monthly corrections, the time series $\overline{\mathbf{X}}^m$ is aggregated to form a seasonal series and the periodic corrections described above are applied, now indexing over the 4 seasons rather than 12 months to give $\bar{\mathbf{S}}^m$ where **S** refers to the seasonal matrix of simulations which is *p* x *n/4* in size. Finally this time series is aggregated to an annual time series and the correlations, standard deviation and mean are corrected to form $\overline{\mathbf{A}}^m$ where **A** is the matrix of yearly data which is *p* x *n/12*.

According to Srikanthan and Pegram (2009), the corrections at each time aggregation can be applied in a single correction step as follows:

$$\overline{\mathbf{X}}^m_{i,s,t} = \left(\frac{\overline{\mathbf{X}}^m_{i,s,t}}{\mathbf{X}^m_{i,s,t}}\right)\left(\frac{\overline{\mathbf{S}}^m_{s,t}}{\mathbf{S}^m_{s,t}}\right)\left(\frac{\overline{\mathbf{A}}^m_{t}}{\overline{\mathbf{A}}^m_{t}}\right)\mathbf{X}^m_{i,s,t} \qquad (3.3)$$

There are some further details in the bias correction that ensure optimum results. A three step correction procedure is used to correct biases firstly in the mean, then the standard deviation and finally the correlations. This ensures that the future climate change signal is not affected by the bias correction. The bias corrections are applied three times in the recursive nature suggested by Mehrotra and Sharma (2012) to achieve even better performance in the bias corrected simulations. To correct the future GCM projections, the statistics from the historical period GCM simulations and the reanalysis data are applied for the corrections (Johnson and Sharma, 2012). This allows the GCM projections to evolve according to the impacts of climate change over time.

After involving the bias correction method with the developed models (dimensionality-reduction and machine-learning methods) in the previous chapter, the credibility of the combined regression-based statistical downscaling model should be validated under the impact of changing conditions (non-stationarity) arising from global warming.

3.2.2 Credibility of model under non-stationary climate

Statistical downscaling models are developed based on quantitative and empirical relations between a target variable and predictors over the historical period. The relations are criticized owing to remaining unaltered despite non-stationary changes arising from global warming in the future. It is therefore important to distinguish between stationarity of the statistical relations and the non-stationarity under global warming. The empirical relations between target hydro-climatic variable and large-scale atmospheric predictors are not expected to change over time. If the best-selected

downscaling model is, however, calibrated under non-stationary conditions, it is adjusted to the changes arising from global warming. The model will consequently be qualified to a better possibility of generalizing to future changing climate. Relying on this assumption, in the present study two design-of-experiment (DOE)-based frameworks proposed by Salvi et al. (2015) are employed to examine the credibility of the best-selected statistical downscaling model for future generalization under approximate non-stationarity. The core of the framework is based on an implicit assumption that "climate conditions in the current or future will have 'signatures' over time and space. For any specific region, future climate states and empirical relations may be assumed to have signatures in the past climate" (Salvi et al., 2015). According to this assumption, if in the future due to global warming, climate gets warmer (colder) or El-Niños become more (less) prevalent, and anthropogenic activities lead to severe radiative forcing, the climate may start to resemble the situations in the past where the similar conditions occurred due to natural variability (Salvi et al., 2015). The details of the two design-of-experiments are discussed in the following subsections.

3.2.2.1 Experiment series 1: Training period selection

The general capability of empirical relations may be validated through carefully selecting the data into the downscaling models for training phase followed by a testing phase. The first series of the DOE experiments is based on the performance evaluation of a model for the period when the condition of atmospheric predictors are different from those used in the calibration or training phase. In other words, the satisfactory performance of a model that has been trained based on a specific condition of climate is expected to be robust for a totally contrasting climate condition to a great extent. The contrasting climate conditions could be hot versus cold years, or ENSO versus non-ENSO years, and vice versa. The different experiments designed to validate the performance of the combined supervised dimensionality reduction and machine-learning models in the current study are discussed in more detail as follows:

I) Base experiment (Tr-RAN-Te-RAN)

A random selection of training and validating periods (K-fold cross-validation) is used as a scenario for the validity of the model. In this method, known also as the leave-one-out cross-validation, all observations are used for both training and validation, and each observation is used for validation exactly once. This random selection of training period ensures complex mixing of large-

scale atmospheric patterns of different climate conditions, leading to the coverage of a wide range of climate variability. This experiment is therefore treated as 'base experiment' and the results of all other experiments in series 1 are compared with this random-selection experiment. The experiment is referred to as 'Tr-RAN-Te-RAN' in the present paper.

II) Chronological order (Tr-CH-Te-CH)

In this scenario the selection of training period is conventionally carried out based on chronological order. The first 30 years of the overall time period (1951-1980) (known as 'Past') are selected for training period and the next 25 years (1981-2005) (known as 'Recent Past') are considered as validation period.

III) Hot and cold years (Tr-C-Te-H and Tr-H-Te-C)

In this experiment relatively warmer/colder years from the time period 1951-2005 are identified as training set. In other words, subset of data that are considered relatively warmer years (in case of colder years as testing) or relatively colder years (in case of warmer years as testing) are selected for training the statistical model.

To identify relatively warmer/colder years, mean annual temperature data can be used for this purpose. In this method, mean annual temperatures are arranged in descending order. First X years will then be considered as relatively warmer years. The same procedure is also carried out for ascending order to select relatively colder years. In the present study to have a realistic criterion, the categorization of warmer/colder years is performed based on average monthly temperature data over the summer months. As the summer months (Jun, July, and Aug) form relatively high-temperature periods compared with other months of year, they can be considered as a better indicator for identification of relatively warmer/colder years.

IV) ENSO and non-ESNO years (Tr-EN-Te-nonEN and Tr-nonEN-Te-EN)

El Niño-Southern Oscillation (ENSO) is an irregularly periodical variation in Sea Surface Temperature (SST) in the equatorial Pacific Ocean having remote influence on global climate systems (Langenbrunner and Neelin, 2013). Different studies (Modarres and Ouarda, 2014; Nazemosadat and Cordery, 2000; Roghani et al., 2015) demonstrate the influence of El Niño (warming) and La Niña (cooling) phases on precipitation behavior in different parts of Iran including the study area. It is

likely that the frequency and the magnitude of El Niño influences may increase by more emission of greenhouse gases in the future. Another experiment set of the first series of DOE is hence formed by the selection of ENSO/nonENSO occurrence years as training period. The list of El Niño and non-El Niño years is obtained from Salvi et al. (2015). In this set of experiments, Tr-nonEN-Te-EN represents the scenario in which non-El Niño years are selected from the time period (1951-2005) as training period. Conversely, Tr-EN-Te-nonEN represents selection of El Niño years from the overall time slice as training period.

The list of selected years for calibration of the downscaling model for different set of experiments in the first series of the DOE approach is given in Table 3-1.

3.2.2.2 Experiment series 2: validation based on climate change signatures

The second series of DOE to validate the proficiency of the downscaling model in predicting changing climate is based on an indirect 'signature based' approach. In this experiment two scenarios are followed: 1) 'Pre-industrial run' corresponding to 'no anthropogenic greenhouse gas emissions', and 2) 'Future RCP8.5 run' corresponding to 'highest greenhouse gas emissions' and representing the strongest radiative forcing in the future. In this experiment, signatures of 'Pre-industrial' scenario (PI) and 'Future RCP8.5' scenario are identified (based on large-scale atmospheric predictors) in the recent past time period (1980-2005). For each individual year in the recent past time period, the Euclidean distance is computed for centroid of atmospheric predictors between that year and each year in the selected scenarios (PI and RCP8.5). Years that have atmospheric predictor close to the different scenarios, based on the results of the Euclidean distance analysis, form two different subsets. The subset close to Average Climate Conditions (ACCs) of pre-industrial is called 'ACC-PI signatures' and the subset close to average climate conditions of RCP8.5 is called 'ACC-RCP8.5'. The difference in observed monthly mean precipitation for 'ACC-PI' and 'ACC-RCP8.5' signatures represents the possible signature of greenhouse gas emissions to precipitation in future. After implementing supervised PCA method on the projectors, precipitation is projected for both 'ACC-PI' and 'ACC-RCP8.5' signatures as well. Similar difference is also computed for projected precipitation and the results are compared with observed ones. The proficiency of supervised PCA and the downscaling model in predicting the expected difference between 'ACC-PI' and 'ACC-RCP8.5' signatures indicates high credibility of model in precipitation projections under changing (non-

stationary) conditions. The procedure is carried out on different types of GCMs for the PI and RCP8.5 predictors.

Table 3-1. List of time sets selected as training period for different experiments in series 1 of DOE

Tr-CH-Te-CH	Tr-C-Te-H	Tr-H-Te-C	Tr-nonEN-Te-EN	Tr-EN-Te-nonEN
1951	1951	1964	1951	1957
1952	1952	1966	1952	1958
1953	1953	1973	1953	1965
1954	1954	1975	1954	1966
1955	1955	1976	1955	1968
1956	1956	1977	1956	1969
1957	1957	1980	1959	1972
1958	1958	1983	1960	1973
1959	1959	1984	1961	1982
1960	1960	1985	1962	1983
1961	1961	1987	1963	1986
1962	1962	1989	1964	1987
1963	1963	1990	1967	1991
1964	1965	1994	1970	1992
1965	1967	1995	1971	1994
1966	1968	1997	1974	1995
1967	1969	1998	1975	1997
1968	1970	1999	1976	1998
1969	1971	2000	1977	
1970	1972	2001	1978	
1971	1974	2002	1979	
1972	1978	2003	1980	
1973	1979	2004	1981	
1974	1981	2005	1984	
1975	1982	2006	1985	
1976	1986	2007	1988	
1977	1988	2008	1989	
1978	1991	2009	1990	
1979	1992	2010	1993	
1980	1993	2011	1996	
	1996		2000	
			2001	
			2002	
			2003	
			2004	
			2005	

3.2.3 Projection for a future climate

After correcting biases and errors in the large-scale atmospheric predictors, and also examining the credibility of the combined statistical downscaling model, the next phase is to project the accurate behavior of the target variable for future climate simulations.

Therefore, in the procedure, the simulated GCMs for different climate change scenarios are first corrected using the MRNBC method in the preprocessing step of downscaling. The bias corrected atmospheric predictors are subsequently imported into the supervised dimensionality reduction model (Kernel Supervised PCA) developed and discussed in the previous chapter to generate principal components. Consequently, the principal components are substituted in the best-selected machine-learning method (RVM) to downscale the target variable for long term projection. The complete downscaling procedure is illustrated in Figure 3-1.

3.3 Results and discussion

3.3.1 Bias correction

To correct the biases in GCMs of the multi-model ensemble, NCEP/NCAR-based atmospheric projectors are used as the bench mark. The bias corrected results are presented in Table 3-2 where it is clear that the MRNBC has led to substantial improvements in the representation of the statistics of each of the predictors compared to the raw GCM simulations for the current climate. Due to space limitations, results are provided for a single GCM (BCC-CSM1-1) but the performance of the bias correction is similar for all GCMs.

Table 3-2. Root mean square error (RMSE) in estimates of annual statistics from GCM simulations compared to NCEP/NCAR estimates. RMSE calculated across 9 grid cells for BCC-CSM1-1 GCM.

Statistic	GCM case	AIR	RHUM	SHUM	SLP	TMAX	TMIN	HGT3	PRECFLUX
Annual Mean	Raw	2.83	12.05	4.3	3.69	2.69	4	17.68	5.6
	MRNBC	0.01	0.17	0.01	0.03	0.02	0.03	0.22	0.09
Annual Standard Deviation	Raw	0.11	1.23	0.38	0.7	0.21	0.3	1.76	0.41
	MRNBC	0.02	0.49	0.06	0.24	0.08	0.1	0.77	0.10
2 year Standard Deviation	Raw	0.11	1.42	0.38	0.86	0.23	0.31	2.75	0.45
	MRNBC	0.02	0.44	0.06	0.2	0.06	0.08	0.43	0.09

Figures 3-2, 3-3 and 3.4 show the performance of the bias correction across all GCMs, grid cells and, in the case of the monthly level statistics, all 12 months. Again it is clear that the bias correction leads to substantial improvements in all three statistics (monthly mean, monthly standard deviation, and annual standard deviation) for the current climate. The observed monthly means (and therefore seasonal and annual means) are almost exactly reproduced. The variance and persistence (standard deviation at the monthly and annual level) also show good improvements although there are some remaining biases compared to the mean corrections, for example the positive bias in all models at all

locations for Sea Level Pressure variance. This is because the corrections are applied in the multivariate setting so it is not possible to correct each variable perfectly as well as correcting the inter-variable relationship. Larger reductions in bias could be expected if the corrections were applied separately for each variable but this would not preserve the physical relationship between variables, which is important as they form the inputs to the downscaling models.

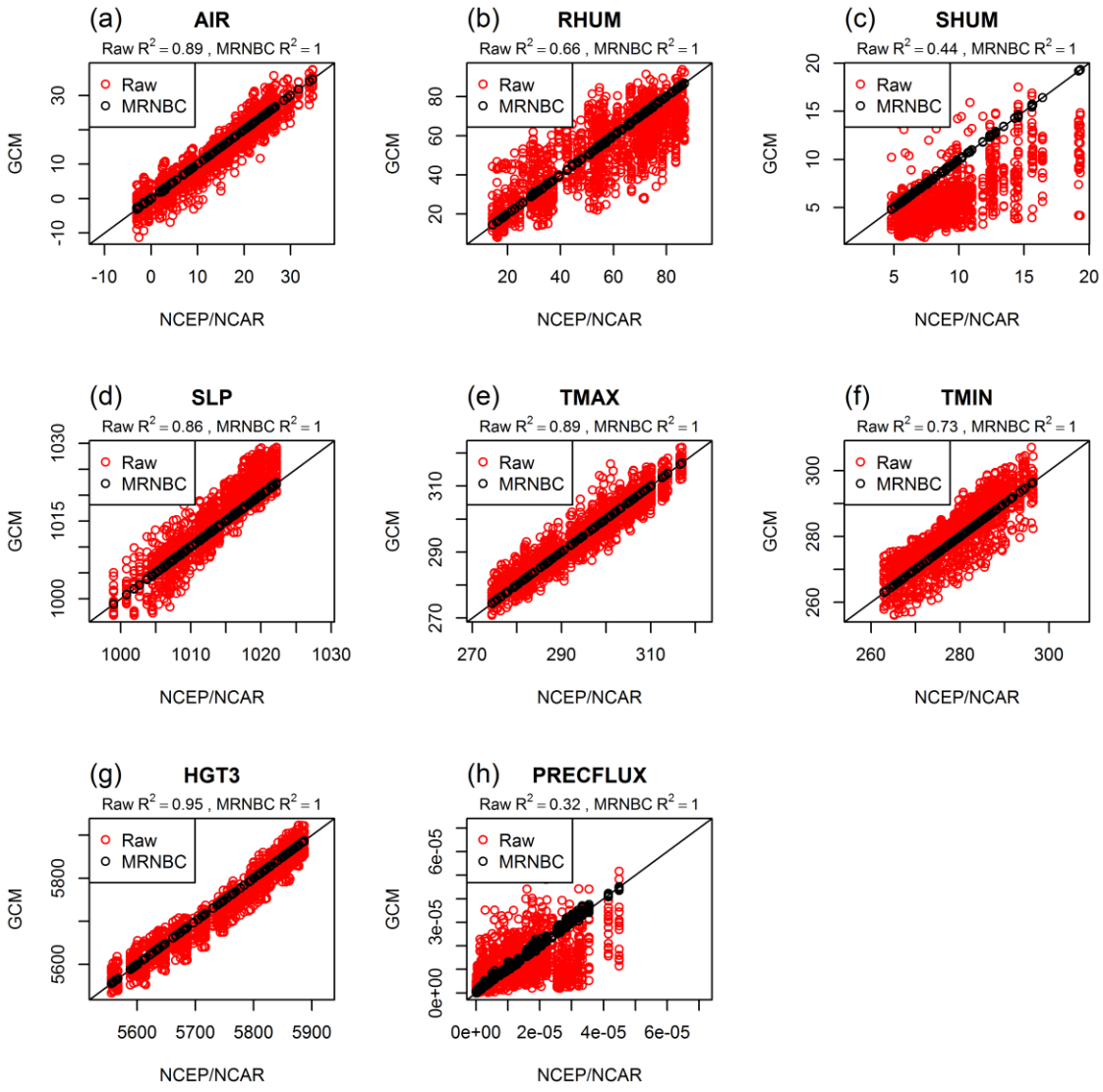

Figure 3-2 Monthly mean values for each predictor variable for all GCMs and all grid locations for raw and bias corrected GCM simulations. Each plot contains 1620 points representing 15 GCMs, 9 grid locations and 12 months. R^2 values are provided for both cases below the title for each panel.

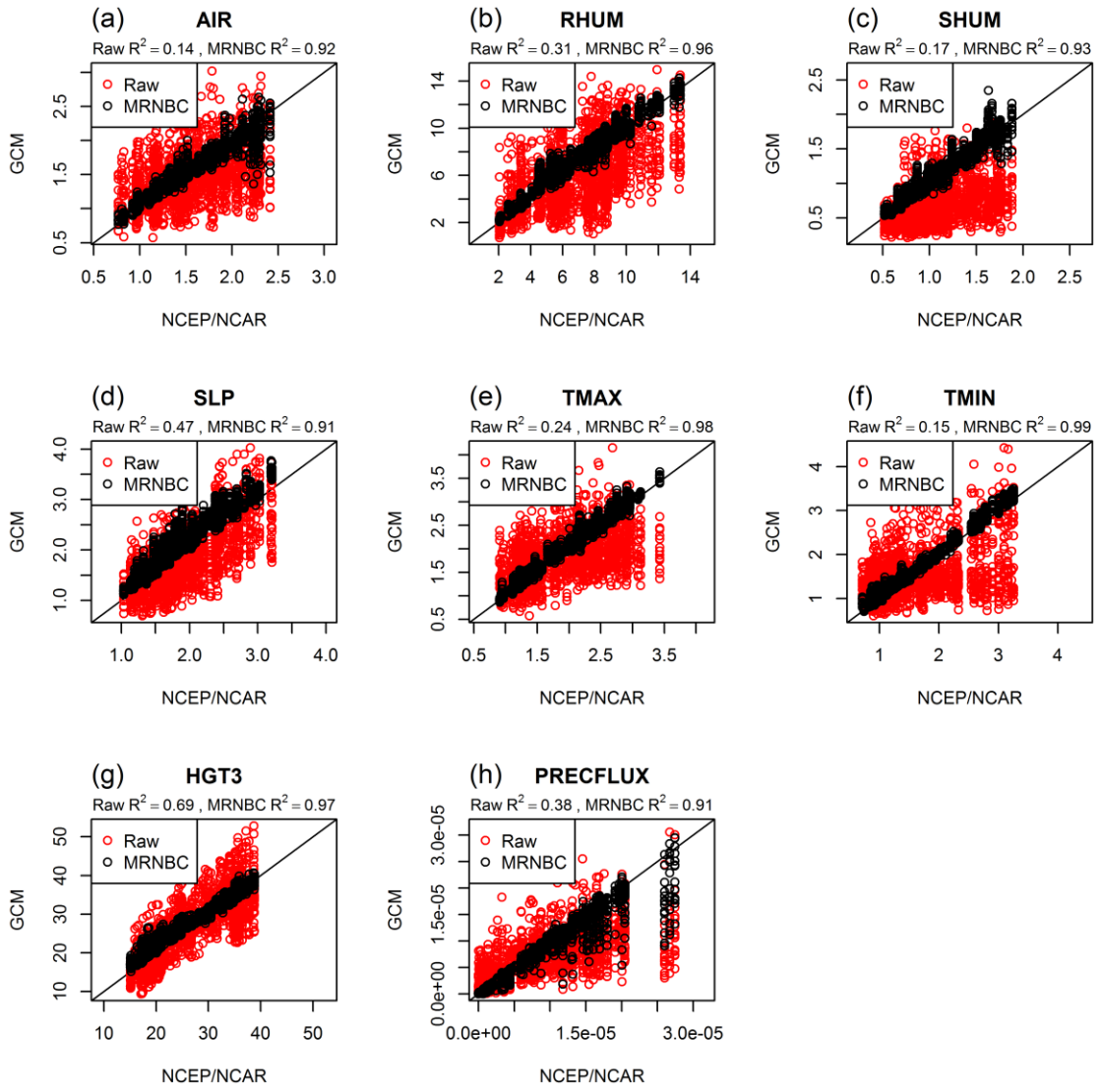

Figure 3-3 Monthly standard deviation values for each predictor variable for all GCMs and all grid locations for raw and bias corrected GCM simulations. Each plot contains 1620 points representing 15 GCMs, 9 grid locations and 12 months. R^2 values are provided for both cases below the title for each panel.

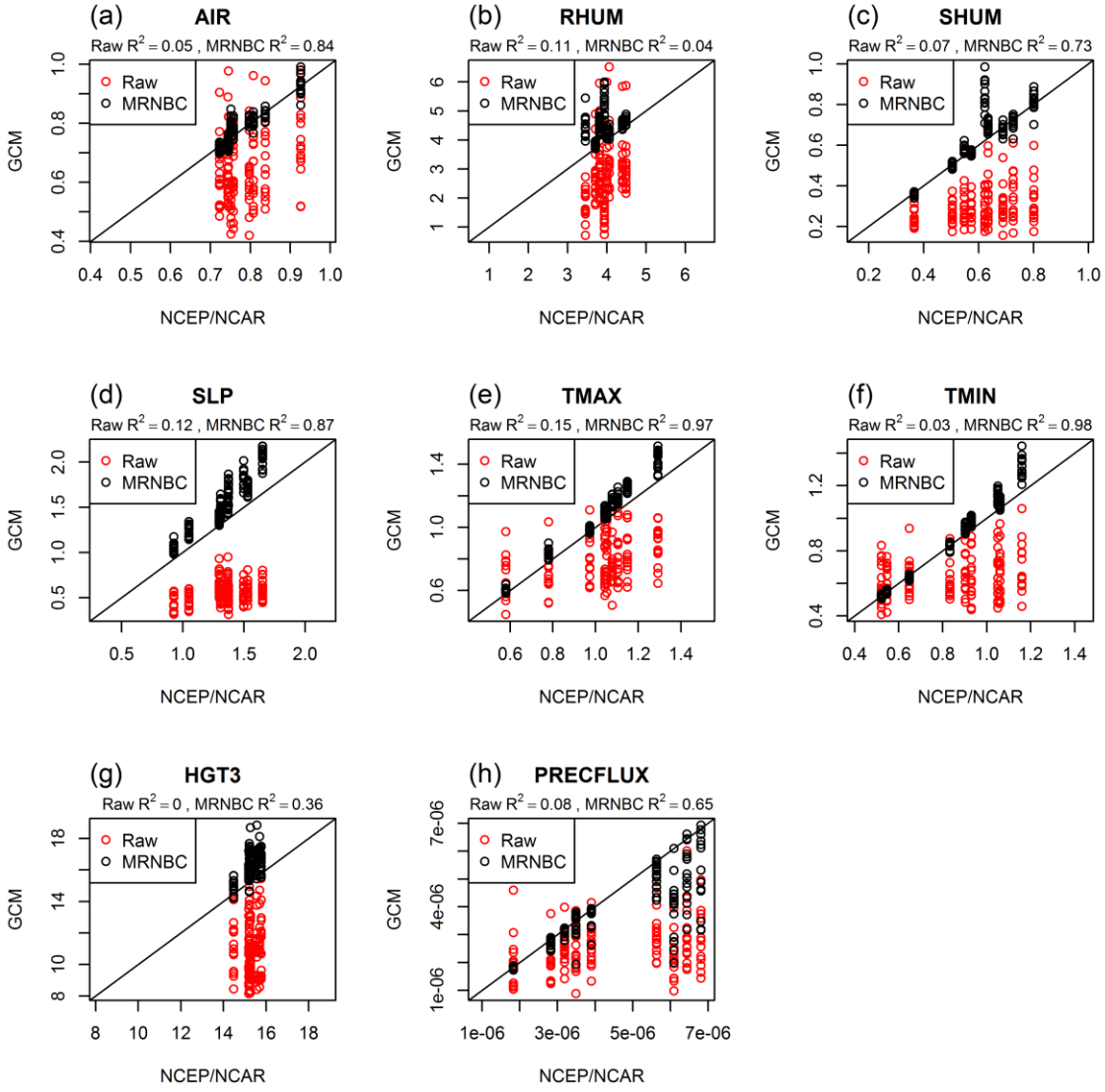

Figure 3-4 Annual standard deviation values for each predictor variable for all GCMs and all grid locations for raw and bias corrected GCM simulations. Each plot contains 135 points representing 15 GCMs and 9 grid locations. R^2 values are provided for both cases below the title for each panel.

3.3.2 Historical precipitation representation in GCMs

In this section, to assess the impact of the bias corrections on each GCM-based input atmospheric projector of the downscaling model, the representations of precipitation downscaled with different ensemble GCM models are extracted for the historical period and compared with observed precipitation during the same time period (1951-2005).

Doing so, the same raw atmospheric projectors used in the modelling step, and the bias-corrected ones derived from the previous section for each GCM model, are used as input to the best selected dimensionality reduction method from the previous chapter (Kernel Supervised PCA). Using the same tuned parameters derived in the modelling step (Chapter 2) for the Kernel Supervised PCA, low dimensional projectors of the both raw and corrected historical atmospheric projectors are retained. The derived transformed projectors (in the same reduced-dimension as the modelling section, Z=10) for CMIP5 GCM models are imported to the best selected machine-learning model (RVM) for probabilistic precipitation projection of the multiple-GCM-models for the historical time period. The results of reproduced precipitations from both bias-corrected and raw GCM models are compared against observed precipitation for the same time period, in the form of the empirical cumulative distributions in Figure 3-5. As illustrated in Figure 3-5 (a), a significant bias exists between observed and projected precipitation for the raw GCM models across the different exceedance probabilities, especially rare high-magnitude observations. This error, related to variability and persistence biases in atmospheric projectors, is significantly reduced for the corrected multiple-GCM-derived precipitation through using the MRNBC bias correction model. As current precipitation variability in the GCMs should be the same as that in the observed data, Figure 3-5 (b) depicts that all the GCM-derived projected precipitations follow similar distributional behavior and show a good fit with observed precipitation. The MRNBC technique in the bias correction procedure is thus able to remove the difference between observed and the raw simulated multiple-GCMs through addressing variability and biases in serial and cross dependence of large-scale atmospheric projectors, thereby enhancing the quality of GCM outputs. Accordingly, relying on the MRNBC model is expected to improve the performance of precipitation projection under different climate change scenarios for the upcoming decades.

3.3.3 Performance evaluation under non-stationary conditions

To examine the credibility of the downscaling model under non-stationary conditions arising from climate change, the two DOE experiment series (described in section 3.3) are executed on the best selected model (K-S-PCA and RVM). The results of each experiment series are discussed in the following sections.

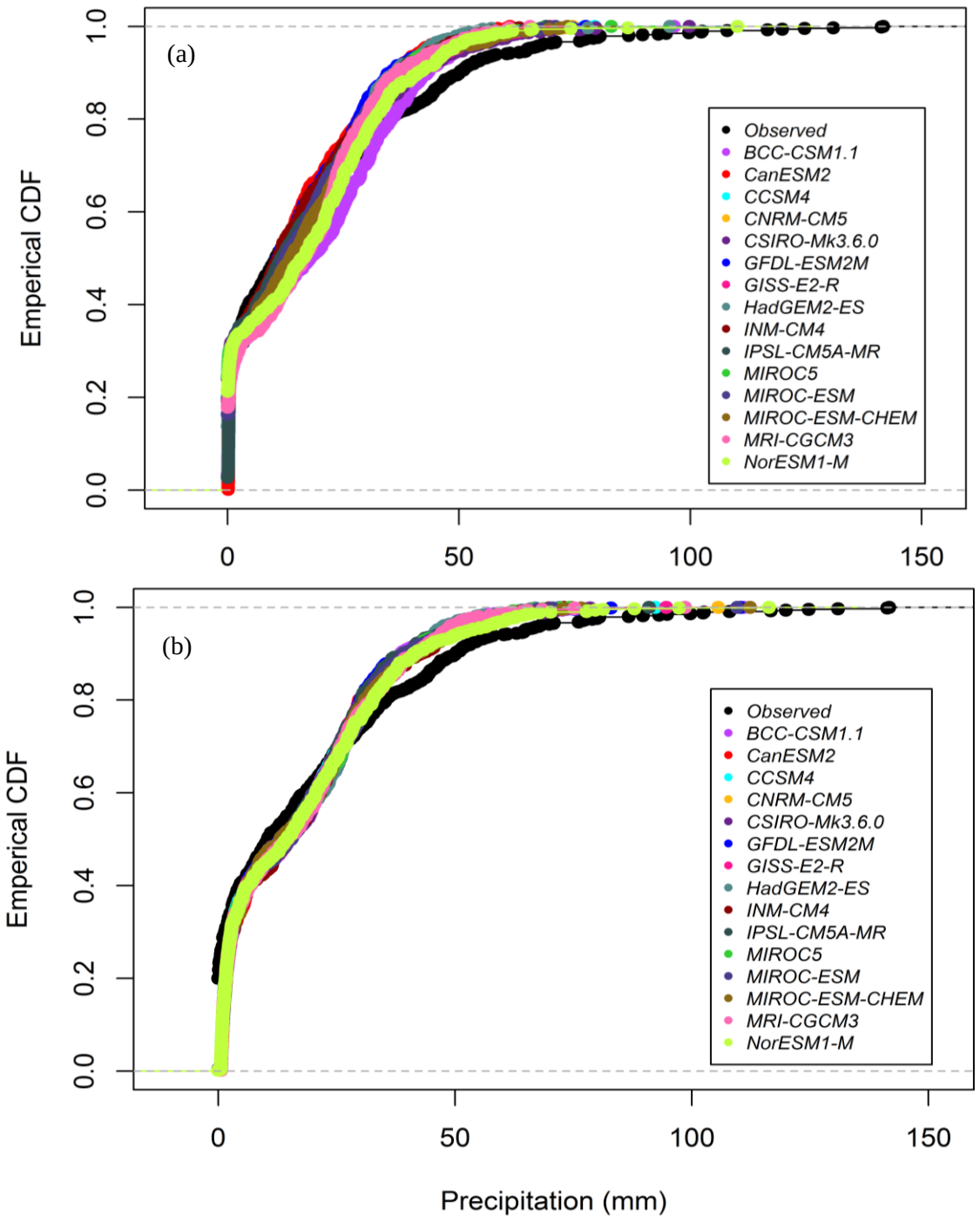

Figure 3-5. Empirical cumulative distribution functions of reproduced precipitation from a) raw-multiple-GCM models, and b) bias-corrected multiple-GCM models for the historical time period (1951-2005) against observed precipitation in the same time period.

3.3.3.1 Training period-selection-based approach (series 1)

In this series, the best tuned statistical downscaling model consisting of the Kernel Supervised PCA and the RVM model is trained with the hypothetical scenarios taking reverse climate conditions for validation. The results of these series of experiments are given in Table 3-3, where the model is trained with cold years and validated for hot years (Tr-C-Te-H), trained with non-El-Niño years and validated for El-Niño years (Tr-nonEN-Te-EN), and also dramatically opposite climate conditions (Te-H-Te-C and Tr-EN-Te-nonEN) along with chronological order (Tr-CH-Te-CH). The small magnitude of RMSE in Table 3-3 reveals that the best selected downscaling model performs satisfactorily under reverse changing climates. The difference between RMSE of the Tr-RAN-Te-RAN (as the base experiment) and RMSE of the other experiments in this DOE series is also small, which indicates high performance accuracy of the model for the conditions defined in each experiment. Figure 3-6 also illustrates observed and predicted precipitation time series derived for the validation time period in each experiment. The graphs depict a good agreement between observed and predicted precipitation time series through the model under different changing climates. It should be noted that the model preforms satisfactorily in terms of extreme events in all experiments as well. The results demonstrate that the combination of the developed Kernel Supervised PCA and RVM model is capable of capturing all the expected changes arising from dynamically complicated and changing climates.

Table 3-3. Performance accuracy of the best selected statistical downscaling model under the first series of DOE experiments

DOE Methods	Dimensionality Reduction Method	Machine-Learning Method	Kernel Function	RMSE	Diff*
Tr-RAN-Te-RAN	**K-S-PCA**	**RVM**	**RBF**	**1.39**	-
Tr-CH-Te-CH				3.18	1.79
Tr-C-Te-H				2.91	1.52
Tr-H-Te-C	K-S-PCA	RVM	RBF	3.93	2.54
Tr-nonEN-Te-EN				3.29	1.9
Tr-EN-Te-nonEN				1.89	0.5

Bold signifies the base experiment (Random Method).
* Difference between the RMSE of the Random Method and each DOE (series1) method.

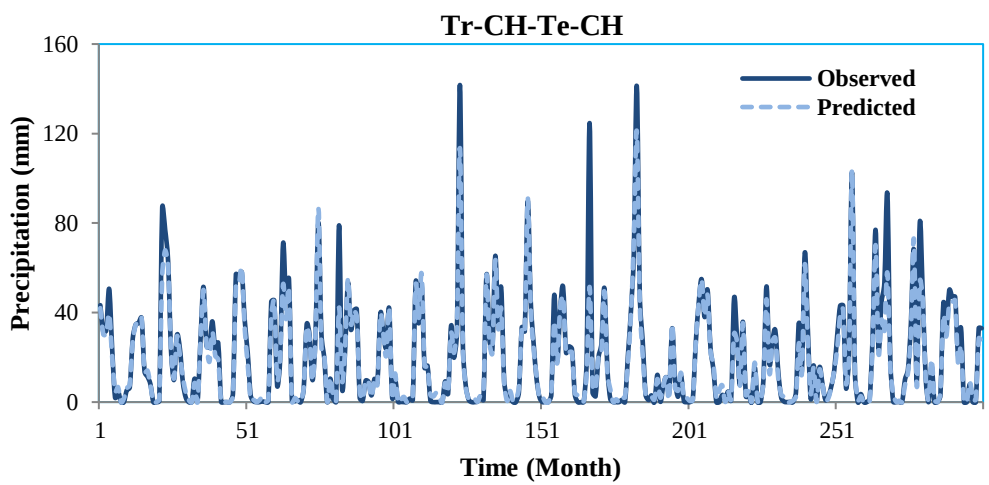

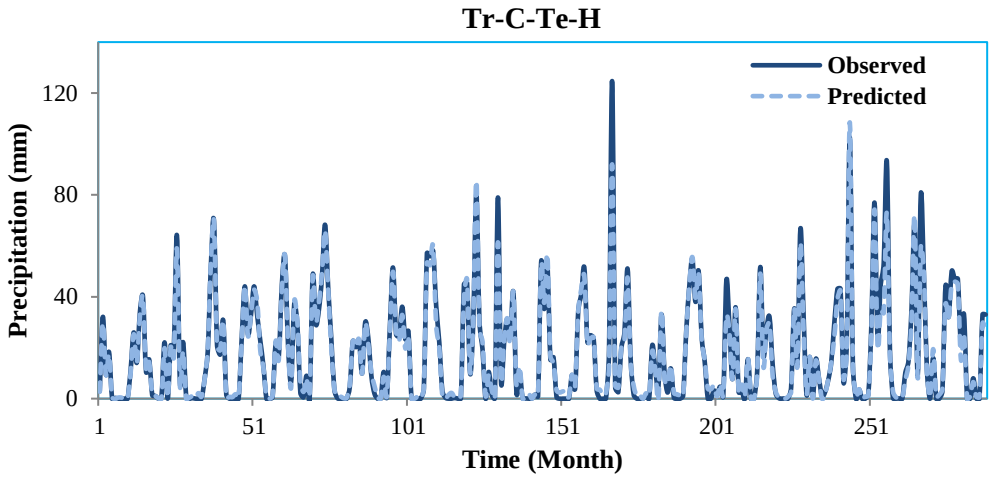

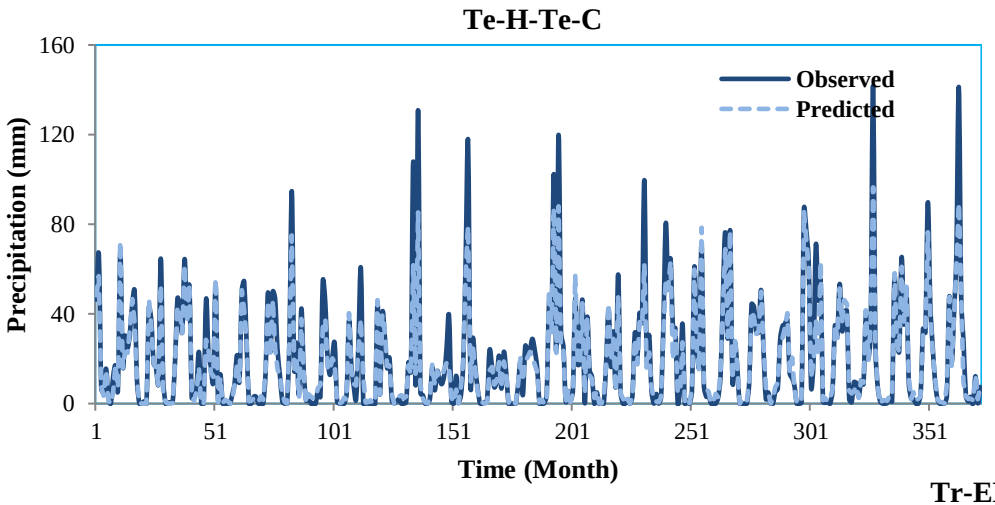

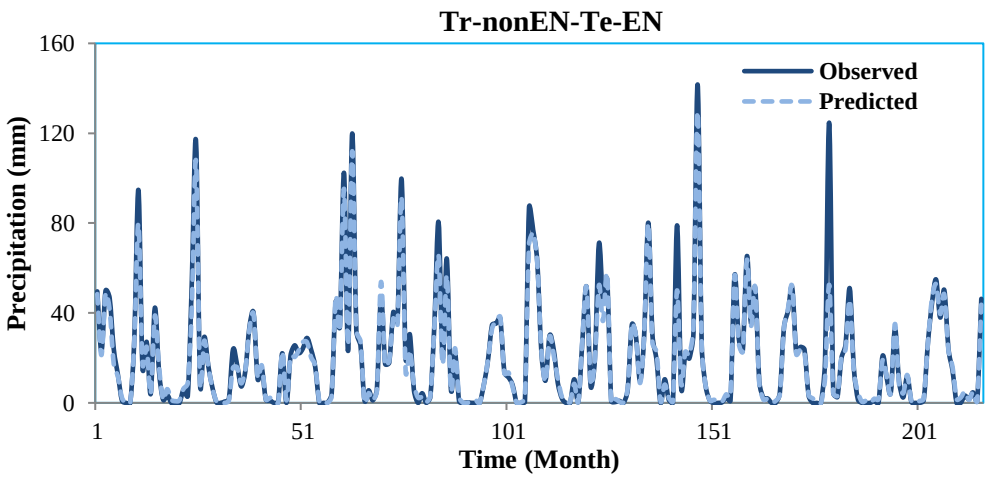

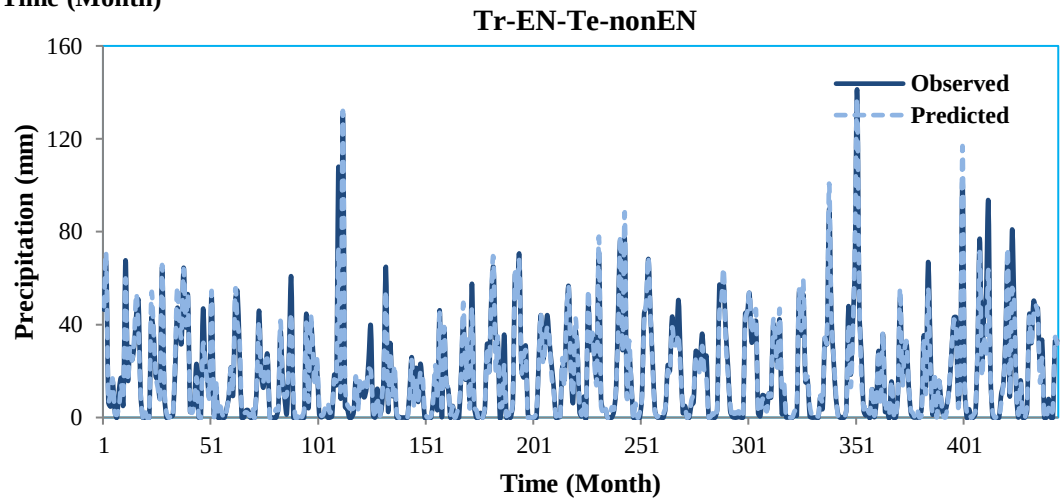

Figure 3-6. Observed and predicted precipitation time series derived from the best selected downscaling model for the validation time periods of DOE series1

3.3.3.2 Signature-based validation approach (Series 2)

The capability of the best selected downscaling model in terms of capturing the expected difference in mean precipitation owing to greenhouse gas emissions is tested with the signature-based method of the DOE approach. In the signature-based method, average climate conditions are obtained for the ACC-PI and ACC-RCP8.5 scenarios. These climate conditions should be obtained for a period of time, in which large-scale atmospheric predictors reflect significant climate change impacts from historical period to the RCP8.5 condition. For this purpose, Probability Density Functions (PDFs) of the atmospheric predictors are examined over the historical period (1981-2005) and a time period reflecting the worse condition of RCP8.5 (2070-2099). After removing systematic errors from different GCMs using the Multivariate Recursive Nesting Bias Correction (MRNBC) method, spatially averaged time series of each predictor are obtained over the 9 grid-cell domain for the PI and RCP8.5 periods. Figure 3-7 illustrates the kernel probability density functions of the atmospheric predictors for INMCM4 GCM as an example. Comparing between PDFs of the predictors simulated by the INMCM4 for historical and RCP8.5 illustrates significant changes. Applying a two sample Kolmogorov-Smirnov (K-S) test indicates that all predictors are statistically changed from historic runs to RCP8.5 at 5% significance level. The same condition exists for all GCMs in scenario RCP8.5 mentioned in Table 2-1.

The Euclidean distance analysis is then applied on multi-predictors of historical and PI/RCP8.5 scenarios as a measure of resemblance to identify associated signatures in the recent historical period (1981-2005). After identifying the signature years, the low dimension of the related atmospheric predictors are projected through the Kernel Supervised PCA. The dimension-reduced predictors are then imported to the developed RVM model to project monthly precipitation time series for the signature periods in the recent historical data. To identify the difference between mean projected and observed precipitation in each ACC-PI and ACC-RCP8.5 signature, and also the difference of mean projected precipitation between both the signatures, the non-parametric Wilcoxon test is employed. The results of the mean difference between observed and predicted precipitation in each signature and the Wilcoxon analysis are given in Table 3-4 for all the GCMs. The results demonstrate that the downscaling model performs satisfactorily in projecting precipitation for both the ACC-PI and ACC-RCP8.5 signatures, so that the difference between mean of observed and projected precipitation is significantly small under all GCMs. This demonstrates good match between the results of projected precipitation through the model and observed precipitation for each signature.

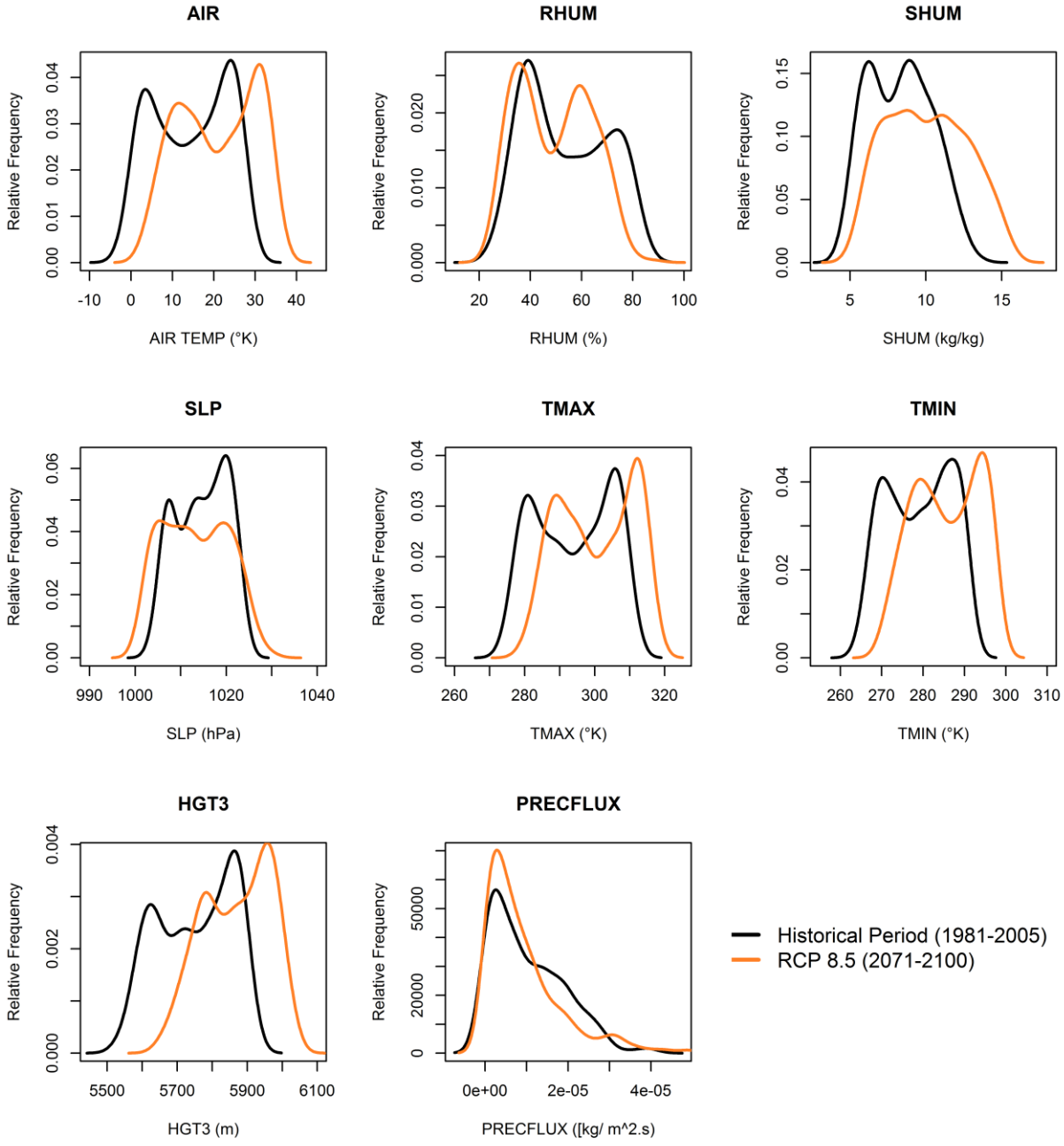

Figure 3-7. Probability density function plots for comparison of atmospheric predictors simulated for 'historic' and 'RCP8.5' scenario over the study area

Table 3-4. Difference between mean of projected and observed precipitation obtained through the downscaling model for ACC-PI and ACC-RCP8.5 signatures and associated Wilcoxon test results

GCM models	ACC-PI Signatures		ACC-RCP8.5 Signatures		(ACC-PI) - (ACC-RCP8.5)
	(Obs)-(Pred)	P-value Will-Cox	(Obs)-(Pred)	P-value Will-Cox	P-value Will-Cox
BCC-CSM1.1	2.6	0.293	0.79	0.923	**0.081**
CNRM-CM5	0.31	0.668	8.12	0.158	**0.044**
CSIRO-MK3.6	1.61	0.950	5.49	0.181	**0.003**
GFDL-ESM2M	1.193	0.394	1.68	0.944	**0.065**
GISS-E2-R	2.24	0.339	4.75	0.439	**0.041**
INM-CM4	3.28	0.611	0.856	0.918	**0.039**
IPSL-CM5A-MR	1.33	0.902	4.67	0.688	**0.052**
MIROC5	3.43	0.589	0.53	0.656	**0.048**
MIROC-ESM	0.305	0.706	0.64	0.569	0.69
MRI-CGCM3	3.51	0.402	4.73	0.280	**0.0004**
NorESM1-M	5.53	0.370	0.29	0.646	**0.064**

*Bold indicates significant at the 10% significance level

The results of the Wilcoxon test also indicate that there is not any significant difference between the mean of projected and observed precipitation in each ACC-PI and ACC-RCP8.5 signature. However, the results of the Wilcoxon test reveal that except one GCM (MIROC-ESM) the mean of projected precipitation between the ACC-PI and ACC-RCP8.5 signatures is significantly different at 10% significance level. The results prove the capability of the model in capturing changes in mean precipitation due to greenhouse gas emissions under the strongest radiative forcing scenario in the future.

Overall, the results of both the DOE experiment series demonstrate the ability of the downscaling modelling in projecting precipitation under all possible future dynamic climates. The high performance of the model in all DOE experiments therefore indicates the credibility of the downscaling model in generalizing under future non-stationary climates.

3.3.4 Future precipitation projections

To project the impact of climate change on the future precipitation behavior, 15 different GCMs of the CMIP5 multi-model ensemble are used under three different forcing emission scenarios. To project future precipitation for each GCM model under climate change scenarios, the same three operational procedures explained in the previous section for the historical dataset (i.e., bias correction, dimensionality reduction, and nonlinear machine-learning based modelling) are implemented on the

future simulated atmospheric projectors in two temporal time scales, near-term (2015-2040) and long-term (2015-2100).

To better explain the projection changes and understand how the bias-correction procedure can influence the behavior of projected precipitation in comparison with the bias-uncorrected projections in the previous chapter, a linear trend is calculated from the annual mean of projected precipitation derived from raw and bias-corrected-multi GCM models under three forcing scenarios for the two temporal scales (Table 3-5). According to the results, the precipitation trend is quite variable across the different GCMs, but the majority of the models indicate a steadily decreasing trend in the twenty-first century under each climate change scenario. This is consistent for both the raw and bias-corrected models showing that the bias correction has not affected the average direction of the climate change signal, even though the absolute magnitude of the future projections is different.

Bias correction does, however, lead to changes in the magnitude of precipitation reduction. For example, before bias correction, the average precipitation change ranges across the different scenarios from -2.92 mm$(10yr)^{-1}$ to -3.59 mm$(10yr)^{-1}$ and from -0.66 to -5.08 mm$(10yr)^{-1}$ for the near-and long-term periods respectively. After employing bias correction on all the GCMs, the precipitation reduction becomes much greater for the near-term, so that average precipitation changes range from -1.20 mm$(10yr)^{-1}$ to -11.30 mm$(10yr)^{-1}$ and for the long-term it varies from -0.87 to -3.43 mm$(10yr)^{-1}$. Interestingly, the RCP2.6 case has the largest reduction in the near-term period, which may be attributed to the availability of more GCMs for this scenario. For the two high emission scenarios the trends are still expected to be negative and of the order of around 10 mm reduction per decade to the current trend for recorded precipitation. Slightly smaller reductions in precipitation are expected over the long-term period. Generally the largest reductions are projected in the near-term under all three emission scenarios.

Overall, the results indicate a more negative trend after employing the bias-correction procedure in the statistical downscaling for both near-term (2015-2040) and long-term (2015-2100) periods. More models agree on the direction of climate change signal after applying bias correction. Similar results were found by Johnson and Sharma (2015) in the context of drought modelling where agreement across the GCMs was improved following bias correction with more consistency in the direction of the change in drought frequency.

Table 3-5. Linear trends for projected precipitation (mm $(10yr)^{-1}$) in near-term (2015-2040) and long-term (2015-2100) periods, before and after bias-correction under different climate change scenarios

	RCP2.6				RCP4.5				RCP8.5			
	Near-Term		Long-Term		Near-Term		Long-Term		Near-Term		Long-Term	
Model	Before	After	Before	After	Before	After	Before	After	Before	After	Before	After
BCC-CSM1.1	-8.69	-16.68	-1.07	-2.25	-9.61	-30.10	-4.80	-1.37	-25.63	-20.53	-6.41	-2.14
CanESM2	-1.11	-5.17	-0.07	-5.89	-9.24	-26.74	-3.58	-1.46	-	-	-	-
CCSM4	0.12	-27.40	-1.85	-1.23	0.58	-27.08	-0.17	0.59	-	-	-	-
CNRM-CM5	6.76	17.98	1.38	11.05	12.31	24.90	0.92	3.62	-	-	-	-
CSIRO-Mk3.6.0	-19.40	-32.08	-0.25	0.78	-	-	-	-	-2.34	-31.74	-2.80	-3.52
GFDL-ESM2M	-	-	-	-	-19.98	-5.68	-6.25	-2.03	4.46	-8.97	-3.90	-1.69
GISS-E2-R	-4.09	-9.89	-0.82	-0.99	19.49	40.60	-1.69	-0.34	3.46	13.85	-1.39	1.07
HadGEM2-ES	10.11	-9.89	2.57	-0.99	-	-		-	-	-	-	-
INM-CM4	-	-	-	-	-6.03	15.00	-4.63	-2.63	1.25	-21.91	-3.80	-4.82
IPSL-CM5A-MR	4.72	8.49	2.26	2.46	-7.29	23.37	-0.14	1.87	7.90	-0.61	-6.60	-5.17
MIROC5	-3.43	-17.27	-3.15	-3.63	-13.72	-12.21	-1.92	-3.13	6.49	3.54	-5.76	-3.60
MIROC-ESM	-22.05	-51.31	-3.72	-5.93	-10.34	-30.75	-8.56	-5.36	3.84	36.30	-9.23	-5.16
MIROC-ESM-CHEM	-8.51	-39.31	-3.34	-2.33	10.38	20.22	-4.78	-3.96	-26.45	-33.73	-5.52	-4.42
MRI-CGCM3	4.88	18.81	1.80	1.24	-1.05	23.66	-0.74	0.01	-2.84	6.87	-1.48	-2.38
NorESM1-M	-2.09	16.81	-2.25	-4.44	-12.16	-30.75	-4.95	-5.57	-2.20	-5.17	-8.94	-5.89
Average	-3.29	-11.30	-0.66	-0.87	-3.59	-1.20	-3.18	-1.52	-2.92	-5.65	-5.08	-3.43
No. of negative models	8/15	9/15	9/15	9/15	9/15	7/15	12/15	9/15	5/15	7/15	11/15	10/15

* It should be noted that the precipitation linear trend analysis for the historical records (1951-2011) shows an increasing trend of 7.29 mm $(10yr)^{-1}$.

Therefore, it is worth noting that the applied bias-correction model (MRNBC) has potential to improve the results of future projections through addressing biases in persistence, which may represent interannual variability arising from large-scale climate modes, and also biases across the atmospheric projectors. Thus, the bias-correction procedure constitutes an important step in the post-processing analysis of large-scale atmospheric projectors in regression-based statistical downscaling and can play a vital role in reducing the uncertainty of hydro-climate variable projections.

Due to the importance of the seasonal precipitation variation in water resources applications, seasonal behavior changes of projected precipitation are also considered under different climate change scenarios. Figure 3-8 illustrates the seasonal changes of derived average projected precipitation based on post-processed (bias-corrected) CMIP5 models under three different emission scenarios for near and long-term periods. The mean of observed precipitation is also shown in Figure 3-8 (as blue marks) for each season to compare the future projected precipitation changes derived from different scenarios to historical recorded precipitation for the study site. The results indicate a decrease of precipitation for winter, compared with the historical time period, under all of the scenarios in both near and long-term periods; less reduction is seen in the near period. The mean reduction of projected precipitation in winter ranges from -6.10% under RCP2.6 to -17.71% under the same scenario. However, over the long-term period the same reduction pattern is also projected for spring, with variation from -2.63% to -7.84% under different forcing scenarios for both time periods. The changes for summer are generally small as this is the dry season but the majority of the scenarios still show reductions in projected precipitation. In fall, no significant changes are projected based on the ensemble averages over the short-term period, even precipitation under RCP2.6 tends to increase. Unlike the short-term period, more reduction is seen in the long-term period for all the scenarios, as the fluctuation varies from -0.12% to -3.20%. Although the most precipitation reduction is projected to occur in winter and spring, other characteristics of precipitation (especially rainfall), i.e., distribution and intensity, may potentially be significantly influenced by climate change under different scenarios. Thus, in addition to studying only the amount of precipitation, it is also important that these two factors are considered and taken into account when projecting the availability of surface water resources at the study site.

According to the results, the precipitation for Tehran city is clearly projected to be influenced by climate change in future decades and the availability of surface water resources will potentially be severely decreased in the near and long-term. Therefore, water resources authorities and managers

need to provide near and long term plans for mitigating adverse consequences arising from water shortages and surface water resources reduction under the impact of climate change in future decades.

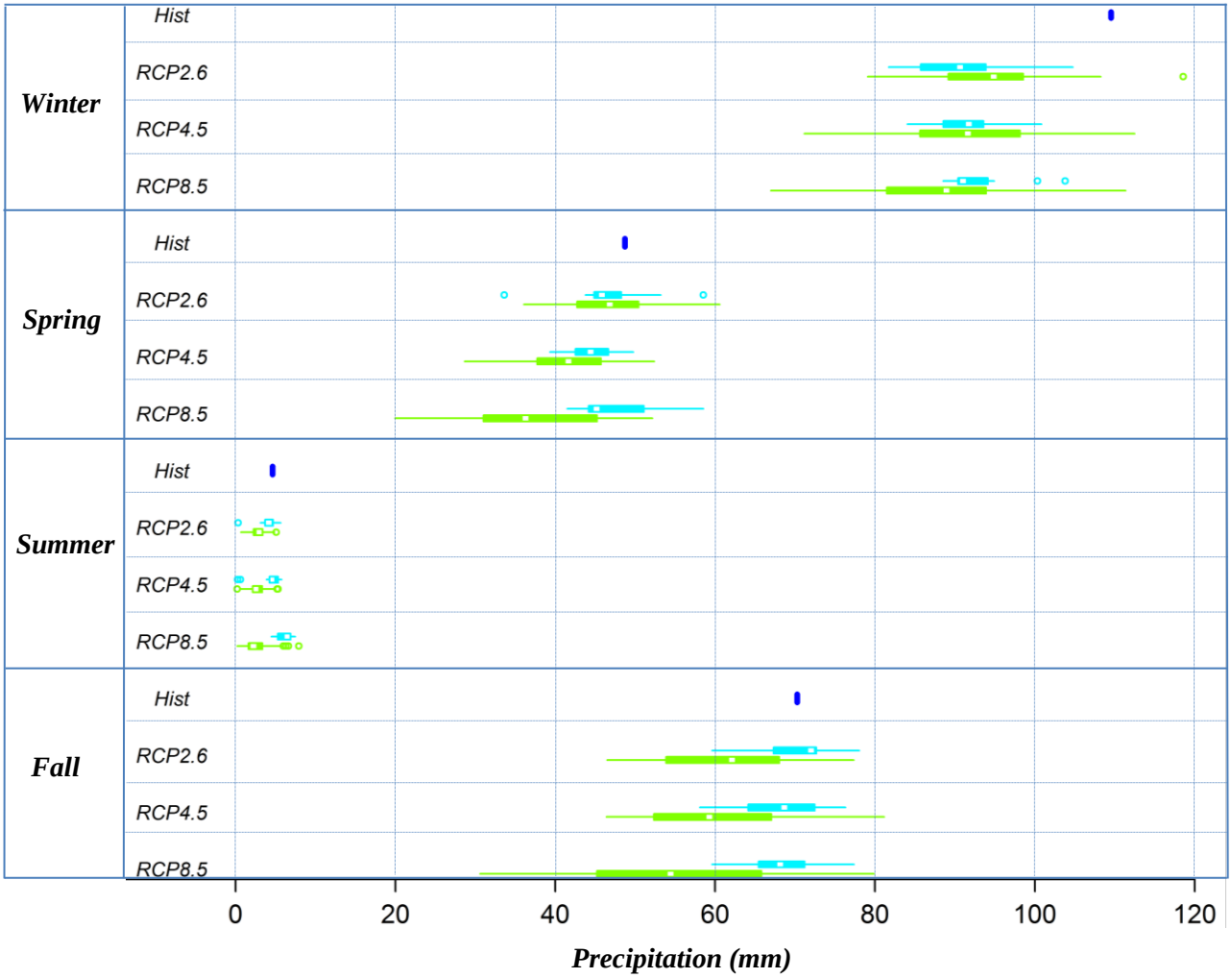

Figure 3-8. Seasonal changes of projected precipitation after bias correction under different emission scenarios relative to the historical (1951-2011) mean for that season. The near-term time periods are illustrated in green color and the long-term ones are in blue.

3.4 Conclusions

Projecting the impact of climate change on the probabilistic behavior of hydro-climate variables in fine local scales is highly complicated due to the existing complex and nonlinear relationship between climate-associated processes and the target hydro-climate variables of interest. This complexity

results in different sources of uncertainty, which influence the projection accuracy of the global warming impacts on the response variable. To improve the accurate projection of hydro-climate variables, this study has presented a comprehensive methodology for enhancing the predictive power of regression-based statistical downscaling through addressing different sources of uncertainty arising from biases in raw data from GCMs, high dimensional space atmospheric projectors, and nonlinearity between hydro-climate predictands and atmospheric projectors.

The results in the dimensionality-reduction section demonstrate that a kernelized form of supervised dimensionality reduction technique is able to efficiently reduce the impact of the high dimensional space of atmospheric projectors in terms of performance accuracy in statistical downscaling. This improvement is achieved through modelling the nonlinear variability and interdependency among bias-corrected atmospheric projectors by taking into account the dependency between the target precipitation variable and explanatory projectors.

Subsequently, the application of nonlinear data-driven machine-learning methods proves the high efficiency of the Bayesian learning algorithm (RVM) in capturing the nonlinearity between dimension-reduced atmospheric projectors and the target variable in the modelling section. The superiority of this model in addressing the complex nonlinear relationships gives rise to minimizing the possibility of overfitting and reducing computational burden in the downscaling modelling as well.

Unlike traditional univariate bias correction approaches, the current study demonstrated the usefulness of the Multivariate Recursive Nesting Bias Correction (MRNBC) approach on simultaneously correcting biases and variability in multiple-GCM-derived variables over multiple time scales for regression-based statistical downscaling. Since multiple projectors in statistical downscaling represent a number of grid cells surrounding a specific study site, it is important to extend the scale-dependent climate model biases to account for the biases in the spatial cross dependence attributes among multi projectors as well. Thus, employing this procedure leads to reducing the uncertainty and improving the future projection accuracy of hydro-climate variables of interest.

It should be noted that the proposed methodology is not restricted to precipitation and can be used for other hydro-climate variables as well. The application of the proposed methodology in the regression-based statistical downscaling in the study site reduces the impact of different sources of

uncertainty and results in more accurate climate change impact assessments on hydro-climate variables in the future. Using more-accurate projections, decision makers of the capital of Iran will be able to better define long-term and effective proactive strategies to be adopted in response to potential future changes. They will thus be better able to mitigate adverse consequences arising from global warming that might threaten the availability of surface water resources in this megacity. However, whether the method is able to globally outperform other methodologies is a challenge that needs be addressed in future work.

Chapter 4

Time Varying Non-stationary Multivariate Risk Analysis Using a Dynamic Bayesian Copula

This chapter is based on the following two papers; one is published in the journal Water Resources Research and the other is under review in the journal Scientific Reports. Organizational changes are made to both the papers to be consistent with the format of the thesis. There are thus differences between the content of this chapter and the papers. There are also minor changes in response to comments from the examining committee.

Sarhadi, A., D. H. Burn, M. Concepción Ausín, and M. P. Wiper (2016b), Time varying nonstationary multivariate risk analysis using a dynamic Bayesian copula, *Water Resources Research*, *52*(3), 2327-2349.

Sarhadi, A., M. C. Ausín, and P. M. Wiper (2016a), A New Time-varying Concept of Risk in a Changing Climate, *Scientific Reports*, Submitted.

Summary

A time varying risk analysis is proposed for an adaptive design framework in non-stationary conditions arising from climate change based on the projections derived in the previous chapters. A Bayesian, dynamic conditional copula is developed for modelling the time-varying dependence structure between mixed continuous and discrete multi-dimensional hydro-meteorological phenomena. Joint Bayesian inference is carried out to fit the marginals and copula in an illustrative example using an adaptive, Gibbs Markov Chain Monte Carlo (MCMC) sampler. Posterior mean estimates and credible intervals are provided for the model parameters and the Deviance Information Criterion (DIC) is used to select the model that best captures different forms of non-stationarity over time. This study also introduces a fully Bayesian, time-varying joint return period for multivariate time-dependent risk analysis in non-stationary environments. The results demonstrate that the nature and the risk of extreme-climate multi-dimensional processes are changed over time under the impact of climate change and accordingly the long-term decision making strategies should be updated based on the anomalies of the non-stationary environment.

4.1 introduction

Global warming is a major threat to the planet. This warming is a result of an increase in human-induced greenhouse gas emissions and is altering Earth's climate. According to the Intergovernmental Panel on Climate Change (IPCC), changes in characteristics of the water cycle due to rising temperatures have hydrological implications (IPCC, 2014; Milly et al., 2015). Thus, global warming will impact hydrological processes and lead to increased risk of climate extremes in different parts of the world.

This chapter deals with the probabilistic aspect of the risk in infrastructure and water resource planning. The risk term is thus defined as the probability of failure of a water system over a planning horizon. The failure may occur under the impact of extreme rare hydro-climate events. To estimate the reliability of the system over its lifetime, the exceedance probability of rare events should be estimated. Water professionals struggle to develop approaches that account for the impact of climate change on hydrological designs to reduce associated risks. Traditional, risk-based decision-making principles in water resources planning are based on the fundamental assumption of statistical stationarity. Under stationarity it is assumed that the probabilistic characteristics of hydro-meteorological processes will not change over time and that future water resources planning can be designed with past records in mind. Milly et al. (2008; 2015) argued that the fundamental assumption of stationarity has been influenced by climate change and anthropogenic effects and therefore stationarity is no longer applicable for water resources risk assessment and planning. Accordingly, water planners must revise current planning and analytic strategies to develop non-stationary probabilistic models based on the anomalies of the changing environment arising from climate change (Read and Vogel, 2015; Salas and Obeysekera, 2013). Therefore, in the changing environment an effective and flexible time-varying design approach must be adopted for risk-based decision-making in water resources planning and infrastructure designs.

Under non-stationary conditions, the behavior of extreme hydro-meteorological processes changes and their probabilistic parameters may no longer be constant. Vogel et al. (2011) introduced a "flood magnification factor" to quantify how the distribution of extreme events shifts from decade to decade under the impact of a broad range of anthropogenic activities, including climate change. In this condition, alternative approaches should be developed in which the effect of non-stationarity is integrated and probabilistic parameters are allowed to change over time. In this case, statistical

distribution parameters are expressed as functions of covariates to model the changing conditions associated with non-stationarity generated by climate change impacts. A covariate could take the form of a time-dependent trend in the moments of hydro-meteorological variable time series or low frequency climatological signals (Du et al., 2015; Katz et al., 2002).

Univariate non-stationarity modelling in hydrological risk assessment has drawn a great deal of attention in hydrological science in recent years (Rosner et al., 2014; Salas and Obeysekera, 2013; Westra et al., 2014). Khaliq et al. (2006) reviewed approaches used for the non-stationary frequency analysis of hydro-meteorological variables. Bayesian approaches have gained more attention for non-stationary modelling in recent years. Studies that use Bayesian techniques for the analysis of hydro-meteorological variables include Cunderlik et al. (2007), Ouarda and El-Adlouni (2011), El-Adlouni and Ouarda (2009) for at-site frequency analysis, and Khaliq et al. (2006) and Leclerc and Ouarda (2007) for regional frequency analysis at ungauged areas. These studies were carried out under non-stationary conditions in a univariate context, while it is well known that natural stochastic hydro-meteorological processes are multivariate phenomena by their very nature characterized by multi-dimensional properties that are statistically dependent. Accordingly, univariate risk analysis methods under non-stationarity conditions cannot fully characterize the properties that are highly correlated. This inability may lead to high uncertainty and failure of risk plans in water resources systems. For a complete understanding of multivariate hydro-meteorological extreme events under the impact of climate change, it is therefore necessary to study the simultaneous, multivariate, probabilistic behavior of two or more hydrological properties. Since being introduced and applied in hydrology and geosciences by De Michele and Salvadori (2003), the application of copulas in modelling the dependence behavior of hydrological processes has grown quickly in recent years (Chebana and Ouarda, 2011; Hao and Singh, 2012; Lee et al., 2013; Madadgar and Moradkhani, 2013; Madadgar and Moradkhani, 2014; Requena et al., 2013; Sadri and Burn, 2012; Santhosh and Srinivas, 2013). However, these studies and similar ones have not taken into account the effects of non-stationarity and assumed a constant dependence relation over time, which is not appropriate under a changing environment. Wahl et al. (2015) also demonstrated increasing risk of compound flooding through exhibiting non-stationarity in the dependence between two natural hazards, heavy precipitation and storm surge, at major US coastal cities. Using the lowest and highest values of dependency separately, they attempted to show changes in joint return periods relevant to flood risk analyses at

the beginning and the end of a time period, ignoring time-varying non-stationarity in a multivariate risk analysis.

Multivariate, non-stationary risk analysis is relatively new and very few publications are available in the literature regarding this area. Chebana et al. (2013) first mentioned the idea of using multivariate functions with changing dependence structure between multivariate hydrological dimensions over time. Corbella and Stretch (2013) also applied conditional copula functions with invariant dependence metrics. Despite their importance, dependence structures affected by the changing environments between different individual hydrological dimensions have scarcely been investigated. Bender et al. (2014) presented a bivariate non-stationary approach to study the time dependent behavior of bivariate hydrological design parameters. Jiang et al. (2015) also performed a bivariate frequency analysis with time variation in dependence structure for the low-flow series from two hydrological neighbor stations. Nevertheless, practical mathematical issues arise when dealing with time-varying dependence of two or more dimensions over time in multivariate non-stationary stochastic modelling. For example existing studies only use simple, linear trend estimators to model the distribution function parameters. The methods are not fully time-varying in terms of functions, especially in the definition of the return period concept. Furthermore, they are not assessing time varying risk concept for an adaptive multivariate design framework over future long time periods. Thus, few theoretical hydrological studies on the concept of time-varying multivariate non-stationary modelling exist. This is partly related to the unavailability of robust methods and the complexity of parameter estimation techniques.

While frequentist methods have been preferred for estimating distribution parameters, Bayesian inference offers a more attractive framework in terms of time-varying copula estimation (Smith, 2013). In particular, Bayesian inference for dynamic copulas has been studied in the financial context by Ausin and Lopes (2010) and Creal and Tsay (2015). However, to the best of our knowledge, no study is available in the literature that discusses adapting Bayesian inference for multivariate conditional dynamic copula modelling in the water resource management area. Thus, this insight is new in hydrology and should prompt a strong interest in multivariate copula-based models with time-varying dependence parameters under non-stationary conditions. To promote a robust methodology to deal with the concept, the present study proposes a time varying copula capturing the time evolution in the changing dependence structures under multi-model ensembles of climate change scenarios. Full

likelihood-based Bayesian inference is developed where the whole set of the model parameters are estimated in an adaptive multivariate time-varying design framework. The proposed methodology is employed on the complex natural phenomenon, drought, which stands first among all others affecting the most people (Tallaksen and van Lanen, 2004), as an illustrative case study.

This chapter is organized as follows: Section 4.2 describes the main properties of drought process that is used as an illustrative case study and the climate dataset used in this study. Section 4.3 presents the mathematical background of the Bayesian dynamic copula model used to assess time varying risk in an adaptive non-stationary water-planning framework under changing climate conditions. The results and discussion of the case study follow in the Section 4.4, and finally the conclusions and potential future work for wider applications are drawn.

4.2 Illustrative study and dataset

4.2.1 Definition of drought characteristics

Drought is a complex natural hazard. The reasons arise from the dynamic complexity and lack of knowledge about this natural hazard and can be summarized in several ways. First, drought is recognized as a creeping process whose impacts start slowly and then accumulate over a considerable period of time and may linger for a long time after the termination of the drought event. Second, there is no precise and universal definition for drought, which makes it difficult to deal with such a phenomenon (Mishra and Singh, 2010). Third, the impacts of drought result in non-structural damages spreading over a large geographical area varying in spatial and temporal scales (Mishra and Singh, 2010; Wilhite, 2000). Unlike some other natural hazards, humans can directly trigger drought and aggravate it through impacting land's capacity for receiving and holding water (Mishra and Singh, 2010). The other way that humans affect drought is by the indirect impact of climate change, which is created by global warming from greenhouse gas emissions. This process can adversely exacerbate drought characteristics.

Droughts are dynamic and multi-dimensional in nature. One cannot assess and describe them by characterizing a single feature for any type of analysis. There is a need to find an appropriate way to define different properties of drought using underlying indices. A list of the most prominent indices, which have been widely used to define different types of droughts, is found in Mishra and Singh (2010). One of these, formed by monthly time series of precipitation—Standardized Precipitation

Index (SPI)—and developed by McKee et al. (1993), is used to represent multivariate drought characteristics under the run theory context. SPI's simplicity, its spatial invariance in its interpretation, its probabilistic nature, and its presentation of better spatial standardization with respect to extreme events, have made it a powerful and specialized indicator for precise quantification of drought (Lloyd-Hughes and Saunders, 2002; Mishra and Singh, 2010). The fundamental superiority of SPI relative to other drought indices is that it can be calculated for a variety of time scales. This flexibility enables SPI to monitor precipitation anomalies on short-term and long-term water supplies from soil moisture to streamflow, groundwater, and reservoir storage supplies (Mishra and Singh, 2010). This index is calculated by fitting a Gamma distribution to the monthly precipitation data. The Gamma Cumulative Distribution Function (CDF) is then rescaled so that an index of SPI=0 is the median precipitation. This index applies to different time scales ranging from 1 to 24 months. A drought period is assumed as a consecutive number of time intervals when SPI values are less than the truncation level (SPI=0). Therefore, drought duration is defined as the number of consecutive events with negative-SPI, while drought severity is the cumulative value of the negative-SPI within the drought duration as given in the following form (Mishra and Singh, 2011; Shiau, 2006):

$$S = -\sum_{i=1}^{D} SPI_i \qquad (4.1)$$

where *S* denotes drought severity, and *D* denotes drought duration. In this case, severity dimension is a continuous measurement and is described as a 'continuous random variable', while duration dimension values are discretized to integer numbers and can assume finite or countably infinite number of values. Thus, duration dimension is considered a 'discrete random variable'.

As a dynamic and alternating process, drought occurrences take into account inter-arrival time expression for the recurrence interval of droughts. Inter-arrival time denoted as *X* is thus defined as the period elapsing from the initiation of a drought event to the beginning of the next event (Song and Singh, 2010). Similar to duration dimension, the discretized inter-arrival time dimension is also described as a 'discrete random variable'. The probabilistic characteristics of the defined drought dimensions may be influenced by natural internal climate processes or external forcing as a consequence of human influences. In the changing non-stationary environment, each of the

dimensions may change over time. Figure 4-1 shows the alternating process and time-varying characteristics of droughts defined by the given concept over time.

As mentioned before, the management of surface water resources has been a main challenge for water authorities in Tehran in recent years with respect to rapid expansion of population and occurrence of severe long-term dry spells arising from climate change. It is therefore of crucial importance to have a long-term management plan including the impact of climate change on the occurrence of dry spells and availability of surface water resources in this megacity.

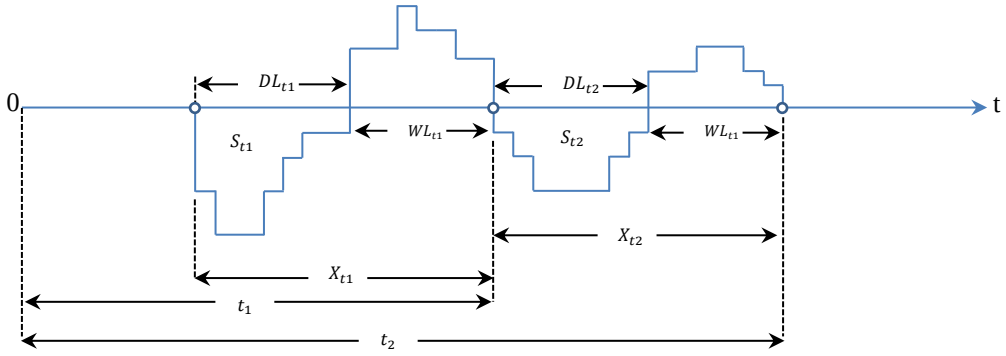

○	Drought event initiation
$t_1, t_2, \ldots$	Real cumulative time occurrence
X_t	Inter-arrival time between drought events
WL_t	Non-drought duration (wet period)
DL_t	Drought duration
S_t	Drought severity

Figure 4-1. Dynamic drought renewal process and definition of drought characteristics in a changing environment

To develop a risk-based water resources plan in a non-stationary condition, the limitations of the relatively short historical hydro-meteorological records, and the uncertainties associated with future climate model projections, are considered major restrictions. To address these limitations, a time varying stochastic model can be developed by synthetizing historical observed records and climate model projections using multiple climate forcing scenarios (Borgomeo et al., 2014; Milly et al., 2008). Although the uncertainty of future projections is still problematic in a changing climate, using climate multi-model ensembles allows to quantify probabilistic uncertainties of hydrological processes in future climate projections. Hence, despite having inherent uncertainties, probabilistic information from multiple-model ensembles under different forcing scenarios helps to identify sources of uncertainty and to measure the degree of influence of extreme events (Bayazit, 2015;

Galloway, 2011). To quantify future extreme dry spells in an adaptive time-varying design framework, based on the concept of design's life period (Rootzén and Katz, 2013), the relatively short historical precipitation time series (1951-2011) in the study site (Tehran) are synthetized with projected precipitation from multi-model ensemble GCMs (spanning from 2015 to 2100) derived in the previous chapter. Synthetizing probabilistic precipitation projections under different forcing scenarios (representing uncertainty of future precipitation behavior) with observed precipitation also helps experts better communicate the certainty of an event occurrence. In this way, assuming that probabilistic projections are reliable, decision makers are able to effectively manage the risk of the event occurring (DeChant and Moradkhani, 2015). To develop a risk-based time-varying framework and to include all the possibilities and avoid additional calculations, one appropriate representative synthetized precipitation time series is selected from each climate change scenario. By making a boxplot of all the synthetized precipitation time series from all ensemble models in the different scenarios, one is able to select two models covering the minimum and the maximum variance of all the synthetized GCM models. In this way, all the possibilities (other models) are located in between these two selected models covering the whole variance of data. Doing so, synthetized MIRO-ESM CHEM model is selected from the scenario RCP2.6 and synthetized INMCM4 model is selected from the scenario RCP8.5, representing minimum and maximum variances of all models, respectively. From the midrange mitigation emission scenario (RCP4.5) synthetized model of CanESM2 is also selected as the representative of this scenario class.

Choosing one representative model from each climate change scenario, the synthetized precipitation time series are used for forming SPI3 (SPI index for 3-month precipitation time series) to define the drought characteristics over the design's life period.

4.3 Methodology

4.3.1 Time-varying multivariate non-stationary risk analysis

Introduced by Sklar (1959), copulas are considered flexible tools for constructing multivariate distributions and modelling the dependence structure between correlated variables. The popularity of copulas is due to their flexibility in forming dependence between variables using any type of marginals. In addition, copulas are able to capture wide variety of dependence structures, including

asymmetry, nonlinear, and tail dependence (Jammazi et al., 2015). More-detailed information about the properties of copulas is given in Nelsen (2007) and Salvadori et al. (2007).

Realizing a changing environment, a time varying or dynamic conditional copula should be taken into account for water resources risk-based decision-making. Introduced by Patton (2006) in a financial framework, a dynamic copula allows a time variant dependence structure to characterize the relationship of underlying variables in a more flexible and time-varying manner. Suppose that $\boldsymbol{y}_t = (y_{1t}, y_{2t})$ represents a pair of hydrological variables whose dependence structure is defined by a copula function. A general form of a time varying joint distribution can be built at any time *t* using a dynamic copula as follows:

$$\boldsymbol{y}_t \sim F(y_t|\theta_t) \tag{4.2}$$

$$F(\boldsymbol{y}_t|\theta_t) = C(F_1(y_{1t}|\theta_{1t}), F_2(y_{2t}|\theta_{2t})|\theta_{ct})$$

$$F(\boldsymbol{y}_t|\theta_t) = C(u_{1t}, u_{2t}|\theta_{ct})$$

where $F(.)$ denotes cumulative distribution function, $C(.)$ is the copula function, θ_{1t} and θ_{2t} are parameters for the time-varying marginal models, θ_{ct} is the time varying copula parameter, and u_{1t} and u_{2t} are marginal probabilities in the dynamic copula in the unit hypercube with uniform $U[0,1]$ marginal distributions.

In a multivariate, risk analysis framework, non-stationarity could be identified in the statistical characteristics of either one or two marginal variables and not in the dependence structure or vice versa. It might also happen that both the marginals and the dependence structure show non-stationary behavior. Non-stationarity can be via a trend component (i.e., linear or nonlinear) and (or) sudden changes in statistical attributes of the variables. The presence of trend or change point may have a considerable effect on the interpretation of results in fitting different probability distributions (Khaliq et al., 2006). To capture the possible non-stationarity of the marginals and the dependence in fitting probability distributions, various time dependent approaches are employed in the context of univariate and multivariate non-stationary frequency analysis (AghaKouchak et al., 2012; Khaliq et al., 2006). Local likelihood-based methods have gained more popularity and proven to be useful explanatory tools. These methods can be developed to include covariates to estimate distribution and copula parameters such that they vary over time. Various techniques have been utilized for this purpose, including the Full Maximum Likelihood (FML) estimation, the Canonical Maximum Likelihood

(CML) method, Inference Functions for Marginals (IFM) approach and empirical copulas (El Adlouni et al., 2007; Jammazi et al., 2015; Ouarda and El-Adlouni, 2011).

In this study, marginal distribution parameters are specified as functions of time, which is viewed as a covariate, and are estimated via the generalized additive model approach capturing linear or nonlinear trends. Different forms of non-stationarity (sudden jump, periodicity, and trend) on the synthetized long-term drought observations are detected using classical statistical techniques such as nonparameteric, univariate and multivariate Mann-Kendall tests (Chebana et al., 2013) on both the marginals and the dependence functions. The null hypothesis of no trend is rejected if the trend test statistic is different from zero at 5% significance level. In the following, the parameter estimation methods of the marginal distributions in the presence of the non-stationarities are discussed for each drought dimension.

4.3.1.1 Time-varying marginal distributions

As in the illustrative example of this study, two correlated drought dimensions are different in terms of probabilistic behaviour; different classes of independent distributions are used to construct their marginal distributions. In a non-stationary process, the parameters of the underlying marginal distributions are time-dependent, and hence, the stochastic behavior of these distributions varies over time (Cheng and AghaKouchak, 2014). Upon detection of a significant trend, to capture the non-stationarity behavior, in this study, different forms of linear and nonlinear functions of time are discussed with respect to location parameter (μ_t) of the different marginal distributions. Other distribution parameters are kept constant in this case, although they could be similarly assumed to be time-varying. This leads to estimating drought quantiles in a more realistic way consistent with the behavior of observed and projected extreme drought events (Cheng and AghaKouchak, 2014). In the following, different forms of trend in regard with the time dependent distribution parameters are discussed for the two drought dimensions.

I. Drought severity models

As drought severity is considered a continuous random variable, the most popular and well-fitted distributions in respect to this variable are Gamma and Log-Normal distributions (Janga Reddy and Ganguli, 2012; Shiau, 2006). Let S_t be the severity dimension starting at (real) time t. Then the two proposed time varying model possibilities will be as follows:

Log-Normal severity model:

$$\log S_t \mid \mu_t, \sigma \sim N(\mu_t, \sigma^2) \qquad (4.3)$$

Gamma severity model:

$$S_t \mid \mu_t, \phi \sim Ga(\mu_t \phi, \phi) \qquad (4.4)$$

with density function given by

$$f(s_t \mid \mu_t, \phi) = \frac{\phi^{\mu_t \phi - 1}}{\Gamma(\mu_t \phi)} s_t^{\mu_t \phi - 1} exp(-\phi s_t), \qquad s_t > 0$$

with E[S_t]= μ_t. In both models, the location parameter (μ_t) is assumed to be a function of time. Then, we consider different forms of constant, linear, and quadratic models for the location parameter as follows:

$$\mu_t = \delta \qquad (4.5)$$

$$\mu_t = \delta + \epsilon t$$

$$\mu_t = \delta + \epsilon t + \zeta t^2$$

where *t* is time. A similar structure can also be used in the case of the Gamma distribution such that, here we assume (for the quadratic model),

$$log\ \mu_t = \delta + \epsilon t + \zeta t^2$$

Therefore, the set of severity model parameters is given by $\beta_S = (\delta, \epsilon, \zeta, \sigma)$ if a Log-Normal model is chosen or, alternatively, by $\beta_S = (\partial, \varrho, \iota, \phi)$ if a Gamma model is selected.

II. Drought duration models

According to the run-theory definition, droughts last as integer numbers of months, and drought duration is thus considered as a 'discrete random variable'. The majority of studies in multivariate frequency area have assumed drought duration as a continuous random variable. For example, Madadgar and Moradkhani (2013), Shiau (2006), Shiau and Modarres (2009), Halwatura et al. (2015), and other associated studies have fitted continuous probability distributions to discrete drought duration values. Other studies such as De Michele et al. (2013) suggested using a

randomization technique known as "jittering" to transform discrete drought duration dimension to a continuous variable.

In this study, however, drought duration dimension is considered as a 'discrete random variable' and 'discrete distributions' are fitted to the drought duration time series. Assume droughts last an integer number of months, $d \in \{1, 2, \ldots\}$, and that in a changing environment, as time goes on, drought durations and their variability may be increasing or decreasing. In this condition we consider a time varying duration model.

Let D_t be the duration of a drought, which starts at (real) time *t*. Then one possibility could be a Negative Binomial duration model:

$$Let\ Z_t = D_t - 1 \qquad (4.6)$$

$$\text{Then } Z_t | r, p_t \sim NB(r, p_t)$$

$$\text{where } p_t = r/(r + \lambda_t)$$

with probability mass function given by,

$$\Pr(Z_t = z|\ r, p_t) = \binom{z + r - 1}{z} {p_t}^r (1 - p_t)^z, \quad z = 0,1,2, \ldots$$

Note that the Negative Binomial model generally allows for capturing overdispersed data. An alternative model could be a Poisson duration model:

$$Z_t | \lambda_t \sim P_o(\lambda_t) \qquad (4.7)$$

with probability mass function:

$$\Pr(\mathrm{Z_t} = \mathrm{z}|\ \lambda_t) = \frac{{\lambda_t}^z e^{-\lambda_t}}{z!}, \qquad z = 0,1,2, \ldots$$

This model could be sometimes overly restrictive when there are many zeros in observations.

Another possible model for duration data is a Geometric distribution. This model corresponds to a particular case of the Negative Binomial model with r set to 1 although it is restricted to data that show strictly decreasing probabilities for higher durations.

In a changing climate, the rate of drought occurrence (λ_t) is assumed to be time-dependent and varies over time. Similar to severity, different log trend forms, including constant, linear, and quadratic models can be employed for λ_t as follows:

$$\log \lambda_t = \eta \tag{4.8}$$

$$\log \lambda_t = \eta + \theta t$$

$$\log \lambda_t = \eta + \theta t + \kappa t^2$$

where *t* is time and the set of duration model parameters is given by $\beta_D = (\eta, \theta, \kappa, r)$.

4.3.1.2 Dynamic copula

To model the dependence between severity and duration dimensions under a changing non-stationary condition, a dynamic copula needs to be developed. In the static states, and even in the existing multivariate time-varying studies, it is assumed that marginal distributions come from the same type of random variables. For example, a copula can model marginal dimensions that are only continuous or discrete random variables. This assumption indicates the uniqueness aspect of copulas and has been mentioned in the literature (Nelson, 2007). In performing statistical inference for copula models in water resource risk studies, it happens some of marginals are discrete and the others are continuous, such as the illustrative example (drought). Here, a non-uniqueness aspect of copula can also be used to model dependency between two different mixed random variables (discrete and continuous) based on the Sklar's theorem (Sklar, 1959). To the best of our knowledge, no studies exist in this area to consider the application of a dynamic copula for mixed dimensions (discrete and continuous). By extending the classical copula model, one is able to develop a dynamic copula so that its parameters vary over time. This study presents an original approach, which can handle realistic, dynamic copula modelling in the case of mixed outcomes.

Let $C_t(u_t, v_t)$ represent the dependence structure between severity and duration for a drought that begins at (real) time *t*, where $u_t = F_{S_t}(s_t)$ and $v_t = F_{D_t}(d_t)$ are the cumulative distribution functions of the severity and duration, respectively, at time *t*. In the current study, a time varying Gumbel copula $C(u_t, v_t|\theta_{ct})$ is developed for drought observations, as this exhibits greater dependence in the positive tail than in the negative and is therefore one of the possible copula functions for extreme

value analyses (AghaKouchak et al., 2012; Chebana and Ouarda, 2011). The time varying distribution function of a Gumbel copula is given by:

$$C(u_t, v_t|\theta_{ct}) = \exp\left\{-[(-\log u_t)^{\theta_{ct}} + (-log\ v_t)^{\theta_{ct}}]^{\frac{1}{\theta_{ct}}}\right\} \quad (4.9)$$

where $\theta_{ct} \in [1, \infty]$ and the density function is given by:

$$c(u_t, v_t|\theta_{ct}) = C(u_t, v_t|\theta_{ct}) u_t^{-1}\, v_t^{-1}[(-log\ u_t)^{\theta_{ct}} + (-log\ v_t)^{\theta_{ct}}]^{-2+\frac{2}{\theta_{ct}}} \times$$

$$[(\log u_t)\,(\log v_t)]^{\theta_{ct}-1}\{1 + (\theta_{ct} - 1)\left[(-\log u_t)^{\theta_{ct}} + (-\log v_t)^{\theta_{ct}}\right]^{-\frac{1}{\theta_{ct}}}\} \quad (4.10)$$

The relation between the dependence parameter of the Gumbel copula and the standard, Kendall's tau dependence values can be expressed as:

$$\tau_t = 1 - 1/\theta_{ct} \quad (4.11)$$

where the Gumbel copula parameter is defined for τ_t in (0,1) so that there is positive dependence as reflected in the real drought observations.

To capture different forms of Kendall's tau under changing non-stationary conditions, the following models are assumed:

$$log\frac{\tau_t}{1-\tau_t} = \xi \quad (4.12)$$

$$log\frac{\tau_t}{1-\tau_t} = \xi + \nu t$$

$$log\frac{\tau_t}{1-\tau_t} = \xi + \nu t + \chi t^2$$

The copula parameter, θ_{ct}, is thus defined as a deterministic function of time, *t*, and a vector of unknown parameters, $\beta_C = (\xi, \nu, \chi)$.

Following the same concept, other members of the Archimedean or elliptical families of copulas could also be considered.

4.3.1.3 Time-varying joint return period

In planning and management of water resources, risk assessment is a crucial task requiring estimation of the recurrence intervals of extreme events. Recurrence intervals of events are characterized by the concept of return periods in hydrology. In the multivariate domain, different transformation types of the joint exceedance probability to a joint return period (JRP) have been suggested in literature (Gräler et al., 2013; Salvadori et al., 2007; Shiau, 2006). There is still discussion on which form of the JRP could be more appropriate in water resources planning and project design (Bender et al., 2014). Following the method introduced by De Michele et al. (2013) and Gräler et al. (2013), in this study, a fully time-varying framework evolving through time is proposed for joint return period. We define the time-varying joint return period at time *t*, denoted by $JRP_t(d_0, s_0)$, as the expected time between droughts with duration larger than d_0 and severity larger than s_0 at time *t*:

$$JRP_t(d_0, s_0) = \frac{E[X_t]}{1 - F_{D_t}(d_0) - F_{S_t}(s_0) + P(D_t \leq d_0, S_t \leq s_0)} \qquad (4.13)$$

where X_t is the mean inter-arrival time between drought events.

Since with the evolution of a drought, inter-arrival time between events may vary over time, the behavior of this variable may be time-dependent; this dimension can also be modelled through potential discrete probability distributions such as those fitted to drought duration in the previous section.

Let X_t be the inter-arrival time between drought events, which starts at (real) time *t*. Then similar to drought duration, one possible model could be a Negative Binomial inter-arrival model:

$$Let\ M_t = X_t - 2 \qquad (4.14)$$

$$\text{Then } M_t | s, q_t \sim NB(s, q_t)$$

$$\text{where } q_t = s/(s + \gamma_t)$$

Other discrete distributions, including Poisson and Geometric can also be fitted. Similar to the drought duration, constant, linear, and quadratic models (shown in equation 4.8) are also used to express the time varying γ_t. In this case, a set of inter-arrival model parameters is given by $\beta_A = (\psi, \omega, \vartheta)$.

Taking into account the inter-arrival time as a time varying variable, and given the time dependent marginal distributions for the duration and severity, the fully time-varying joint return period is given by:

$$JRP_t(d_0, s_0) = \frac{\gamma_t + 2}{1 - u_{t_0} - v_{t_0} + C(u_{t_0}, v_{t_0}|\theta_{ct})} \qquad (4.15)$$

Observe that if we have non-stationary drought durations and severities, such that these increase with time, it is expected that the time-varying joint return period, $JRP_t(d_0, s_0)$ will decrease as t increases for each pair of values, d_0, s_0. Therefore, the time-varying return period in a non-stationary condition depends on the time-varying parameters of the inter-arrival times, marginal distribution and dynamic copula. It should be noted that the other forms of the joint return period can also be developed using the same concept.

4.3.2 Bayesian Inference of dynamic copula

In a multivariate, non-stationary risk analysis framework under a non-stationary environment, uncertainty assessment of the dynamic copula using time as a covariate is of fundamental importance. In this study, a Bayesian Markov Chain Monte Carlo (MCMC) approach is integrated to the non-stationary marginal and copula models to characterize the uncertainty. In this approach, for all the time-varying variables (including marginals, inter-arrival-time, and copula) a Bayesian inference scheme is implemented to indirectly estimate the time varying distribution parameters, $\mu_t, \lambda_t, \theta_{ct}$ and γ_t. For this purpose, instead of directly inferring these distribution parameters, Bayesian inferences are employed to estimate the generalized additive model parameters $\beta_S, \beta_D, \beta_A$ and β_c, respectively, linking the parameter values at time *t* with the time as a covariate.

Bayesian inference defines prior distributions for all unknown generalized additive model parameters $\beta_S, \beta_D, \beta_A$ and β_c. Then, the knowledge brought by a prior distribution is combined with the given observations to generate posterior distribution by Bayes theorem. More specifically, we consider a two-step Bayesian approach where we first make inference for the marginal parameters of the drought severity, β_S, duration, β_D and inter-arrival time, β_A. Then, in the second step, we make inference for the copula parameters, β_c, given the results for the marginal parameters. Assume for example that we have a sample of severities, $s_{t_1}, \ldots, s_{t_n}$, observed at n instant times, $t_1, \ldots, t_n$.

Suppose that we have considered a time-varying Gamma model for the severity as defined in (4.4). Then, the posterior distribution for the severity parameters $\beta_S = (\partial, \varrho, \iota, \phi)$, is given by,

$$p(\beta_S | s_{t_1}, \dots, s_{t_n}) \propto p(\beta_S) \prod_{i=1}^{n} p(s_{t_i} | \beta_S) \qquad (4.16)$$

where $p(\beta_S)$ is the prior density and

$$p(s_{t_i} | \beta_S) = \frac{\phi^{\mu_{t_i}\phi-1}}{\Gamma(\mu_{t_i}\phi)} s_t^{\mu_{t_i}\phi-1} \exp(-\phi s_{t_i}),$$

and where $\log \mu_{t_i} = \partial + \varrho t_i + \iota {t_i}^2$. Consequently, the generated posterior distribution, $p(\beta_S | s_{t_1}, \dots, s_{t_n})$, provides information on the posterior distribution of the time-varying parameter, μ_t, for each time, *t*. Note that in the case of stationarity ϱ and ι are equal to zero and the parameter μ_t remains constant and consequently, the severity observations are independent and identically distributed.

4.3.2.1 Prior distributions

The prior distributions are used to provide any prior knowledge on the parameters, $\beta_S, \beta_D, \beta_A$ and β_c. Thus, prior distributions are independent from observations and are preferably specified using external source of knowledge (AghaKouchak et al., 2012). In the current illustrative example, proper but weakly informative priors are assumed in the case of drought severity model as:

$$\partial \sim N(0, 1000) \qquad (4.17)$$

$$\varrho \sim N(0, 1000)$$

$$\iota \sim N(0, 1000)$$

and $\phi \sim Ga(0.01, 0.01)$, if a Gamma model is considered for the severity distribution. In the case of the lognormal model, N(0,1000) prior distributions are also used for δ, ε and ζ and $\tau \sim Ga(0.01, 0.01)$ where $\tau = \frac{1}{\sigma^2}$.

Similarly, for the duration parameters, $N(0, 1000)$ priors are set for θ, κ and a Gamma prior $Ga(0.01, 0.01)$ is also used for r. Likewise, priors of the same form are used for the equivalent parameters of the inter-arrival time distribution.

For the copula parameters, it is assumed that $\xi \sim N\,(0, 1000)$, and $\nu \sim N\,(0, 1000)$, as well as $\chi \sim N\,(0, 10^{-9})$ to avoid numerical problems with the increase of *t*. Note that if good expert information were available, then this could be used to define more informative prior distributions.

4.3.2.2 Bayesian MCMC inference

In general for our models, analytic evaluation of the posterior distributions is not possible. To estimate parameters inferred by Bayes, an MCMC sampling method is integrated to generate an approximate Monte Carlo sample of realizations from the posterior distributions. While there are different types of MCMC sampling algorithms, the Gibbs sampler approach is employed in the current study to obtain samples from a joint distribution through iterative sampling from the full conditional distributions. For example, in order to generate a sample from the joint posterior distribution (4.16) of the severity parameters, under a given model, $\beta_S = (\delta, \epsilon, \zeta, \phi)$, a systematic form of the Gibbs sampler algorithm proceeds as follows (Dellaportas and Smith, 1993):

0. Set initial values $\delta^{(0)},\ \epsilon^{(0)},\ \zeta^{(0)}, \phi^{(0)}$.
1. Repeat for *m = 1,..., M*.
2. Sample from $p(\delta|\ \epsilon^{(m-1)},\ \zeta^{(m-1)}, \phi^{(m-1)}, s_{t_1}, \dots, s_{t_n})$ (4.18)
3. Sample from $p(\epsilon|\ \delta^{(m)},\ \zeta^{(m-1)}, \phi^{(m-1)}, s_{t_1}, \dots, s_{t_n})$
4. Sample from $p(\zeta|\ \delta^{(m)},\ \epsilon^{(m)},\ \phi^{(m-1)}, s_{t_1}, \dots, s_{t_n})$
5. Sample from $p(\phi|\ \delta^{(m)},\ \epsilon^{(m)},\ \zeta^{(m)}, s_{t_1}, \dots, s_{t_n})$

Repeated iteration of the above procedure yields a sequence, ${\beta_S}^{(m)} = \left(\delta^{(m)}, \epsilon^{(m)}, \zeta^{(m)}, \phi^{(m)}\right)$, which is a realization of the MCMC. To ensure the full convergence of the chains and also minimizing the influence of initialization, the so-called burn-in samples are discarded from the chain. The remaining samples are then used for inference. This procedure can be implemented using the free software WinBUGS (http://www.mrc-bsu.cam.ac.uk/software/bugs/), which is run via the R2WinBUGS interface in R software.

To assess the convergence of the Markov chain, a convergence diagnosis method proposed by Geweke (1991) is used. According to the Geweke test, if the convergence is achieved, the Geweke statistic will have an asymptotically standard Gaussian distribution. More information about this test is given in Geweke (1991). Following the underlying MCMC Bayesian inference, the credibility

intervals and the uncertainty of non-stationary probabilities of the generalized additive models' parameters can also be obtained.

4.3.2.3 Model selection

To select the best proposed models, a Bayesian discrimination criterion is employed. The Deviance Information Criterion (DIC) defined by Spiegelhalter et al. (2002) is a measure specifically designed for model selection under Bayesian inference and can be thought of as a Bayesian alternative to the standard AIC. Once samples of the posterior distributions for the parameters of the different trend models (including constant, linear, and quadratic) are obtained using Bayesian MCMC inference, the DIC measure can be easily calculated. For example, the DIC value for a severity model is obtained as (Spiegelhalter et al., 2002):

$$DIC = D(\overline{\beta_S}) + 2n_D \qquad (4.19)$$

where $D(\beta_S)$ is the deviance:

$$D(\beta_S) = -2\sum_{i=1}^{n} \log \mathrm{p}(\mathrm{s}_{\mathrm{t_i}}|\beta_{\mathrm{S}})$$

and $\overline{\beta_S} = E(\beta_S|\mathrm{s}_{\mathrm{t}_1}, \dots, \mathrm{s}_{\mathrm{t}_n})$, is the posterior mean, which can be approximated from the MCMC output using,

$$\overline{\beta_S} \simeq \frac{1}{M-B}\sum_{m=1}^{M-B} {\beta_S}^{(m)},$$

where B is the number of burn-in iterations, and n_D is the effective number of parameters of the model which is given by:

$$n_D = \overline{D} - D(\overline{\beta_S}) \qquad (4.20)$$

where $\overline{D} = E(D(\beta_S)|\mathrm{s}_{\mathrm{t}_1}, \dots, \mathrm{s}_{\mathrm{t}_n})$ is the posterior deviance, which assesses the model's goodness of fit and can be approximated by,

$$\overline{D} \simeq \frac{1}{M-B}\sum_{m=1}^{M-B} D({\beta_S}^{(m)}) \qquad (4.21)$$

The DIC can be measured in a straightforward way from the WinBUGS output. Note that the minimum value of the DIC indicates the best model.

4.4 Results and discussion

4.4.1 Pre-processing analyses

For selection of an appropriate model in frequency analysis process, the first step is to check if there is any non-stationarity in the dataset. Prior to this step, based on nonparametric goodness-of-fit tests (Chi-square test for discrete drought dimensions and Kolmogorov-Smirnov test for continuous one) the best distribution functions are fitted to the synthetized drought characteristics for the selected GCM models under different forcing climate change scenarios. Table 4-1 shows the best selected distribution for each dimension in different selected scenarios.

According to Chebana et al. (2013) it is recommended to jointly analyze univariate and multivariate trend tests to capture all existing trend components as the signs of non-stationarity. The output of the Mann-Kendall test in univariate and multivariate cases of the drought dimensions in different models are shown in Table 4-1. It should be noted that the trend results are achieved after testing serial correlation and change point detection for univariate properties, and change point detection for multivariate copula dimension. The results indicate that in the low and midrange emission scenarios (RCP2.6 and RCP4.5) only duration dimensions exhibit the presence of non-stationarity, whereas in a severe forcing scenario (RCP8.5) all the univariate and multivariate dimensions of the selected synthetized model show significant trend. In the latter model, all severity, duration, and copula variables exhibit significant upward trend, while inter-arrival time dimension shows significant downward trend.

Table 4-1. Results of the best selected distribution and univariate and multivariate Mann-Kendall trend statistics for each drought dimension in different scenarios

Scenario	Models	Dimensions	Selected Dist.	Univariate MK (Z-value)	P-value	Multivariate MK (Z-value)	P-value
RCP2.6	MIRO-ESM CHEM	Severity	Gamma	0.67	0.49	-	-
		Duration	Neg. Binomial	2.07	**0.04***	-	-
		Copula	Gumbel	-	-	1.39	0.16
		Inter-arrival	Neg. Binomial	-1.54	0.12	-	-
RCP4.5	CanESM2	Severity	Gamma	1.25	0.21	-	-
		Duration	Neg. Binomial	2.39	**0.01***	-	-
		Copula	Gumbel	-	-	1.85	0.06
		Inter-arrival	Neg. Binomial	-2.35	**0.02***	-	-
RCP8.5	INMCM4	Severity	Gamma	1.86	**0.04***	-	-
		Duration	Neg. Binomial	2.47	**0.01***	-	-
		Copula	Gumbel	-	-	2.21	**0.02***
		Inter-arrival	Neg. Binomial	-3.09	**0.001****	-	-

* 5% Significance level
** 1% Significance level

4.4.2 Estimation and selection of time-varying models using MCMC sampling

The distribution parameters of the marginals and copula are estimated through the posterior distribution of the MCMC samples. Considering a trend imposes a certain type of non-stationarity, outputs of posterior distributions should be actively checked to select the best statistical model capturing the non-stationarity form. Three different modes of the posterior distributions are employed in the parameter estimations to select the best fitted model. Mode 0 (M0) is used when non-stationary model does not fit to the model, indicating the mean parameter of distribution (μ) or dependence θ_{ct} is time invariant. Mode 1 (M1) is accounted for a non-stationary condition by assuming the model parameter is a linear function of time. In mode 2 (M2), a quadratic function is used to model the non-stationarity in the distribution parameters and dependence structure.

In all climate change scenarios, the Gibbs algorithm is used to generate independent Monte Carlo samples that are used for convergence diagnosis. In each case, the MCMC algorithm is run for 30000 iterations, which are drawn from the posterior distribution. The first 3000 samples are discarded as burn-in and the rest are used for computing the parameter estimations. Having an asymptotically standard normal distribution, the results of the Geweke's statistic (with absolute values less than 1.96) indicate the chains have converged in all cases. For the sake of brevity, the values of the Geweke's statistic are not reported here.

Figure 4-2 illustrates the trace plot and Auto-Correlation Function (ACF) of the posterior samples obtained for the linear model's parameters of the drought duration dimension under the RCP4.5 scenario as an example. The trace plots reveal no upward and downward trend in simulated samples, which is consistent with the convergence results. The ACF plots also demonstrate that the samples are independent within chains, indicating a good mixing performance of the Markov chain through time. The trace plots obtained for the parameters of the other modes and other dimensions also indicate good mixing, but they are not reported here for the sake of saving space.

Having multiple forms of models capturing stationarity and different complex types of non-stationarity, the performance of the DIC measure is examined to select the best Bayesian model for estimation of the time dependent marginal distributions, inter-arrival time and copula parameters. After selection of the best Bayesian model, the Bayesian posterior mean is used to produce estimates for the distribution parameters of interest over time that are subsequently used for the time-varying

multivariate risk analysis. In the following, the results of the procedure are described for the marginal, the dependence structure of drought severity and duration characteristics, and inter-arrival time dimension under the three selected climate change scenarios.

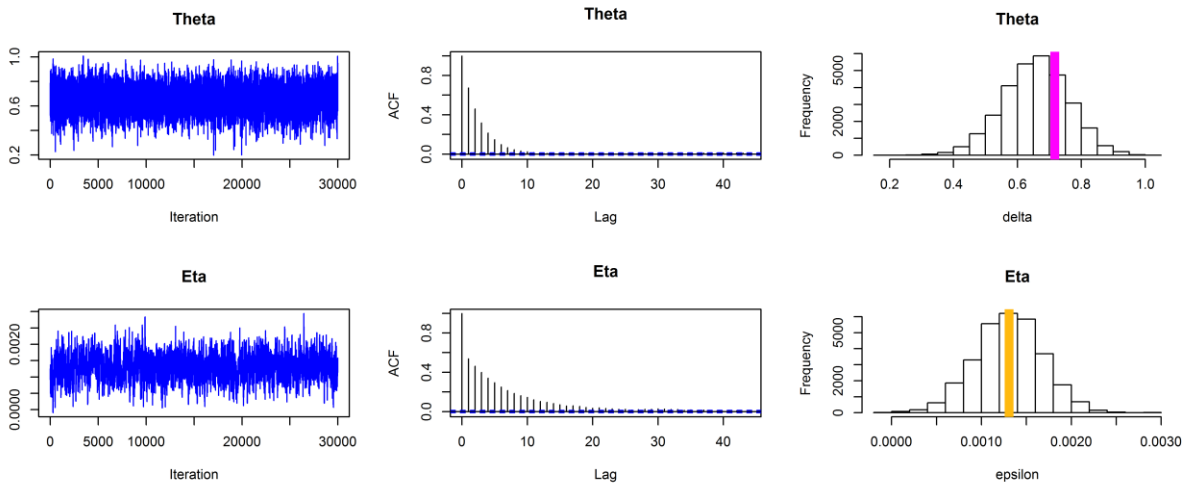

Figure 4-2. Trace plots for posterior samples obtained using MCMC chains for the parameters of the linear non-stationarity model on drought duration under the RCP4.5 scenario

4.4.2.1 RCP2.6 Bayesian model

The results of the DIC for each drought dimension in different forms of non-stationarity under the scenario RCP2.6 are given in Table 4-2. In this scenario for the severity dimension, the results of the DIC show that the constant stationary model presents better fit to severity data. Thus, none of the non-stationary models is adequate to describe the behaviour of severity characteristic over time.

Unlike the severity, and consistent with the trend analysis output, the results of the DIC indicate that the drought duration follows a non-stationary probabilistic time dependent behavior. Although the DIC values of the linear and the quadratic models are not very different, the quadratic Bayesian model shows the least DIC and it is therefore selected as the best model for estimation of the time dependent negative binomial distribution. Similar to the duration, the quadratic model is also selected as the best model to describe the probabilistic time-varying behavior of the inter-arrival time variable in a non-stationary condition.

In terms of the dependency between the severity and duration characteristics (copula variable), the results indicate that a linear non-stationary model provides the best result. Although one of the marginals (duration) exhibits a quadratic non-stationary time dependent behavior, analogously the

DIC results reveal that the linear non-stationary model is required to describe the copula over time. Therefore, it can be concluded that under the RCP2.6 scenario, which is called a peak-decline scenario, the influence of non-stationarity on the marginal distribution (here duration) is larger than the copula dependence measure. The results of the mean and standard deviation of the estimated parameters for each Bayesian model are given in Table 4-2. Figure 4-3 illustrates the smoothed log form of drought multi-dimension time series as function of time and the best-fitted time dependent models.

Table 4-2. Parameter estimation and DIC results of the different forms of the generalized Bayesian models under RCP2.6 scenario

Scenario	Dimension	Statistical Model	Parameters	Posterior mean	Posterior St.	DIC
RCP2.6	Severity	**M0**	∂	1.207	0.109	**646.39**
		M1	∂	1.15	0.15	648.02
			ϱ	0.001	0.002	
		M2	∂	1.15	0.20	650.50
			ϱ	0.001	0.012	
			ι	-1.27	0.0001	
	Duration	M0	η	1.32	0.11	749.8
		M1	η	0.733	0.22	743.23
			θ	0.001	0.0003	
		M2	η	0.512	0.220	**742.08**
			θ	0.002	0.0005	
			κ	-1.355	4.476	
	Inter-arrival time	M0	ψ	1.43	0.08	792.62
		M1	ψ	1.65	0.17	792.29
			ω	-0.0004	0.0003	
		M2	ψ	1.36	0.18	**786.54**
			ω	0.001	0.0006	
			ϑ	-1.92	5.91	
	Copula	M0	ξ	0.620	0.102	-191.44
		M1	ξ	0.110	0.214	**-195.48**
			ν	0.105	0.033	
		M2	ξ	-0.401	0.521	-193.9
			ν	0.386	0.217	
			χ	-0.027	0.020	

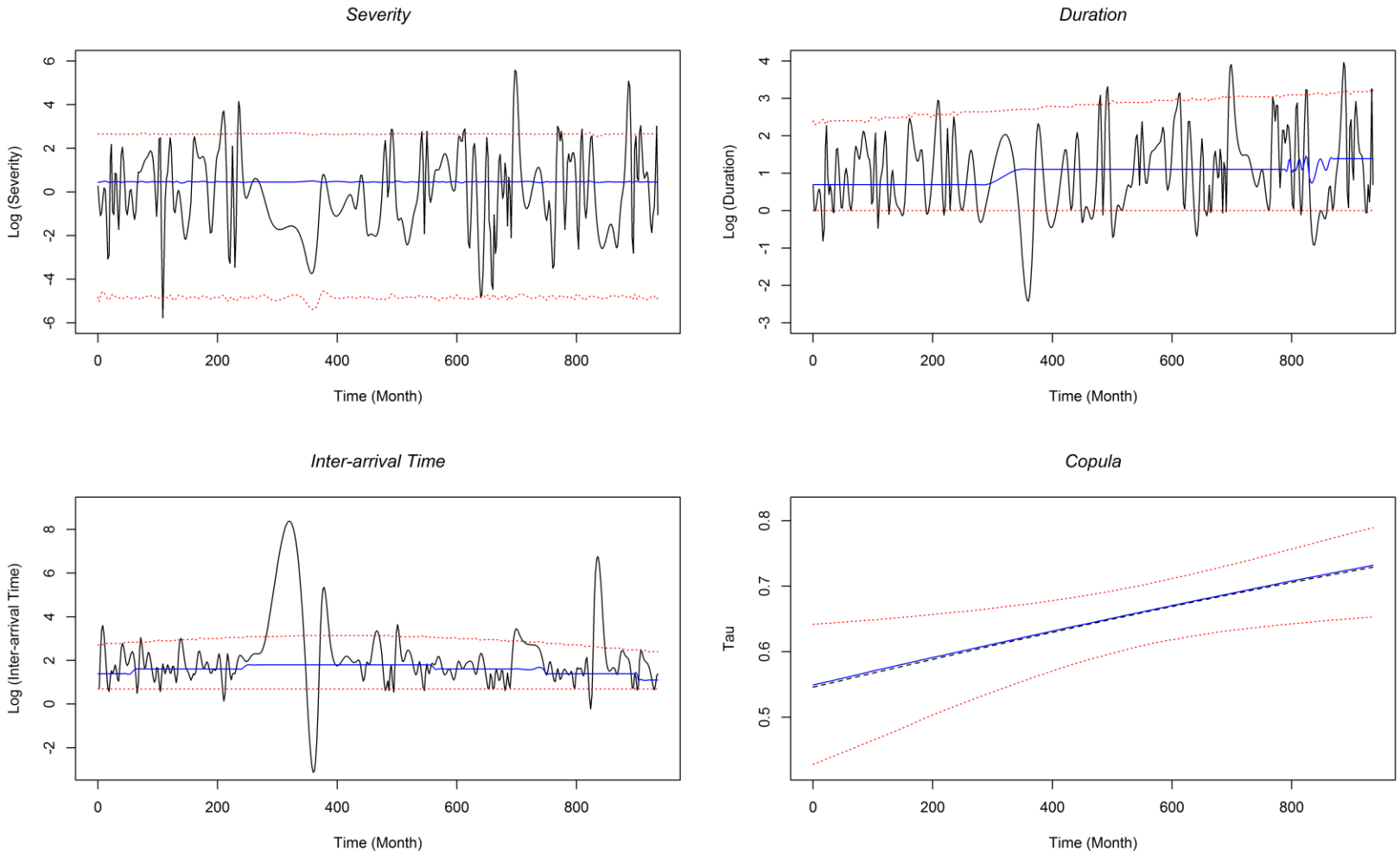

Figure 4-3. Predictive mean (blue dashed lines), true mean of Kendall's τ_t(black dashed line), 95 % Bayesian confidence intervals (red dotted lines), and drought multi-dimension time series (solid black lines) under forcing scenario RCP2.6

4.4.2.2 RCP4.5 Bayesian model

The results of the time varying models for the drought dimensions under the scenario of RCP4.5 are given in Table 4-3. For the severity characteristic, the derived DIC values indicate that the constant model is the most adequate model to describe the probabilistic behavior of severity observations. In terms of the drought duration dimension, the time varying negative binomial distribution is described in different forms of non-stationarity. The results indicate that the linear model is the best model to capture the time varying rate of drought occurrence over time under this climate change forcing scenario. Quite similar to the low emission scenario (RCP2.6) the results of the DICs indicate the superiority of the quadratic model with respect to the time-varying inter-arrival time dimension. The results of the predictive posterior mean and the Bayesian predictive intervals are illustrated in Figure 4-4. Observe that the 95% predictive intervals for the inter-arrival time dimension are narrow with the selected model, as some of the observations lie outside of the intervals. This seems realistic as around 5% of the observed data should be outside of these predictive intervals.

Similar to the RCP2.6 scenario, the results of the time varying Gumbel copula show that the linear function fits as the best model to the dependency structure.

4.4.2.3 RCP8.5 Bayesian model

The Bayesian modelling under the RCP8.5 is an interesting example demonstrating the importance of using a fully non-stationary-based Bayesian model for all the dimensions in a temporal evolution of the climate under a worst-case scenario.

Testing three different Bayesian models with respect to the drought dimensions under the current scenario demonstrates that based on the DIC criterion, the quadratic model is the best model describing the time varying selected distributions for all the dimensions (Table 4-4). The results obtained from the time-varying models are completely consistent with the trend analysis outputs and demonstrate the superiority of non-stationary quadratic-based Bayesian models in capturing a multivariate time-varying environment. Unlike the two previous scenarios, since under the current scenario both the severity and duration dimensions exhibit a quadratic non-stationary time dependent probabilistic behavior, the quadratic generalized Bayesian model proves to be an adequate model in describing the multivariate conditional dynamic copula. Figure 4-5 illustrates the drought dimension time series and the time-varying fitted Bayesian models under the RCP8.5 scenario.

Table 4-3. Parameter estimation and DIC results of the different forms of the generalized Bayesian models under RCP4.5 scenario

Scenario	Dimension	Statistical Model	Parameters	Posterior mean	Posterior St.	DIC
RCP4.5	Severity	**M0**	∂	1.298	0.104	**644.21**
		M1	∂	1.14	0.16	644.70
			ϱ	0.003	0.002	
		M2	∂	1.17	0.23	647.21
			ϱ	0.001	0.013	
			ι	3.14	0.0001	
	Duration	M0	η	1.42	0.11	731.94
		M1	η	0.715	0.211	**722.66**
			θ	0.001	0.0003	
		M2	η	0.58	0.23	722.93
			θ	0.002	0.0005	
			κ	-0.976	2.83	
	Inter-arrival time	M0	ψ	1.483	0.089	759.57
		M1	ψ	1.756	0.197	759.51
			ω	-0.0005	0.0003	
		M2	ψ	1.688	0.195	**758.70**
			ω	-0.0003	0.0004	
			ϑ	1.087	0.166	
	Copula	M0	ξ	0.655	0.104	-192.73
		M1	ξ	0.046	0.224	**-206.81**
			ν	0.129	0.036	
		M2	ξ	-0.049	0.383	-203.36
			ν	0.183	0.176	
			χ	-0.005	0.017	

Overall, the results of the Bayesian modelling demonstrate the complex non-stationary environments under three different climate change scenarios. The results also demonstrate the capability of the proposed methodology in modelling the different types of time-varying non-stationarities in the underlying dimensions arising from the complex environments under different radiative forcing scenarios.

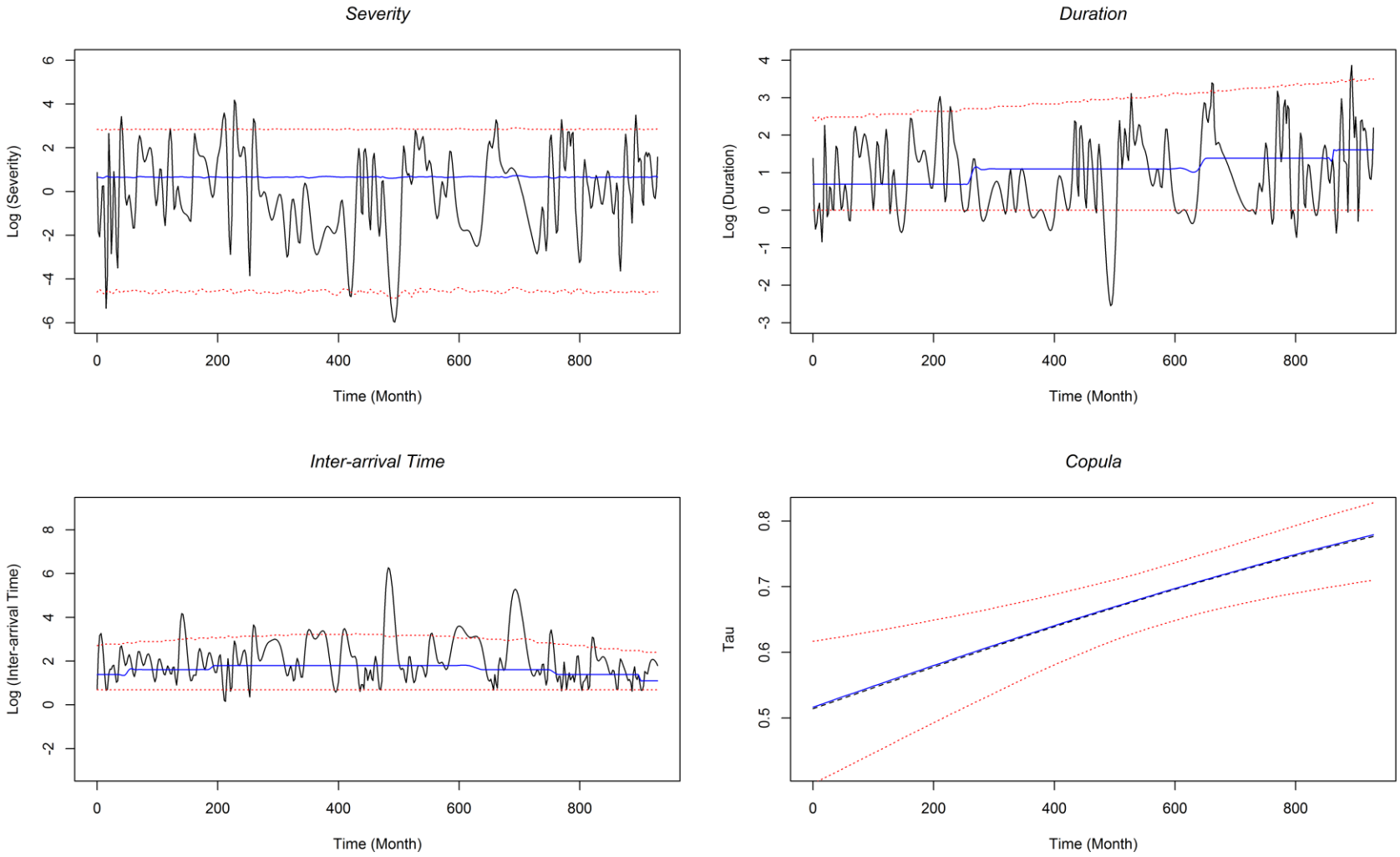

Figure 4-4. Predictive mean (blue dashed lines), true mean of Kendall's τ_t(black dashed line), 95 % Bayesian confidence intervals (red dotted lines), and drought multi-dimension time series (solid black lines) under forcing scenario RCP4.5

Table 4-4. Parameter estimation and DIC results of the different forms of the generalized Bayesian models under RCP8.5 scenario

Scenario	Dimension	Statistical Model	Parameters	Posterior mean	Posterior St.	DIC
RCP8.5	Severity	M0	∂	1.023	0.099	634.49
		M1	∂	0.796	0.172	634.05
			ϱ	0.004	0.003	
		M2	∂	1.267	0.222	**626.53**
			ϱ	-0.032	0.013	
			ι	0.0004	0.0001	
	Duration	M0	η	1.151	0.110	746.35
		M1	η	0.557	0.213	738.21
			θ	0.001	0.0003	
		M2	η	0.570	0.207	**737.39**
			θ	0.0009	0.0003	
			κ	1.660	2.241	
	Inter-arrival time	M0	ψ	1.358	0.090	815.77
		M1	ψ	1.688	0.179	813.20
			ω	-0.0006	0.0003	
		M2	ψ	1.605	0.180	**811.48**
			ω	-0.0002	0.0003	
			ϑ	-4.781	1.965	
	Copula	M0	ξ	0.572	0.100	-183.84
		M1	ξ	0.329	0.219	-186.88
			ν	0.043	0.035	
		M2	ξ	0.570	0.416	**-200.40**
			ν	-0.980	0.190	
			χ	0.013	0.017	

4.4.3 Bayesian time-varying joint return period

After selecting the best Bayesian models and constructing time-varying distributions and copula on the drought multi-dimensions using the MCMC algorithm, the results are employed in creating time varying joint return period in a multivariate risk framework. The results are given for the three forcing scenarios. In each scenario, as the time-varying joint return period plots cannot be shown over time in a 2D plot, three time frames from the design's life time period are selected for illustration of the time variation on the time-varying joint return period.

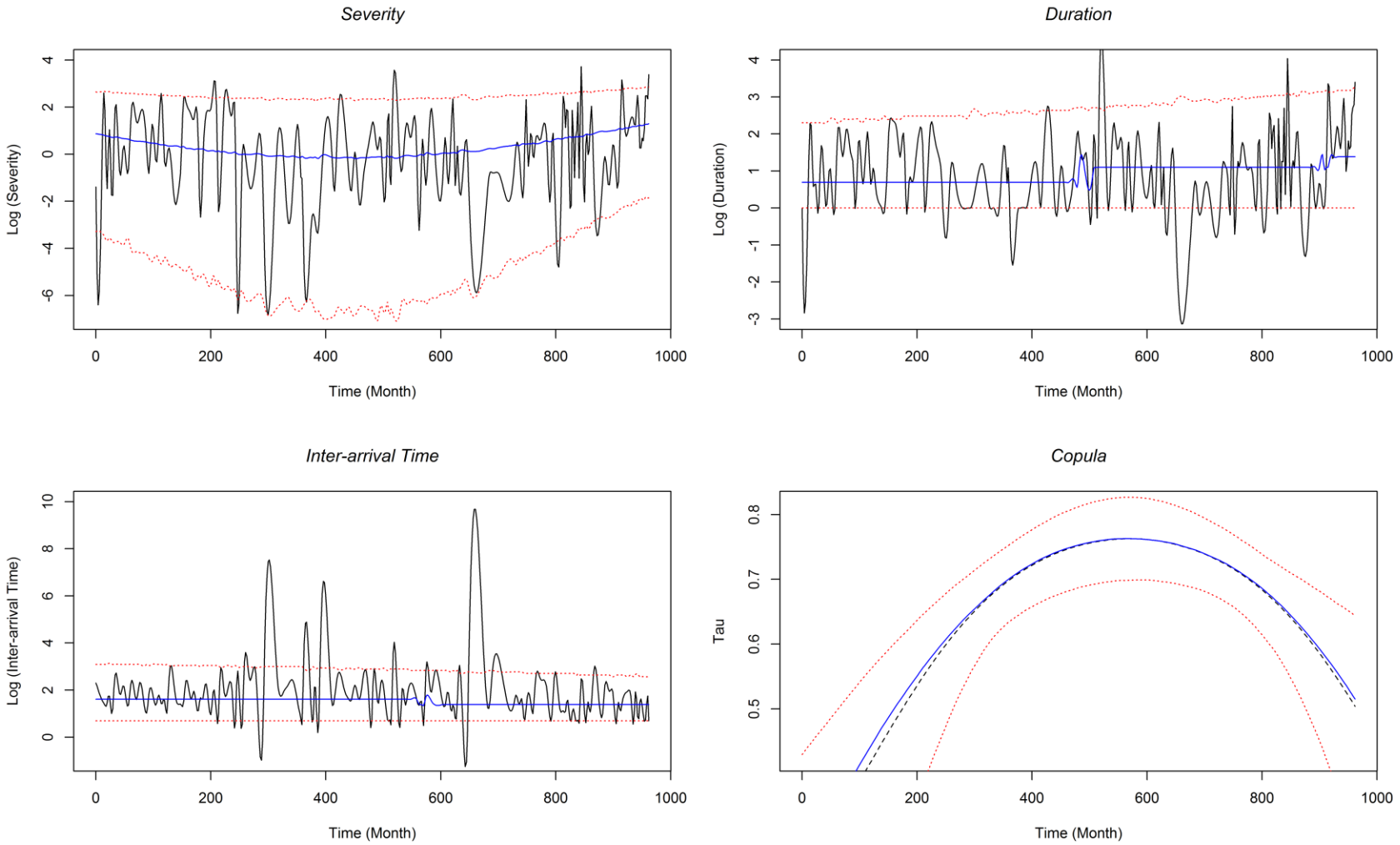

Figure 4-5. Predictive mean (blue solid lines), true mean of Kendall's τ_t(black dashed line), 95 % Bayesian confidence intervals (red dotted lines), and drought multi-dimension time series (black solid lines) under forcing scenario RCP8.5

The first time frame is year 2015, in which the historical observations till this time are employed for creating time-varying joint return period. The second time slice is 2065, a half century after 2015. Over this time period the time-varying joint return period is updated as time goes by. The last time frame is the year 2100. To show the performance of the proposed time-varying framework, the results of the time-varying non-stationary multivariate risk analysis are also compared with the outputs of the currently used time-independent stationary multivariate framework for the same time slices under the three forcing scenarios.

In the following the results of the time-varying non-stationary approach accompany the time-independent stationary multivariate risk analysis for the low and midrange green-house gas emission scenarios (RCP2.6 and RCP4.5) and the worst-case forcing scenario (RCP8.5), respectively.

4.4.3.1 Time-varying joint return period under RCP2.6 and RCP4.5

To show the time-varying non-stationary multivariate risk, the contours of joint probability for drought severity and duration using the dynamic copula and including the time-varying inter-arrival time dimension are illustrated in Figure 4-6(a) for the three time slices under scenario RCP2.6. The results of the time-independent stationary multivariate risk are also illustrated in Figure 4-6(b) for the three time slices under the same scenario. In these plots, historical observations and projected downscaled observations are exhibited separately. A critical return period covering the whole historical drought events is also highlighted as a milestone to better illustrate the flow of time-varying joint return period through time. At the first selected time slice (2015) in the time-varying multivariate framework, the historical drought events are located in the downside of the joint return period plot. This indicates that the majority of drought events occurring in this area have low joint return periods of less than 20 years. By the end of 2065 the majority of drought events are projected to occur with similar characteristics to those of the historical events based on the same framework, whereas some more severe drought events are likely to occur with return period between 20 and 100 years. At the end of the century, as seen in the plot, the number of extreme drought events that are more severe and longer (passing the critical return period) will likely be increased under this climate change scenario.

As illustrated in Figure 4-6(a), as time goes by, the time-varying joint contour plots are moving forward (tractable by following the critical RP contour) indicating that the time between drought events is decreasing and they are becoming more frequent over design's life period. In contrast, in the time-independent stationary framework illustrated in Figure 4-6(b), the risk of droughts is unchanged over the entire century without any changes in the characteristics of historical and projected droughts.

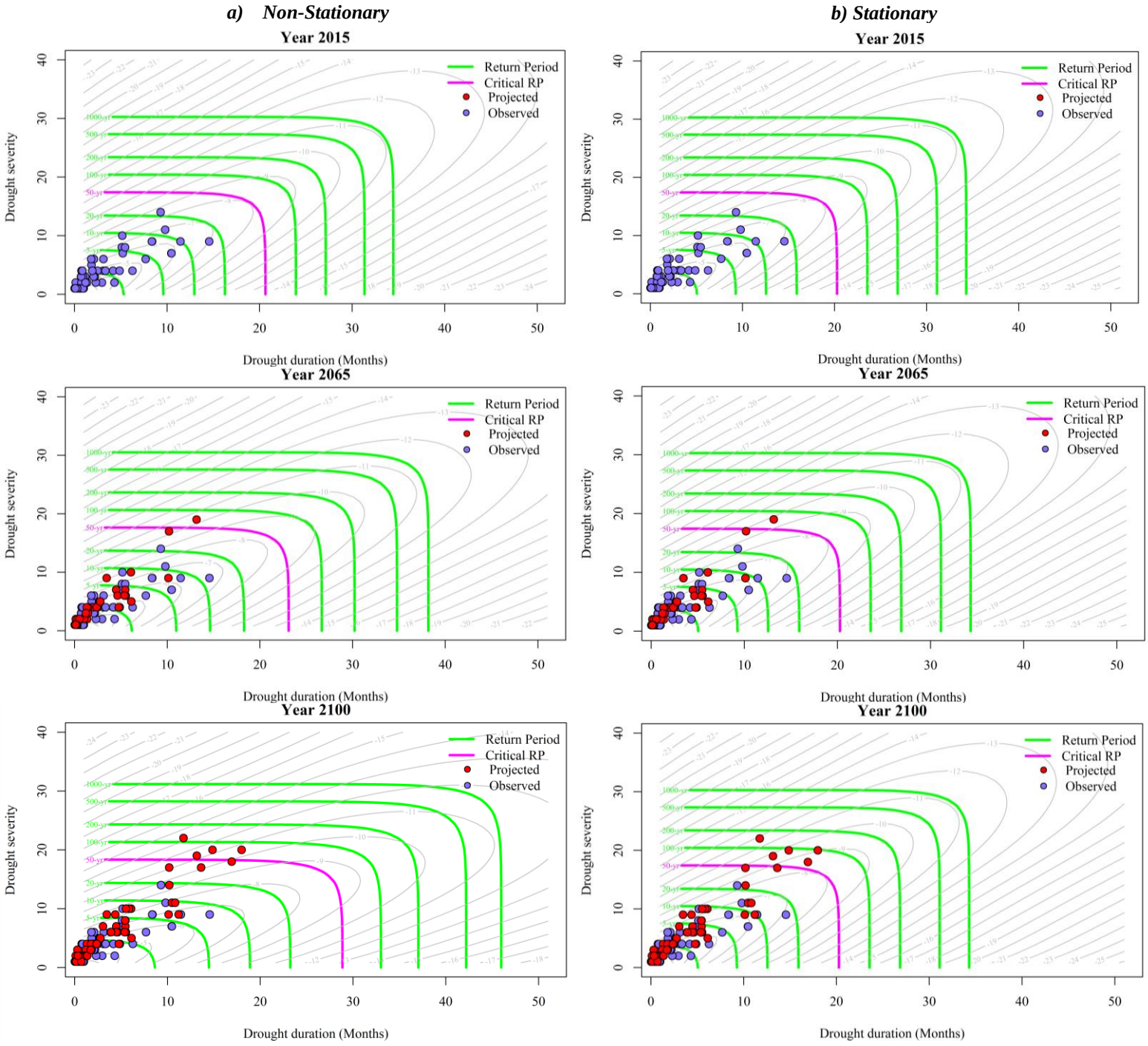

Figure 4-6. Dynamic (non-stationary) versus static (stationary) joint return period plots at three-selected time frames under scenario RCP2.6

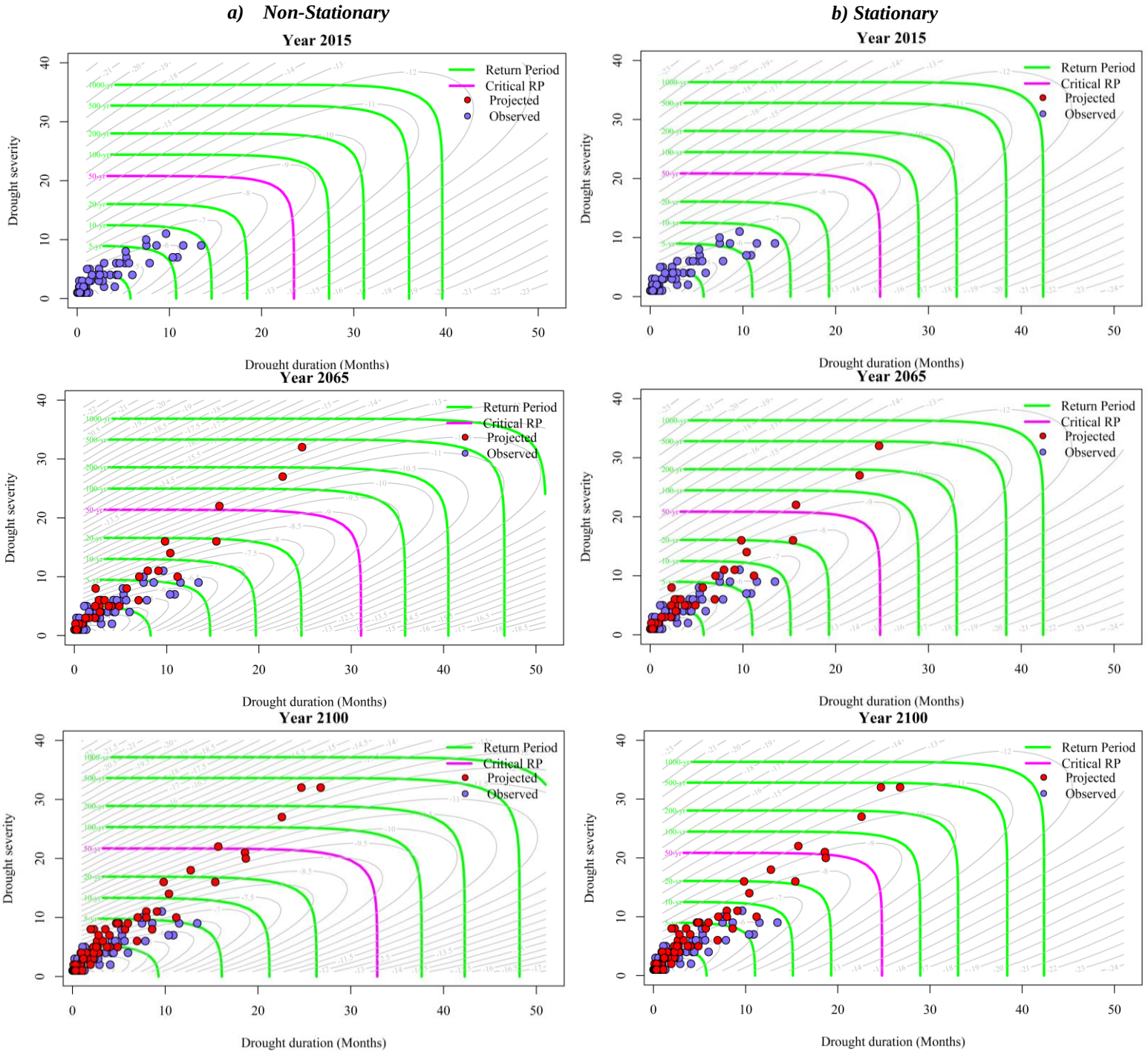

Figure 4-7. Dynamic (non-stationary) versus static (stationary) joint return period plots at three-selected time frames under scenario RCP4.5

In Figure 4-7(a) the results of the joint return period are illustrated based on the selected time-varying non-stationary models under the forcing scenario RCP4.5. As exhibited at the first time frame, all drought events occur under return period 10 years. Compared with the same time in the same framework under scenario RCP2.6, the drought events are much more frequent. It should be noted that the drought characteristics are extracted from the synthetized historical and projected precipitation time series. Synthetizing historical precipitation with different projected precipitation time series under different climate change scenarios leads to different SPI time series and subsequently different drought characteristics. That is the reason that the different time-varying joint probability are achieved over the first time period (2015) under the two underlying scenarios, whereas the historical observations are completely similar in the three scenarios.

4.4.3.2 Time-varying joint return period under RCP8.5

Modelled by quadratic-based Bayesian functions in terms of all the dimensions, the time-varying multivariate risk analysis under this scenario is carried out in a fully non-stationary condition. Figure 4-8(a) illustrates the time-varying joint return period plots at the three selected time frames under this scenario. As shown at the first time slice, the historical droughts over the time period until 2015 are having more severe and lengthier duration in comparison with the other two scenarios, so that more events are observed between return period 20 and 50 year. Ignoring the actual non-stationary environment by this time, the multivariate stationary framework, however, overestimates the risk of multivariate drought occurrences and the drought characteristics (shown in Figure 4-8(b)). As time progresses, in the second time period, the number of extreme events is not increased, and the majority of drought events will probably occur with the same characteristics as the historical events based on the multivariate non-stationary risk framework. However, it is interesting that the time between drought events are decreased in comparison with the other two scenarios. For instance, the events between contour plots of 20-50 years, seen in the previous time slice no longer exist over this time period and they have become much more frequent and moved towards the lower joint return periods. That demonstrates that the drought characteristics are changing over time under the impact of the worst-case climate change scenario. In multivariate stationary framework, however, the risk and the nature of droughts are unchanged over time. In comparison with the non-stationary environment, the time-independent stationary assumption underestimates the length and the risk of droughts (especially frequent droughts) by this time slice.

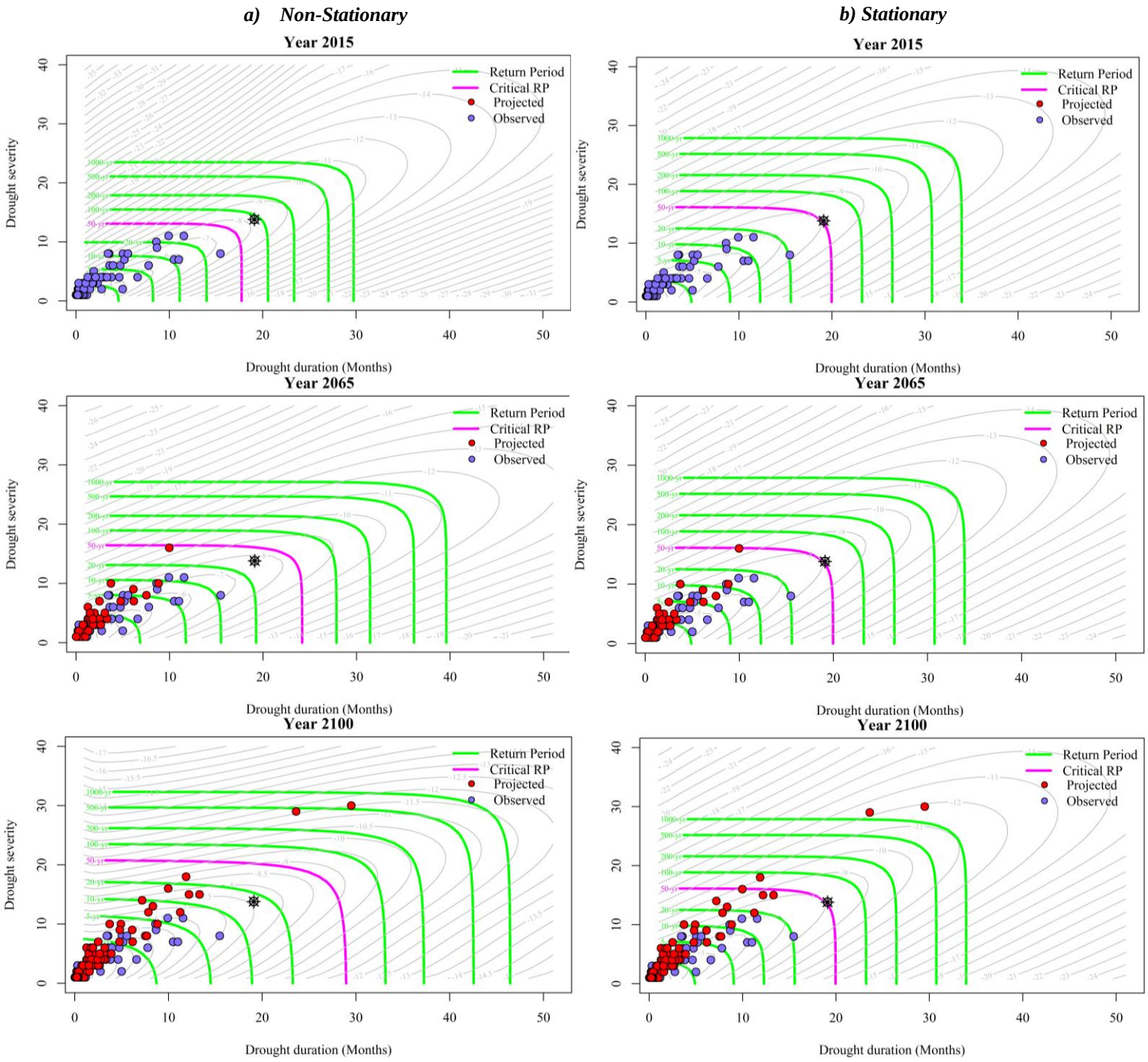

Figure 4-8. Non-stationary (time-varying) versus stationary (static) joint return periods for three time slices of the INM-CM4 model under scenario RCP8.5. The risk changes of the particular assumed drought (symbolized as a black star) are also illustrated in both frameworks

Over the last time period, not only the number of much more severe and lengthy droughts will likely be increased under the critical return period, but also two rare extreme events probably occur under this worst forcing scenario based on the time-varying non-stationary risk framework. The return period of these events are between 500-1000 years, meaning that they are extreme droughts with large potential damage consequences. However, the currently used multivariate time-independent stationary-based risk analysis shows remarkable discrepancy with the multivariate time-varying non-stationary one so that it underestimates the risk of drought occurrences (for all the frequent and extreme events) and both the drought severity and drought duration. Therefore, the adverse consequences arising from ignoring the non-stationary condition and changing the nature and the risk of droughts in the time-independent stationary multivariate framework under this climate change scenario will seriously threaten various sectors of the Tehran city, especially drinking water sector.

In comparison to the other two scenarios (RCP2.6 and RCP4.5), all the multi-dimensions (including marginal, copula, and inter-arrival time) are exhibiting a non-stationary behavior under this scenario. Since the joint return period is also a function of the time-varying multi-dimensions, as time progresses over the design's life period, the speed of the forward moving of the contour plots is consequently greater than the previous scenarios. This indicates that the nature of drought characteristics are severely and fast changed under this worst greenhouse gas emission scenario.

To better compare the concept of risk in the two frameworks, an example is given in Figure 4-8. An assumed symbolized severe drought event (illustrated in black) represents joint multi-dimensions of the severity 14.0 and the duration of 19.0 months. The results indicate that under the currently-used static risk framework, droughts having the same joint multi-dimensions constantly occur in return period of 50yr without any changes over the entire design period. According to the time-varying framework in the dynamic condition, however, the same characterized drought event having a joint return period of about 100yr occurs less frequent than the drought in the static framework at the beginning of the century. Such overestimation of the risk (joint return period) in the static framework raises infrastructure designing costs and the management of water systems, whereas that is not necessarily based on an actual adaptive time-varying risk framework.

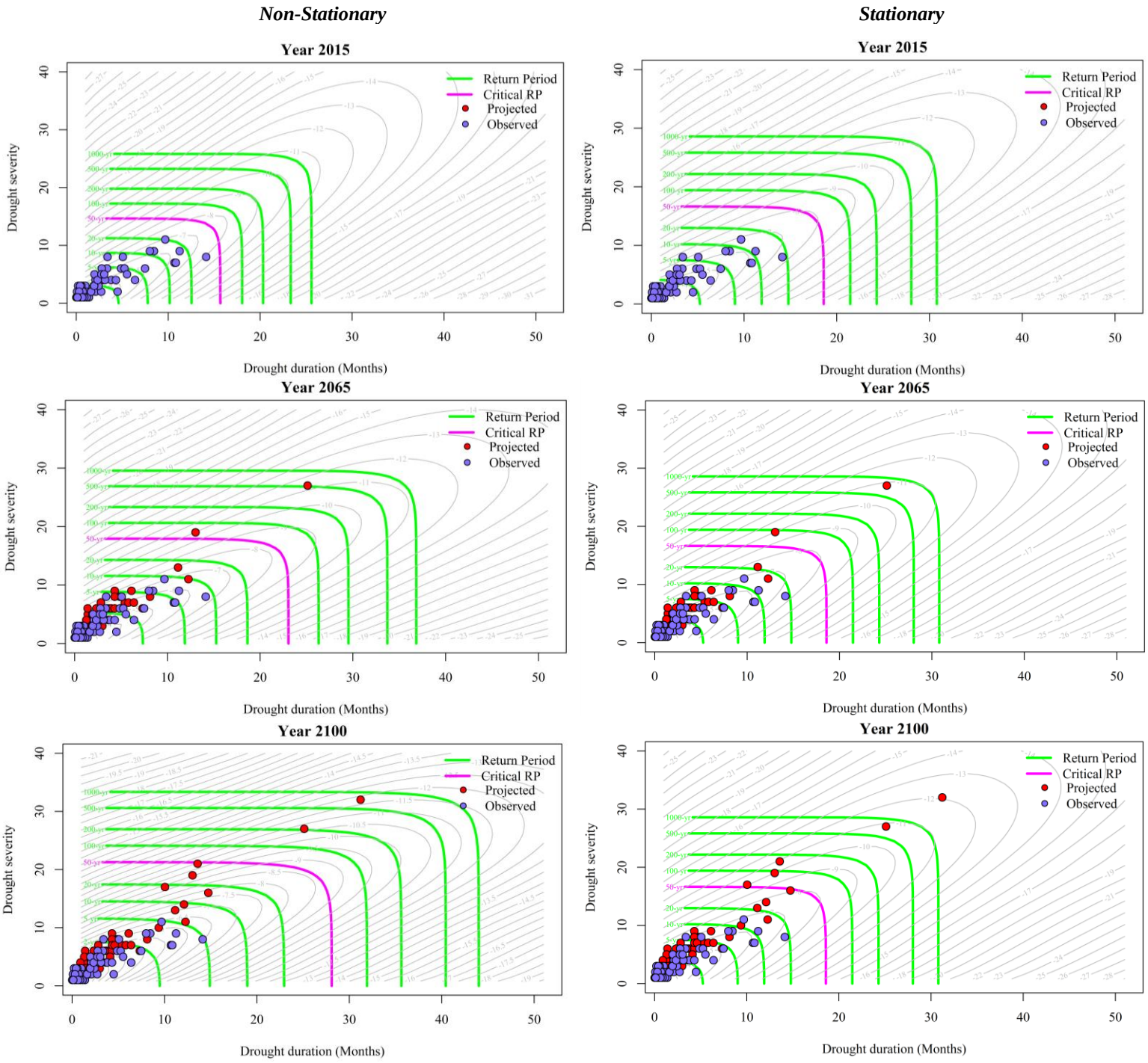

Figure 4-9. Non-stationary versus stationary joint return periods for the three time slices of the GFDL-ESM2M model.

The nature of the joint characterized droughts, however, change over time under the dynamic condition and become much worse in comparison with the static framework, so that the same severe multi-dimensional drought becomes much more frequent with return period of 15yr at the end of the century.

The results indicate that after 2030s the static stationary framework will be underestimating the risk of projected extreme multi-dimensional droughts. That means if the nature-changing assumption of extreme multi-dimensional droughts is overlooked and such a static-based risk framework is used for water system designs, the systems may not be able to withstand drought conditions as the actual risk is higher than that for which the systems are designed. Similar results are achieved for the other synthetized climate models. For example in the GFDL-ESM2M model in Figure 4-9, likewise to the behavior of the INM-CM4 model, the essence of droughts is dynamic and drought characteristics are changing over time in the non-stationary condition for this model as well. In the stationary condition, however, the risk of droughts is constant over the time period.

The results demonstrate that the essence of the complex multi-dimensional droughts is dynamic under altering environment arising from climate change and subsequently the risk of their occurrence will also become dynamic over time.

Figure 4-10 also illustrates the uncertainty in the estimation of joint return period over time in the two stationary and non-stationary based multivariate risk frameworks (based on the GFDL-ESM2M model). The results are shown for a historical event that occurred in 1955 (with the severity $S \geq s = 11.5$ and the duration of $D \geq d = 11$ months). As illustrated in the figure, under the fully nonstationary risk framework, the mean joint return period of such a multi-dimensional event changes over time. The results indicate that the mean joint return period will become less in the future, and such an extreme drought will occur frequently by the end of the century. In the stationary-based risk framework, the mean joint return period of such an extreme event is assumed static without any changes over the entire lifetime. This inability of the currently used multivariate stationary risk framework in capturing actual changing joint return period may lead to high uncertainty and failure of risk plans in water resource systems.

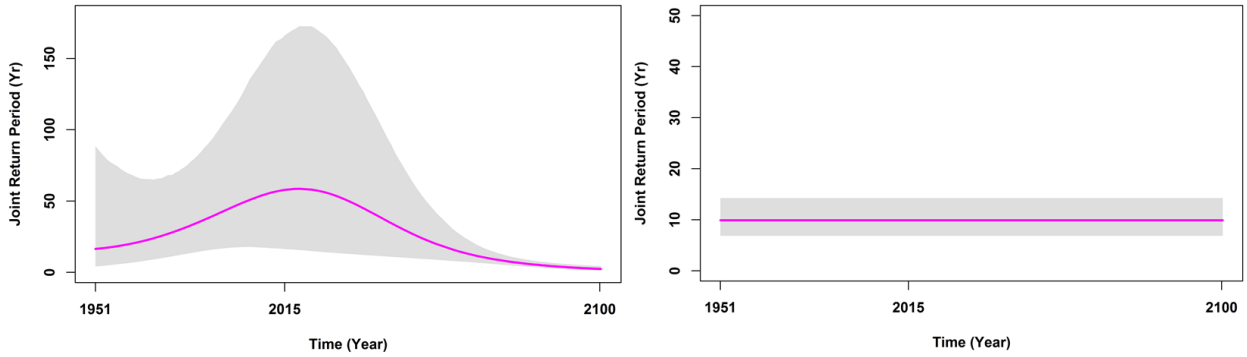

Figure 4-10. The uncertainty of mean joint return period over time with duration and severity equal to or greater than the 1955 Tehran extreme drought in nonstationary and stationary multivariate risk framework. The shaded area illustrate Bayesian Credible Intervals (2.5% and 97.5%) for the return periods

Overall future dynamic-nature extreme droughts will be compounded with severe and long-time impacts. In addition, co-occurrence of more severe droughts accompany with soaring temperature arising from global warming will increase water demand and the challenge of water resources allocation for various sectors, especially drinking water. As drought characteristics change over time through anthropogenic effects, lessons from the past droughts cannot be applied to the future drought events (AghaKouchak et al., 2015). Thus, to mitigate adverse consequences, water resources authorities should be prepared for new characterized drought situations in a warmer environment by defining proactive and long-term effective drought management strategies. Infrastructure adaptations, demand management, improving water-conservation technologies, developing an advanced prediction-monitoring system, raising awareness and public perception, and long-term water policy reforms could be some management long-term mitigation strategies.

The introduced time-varying multivariate risk concept can be effectively used for infrastructure designs and water resources planning. Using the time-varying risk strategy, one is able to estimate to what extent the probability of exceedance associated with extreme multi-dimensional climate event occurrences may change under the intensified non-stationary conditions. Knowing that, engineering designers can reduce uncertainties in the estimation of risk, which results in enhancing reliability of water resources infrastructure designs and reducing the potential costs. In terms of water resources planning and management, using the multivariate nonstationary risk framework, one is also able to project the time-varying frequency and magnitude of multi-dimensional extreme events under the impact of climate change. In this case, ensemble IPCC model runs can be used as an application for

future projection of multi-dimensional extreme events in near and long-term periods. Managers can better operate water supply systems to deliver the water that is demanded with more reliability under a complex and uncertain changing climate. The time-varying risk can be designed for any fine or coarse temporal resolutions. Depending on the context that the time-varying multivariate risk framework is developed for, it can be updated over time by adding new information (observations) for the same time-scale.

4.5 Conclusions

Climate change is impacting hydrological processes leading to increasing the risk of climate extremes. Accordingly, time-varying non-stationary-based multivariate probabilistic modelling concepts should be developed and adopted for risk-based decision-making in water resources planning and designs.

In the present study, a Bayesian procedure is proposed to perform joint Bayesian inference for a conditional copula model describing dependence between continuous (drought severity) and discrete (drought duration) dimensions. The Bayesian inference approach allows estimation of time varying marginal and copula distribution parameters in a two-stage estimation procedure for mixed complicated situations when one of the marginals is discrete. To capture different types of non-stationarity through time, the Bayesian inference is employed to estimate different formats of the generalized additive model parameters. To make the inference and to estimate the parameters, the Gibbs MCMC sampler is employed to generate sample realizations from the posterior distributions. Moreover, the credibility of the Bayesian predictive intervals are also developed providing information about the precision of the estimates. This study has also improved the concept of the joint return period in multivariate risk studies to a fully time-varying joint return period concept through considering inter-arrival time as a time-varying dimension.

The proposed approach in the present study offers a number of advantages. One of the main benefits is producing fully likelihood-based inference to model complex time-varying multivariate non-stationary condition arising from climate change. The approach is able to handle modelling any complex hydro-climate extreme phenomena with complicated time-varying dependence structures consisting of mixed dimensions (continuous and discrete). It is also flexible for modelling mixtures of stationary and non-stationary conditions for multi-dimensions. The study also demonstrates that the

risk of multi-dimensional extreme climate processes becomes time-varying under the impact of climate change. Accordingly, to mitigate adverse consequences arising from these new characterized natural hazards, the associated authorities should keep updating long-term proactive strategies based on anomalies of dynamic anthropogenically forced environments. Updating long-term decision-making strategies, however, requires interdisciplinary cooperation of engineers, policy makers, climate experts, and economists.

Summary, Conclusions, and Future Work

Under the changing climate, the safety and the security of water infrastructure is influenced by the risk of extreme hydro-climatic phenomena. Potential global warming-induced-changes to the extreme hydro-climatic processes call into question the reliability and the accuracy of the currently-used design concepts. The increasing impact of climate change on extreme hydro-climatic phenomena around the world (Coumou and Rahmstorf, 2012) implies that the nature and the risk of these multi-dimensional phenomena are being changed. This thesis first proposes a comprehensive methodology to improve predictive power of the statistical downscaling models for enhancing credibility of climate-related projections in defining long-term strategies and quantifying uncertainties under the impact of climate change. The thesis then outlines a novel framework of a multi-dimensional time-varying risk concept to be incorporated in updating infrastructure design strategies under dynamic environments arising from climate change. This new generation of the adaptive multi-dimensional time-varying risk methodology can be applied for any types of multi-dimensional hydro-climate processes to study anomalies of extreme events arising from climate change.

The following sections outline the concluding remarks as well as recommendations for future work based on the findings in each chapter.

4.6 Summary and Concluding Remarks

Chapter 2 is the first study to introduce a supervised nonlinear dimensionality reduction method to the regression-based statistical downscaling. The algorithm derives a low-dimensional manifold from high-dimensional atmospheric variables conveying relevant climate change information and having maximal dependency with the target variable. The comparison of the results reveals that the proposed supervised PCA methods outperform most of the existing state-of-the-art dimensionality reduction algorithms in terms of the future projection accuracy of the hydro-climate variable in the statistical downscaling process. Specific conclusions from this chapter are outlined as follows:

- The proposed supervised PCA is able to capture certain modes of variability in the atmospheric variables along directions that are associated with the target hydro-climate variable. Using derived subspaces that have maximum dependency with the target variable

improves the predictive power of the regression-based statistical downscaling modelling. It thus leads to projecting more accurate future behavior of hydro-climate variables under the impact of climate change.

- The developed Kernel Supervised PCA algorithm can capture the complexity and nonlinear dependence between the target precipitation and high-dimensional projector variables and also interdependency within atmospheric projectors. The algorithm does this through a nonlinear mapping of the atmospheric projectors using different kernel functions to compute low-dimensional principal components. This ability allows projecting any complexity in climate change signals to improve the accuracy of hydro-climate variable projections under the statistical downscaling process.
- Comparison between precipitation projections derived from the application of conventional PCA (as a standard dimensionality reduction) and Kernel Supervised PCA in the statistical downscaling reveals the former method acts poorly in terms of extreme event projections under RCP scenarios. Using a supervised dimensionality reduction model thus results in reducing this source of uncertainty and improving projection of extreme observations of hydro-climate variables under different GCM models and climate change scenarios for the upcoming decades.

Chapter 3 develops a comprehensive methodology to address other sources of uncertainties in the regression based statistical downscaling. In addition to the impact of high dimensional feature space, this chapter engages soft-computing nonlinear machine learning to capture nonlinear relationships between predictand and atmospheric predictors. In this chapter a Multivariate Recursive Nesting Bias Correction (MRNBC) approach is also proposed to correct biases arising from differences between observed and simulated large-scale atmospheric projectors and to represent anomalies of the large-scale teleconnections in GCM simulations. The following conclusions are drawn in Chapter 3:

- The results demonstrate the effectiveness of the Multivariate Recursive Nesting Bias Correction (MRNBC) in simultaneously correcting temporal and spatial biases over multiple time-scales in cross dependent multi projectors. Applying this procedure in the statistical downscaling leads to reducing different sources of uncertainty and improving

the accuracy of the projections of hydro-climate processes for defining long-term strategies in response to potential future changes.

- The results demonstrate the superiority of the Bayesian learning algorithm (RVM) in capturing any types of complexity and nonlinearity in quantitative empirical relationship between the target variable and atmospheric predictors. The Bayesian based machine learning method shows high efficiency in minimizing the possibility of overfitting and computational time processing. These advantages make RVM a powerful method compared with other learning algorithms to improve performance accuracy of statistical downscaling and future projection of any hydro-climate variables under the impact of climate change.
- The results of the two DOE-based frameworks reveal that the developed downscaling model (consisting of the Kernel Supervised PCA and the RVM model) is credible to project precipitation behaviour under possible future dynamic non-stationary climates arising from global warming. The DOE experiments address unaltered empirical relations in the statistical downscaling models under non-stationary conditions. The experiments demonstrate that the statistical downscaling models are trustworthy and adjusted to the changes arising from global warming.
- The proposed comprehensive methodology enhances the predictive power of regression-based statistical downscaling through addressing the impact of different sources of uncertainties. This leads to more accurate understanding about the impact of climate change on the future behaviour of different types of hydro-climate variables. Relying on the projections, decision makers will thus be able to better define effective and long-term strategies to mitigate adverse consequences arising from global warming on the availability of surface water resources.

It should also be noted that the all analyses in Chapter 2 and Chapter 3 are employed to reduce different sources of uncertainties (high-dimensionality, biases, and nonlinear functional relationships) to project precipitation in a consistent target monthly-based temporal scale. The same procedures can be easily applied to project precipitation (or other hydro-climate variables) for other finer temporal resolutions (e.g. weekly, daily, hourly-based scales) depending on the context. Using other temporal

resolutions for the aforementioned chapters may give rise to dissimilar outcomes in terms of reducing different sources of uncertainties.

Chapter 4 demonstrates that in a changing climate arising from anthropogenic global warming, the nature and the risk of extreme climatic events are changing over time. To strengthen the reliability of infrastructure designs and the management of water systems in the changing environment, existing analytical methods in multi-dimensional risk studies should be replaced with a new adaptive perspective. The results of a comparison indicate that current time-independent (static) multi-dimensional risk frameworks are no longer applicable to projecting the probabilistic behavior under changing multi-dimensional extreme climate processes. Using stationary-based methods may result in undesirable consequences in designing water system infrastructures. The time-independent concept should therefore be replaced with a flexible multi-dimensional time-varying risk framework. Chapter 4 develops a new multi-dimensional time-varying risk concept to be incorporated in updating infrastructure design strategies under changing environments arising from human-induced climate change. Specific conclusions in this chapter are outlined as follows:

- The proposed multivariate time-varying risk framework develops joint Bayesian inference for conditional copula model describing time-varying dependence between mixed continuous and discrete drought marginals over time. The Bayesian framework makes inference by generating iterative samples from the full conditional marginals and joint distribution to estimate related marginals and copula time-dependent parameters. The multivariate framework is full likelihood-based Bayesian inference where the whole set of parameters is allowed to change over time. The framework is thus able to integrate any anomalies in extreme multi-dimensional droughts in non-stationary conditions arising from global warming.
- The framework also introduces a fully Bayesian, time-varying Joint Return Period (JRP) concept. Using the new concept, one is able to compute the extent of risk changes of extreme multi-dimensional droughts over time. It is also possible to exhibit how the nature of extreme climate phenomena is changing under the impact of climate change. The other unique feature of the framework is the computation of the uncertainty in terms of JRP using time-varying multi-dimensions (marginal, copula, and inter-arrival time) in the changing environments under climate change scenarios against stationary condition.

- The credibility of the Bayesian predictive intervals can be developed providing information about the precision of the estimates. The framework also measures uncertainty of time varying distribution parameters of the drought dimensions estimated through the posterior distribution of the MCMC samples in the non-stationary and stationary conditions. Considering a trend imposes a certain type of non-stationarity, the best statistical models are selected on the outputs of posterior distributions to capture different forms of non-stationarity.
- The results demonstrate that using time-independent multivariate risk methodologies may lead to high uncertainty for infrastructure designs and inaccurate estimates of the risk of failure for water resources systems. To avoid undesirable consequences, it is thus of crucial importance to update the current time-independent design concepts and substitute the new generation of the adaptive multi-dimensional time-varying-based methodologies for future risk-based designs in water resources systems. Applying the new concept, one is able to adapt the design of water systems and infrastructure to the dynamic conditions generated by climate change.

4.7 Recommendations for Future Research

Chapter 2 uses the Supervised PCA technique, which focuses on deriving new reduced-dimension features having maximum dependency on the target variable by transformations of the original feature dataset. Supervised PCA therefore does not consider the local structure of the data and subsequently it cannot extract intrinsic dimensionality of the data. Future research can focus on improving this characteristic of Supervised PCA.

Although the Regional Climate Models (RCMs) require expensive and complicated computations and use biased lateral boundary inputs, future research may focus on comparison of the dynamic downscaling results and the comprehensive statistical downscaling methodology in Chapter 3. Such comparison could address the uncertainty arising from the application of GCMs and RCMs in projecting hydro-meteorological processes under different climate change scenarios. Future research can be directed to apply deep structure learning techniques (Deep Learning) in the statistical downscaling. Deep learning is characterized as a class of machine learning that can model multiple levels of representations of large scale atmospheric observations using multiple processing layers.

Deep structure learning can explain entire variance of a response variable in the statistical downscaling and project extreme minimum and maximum hydro-climate events with high accuracy under RCP scenarios. In Chapter 3, the Euclidean distance approach is used to obtain signatures of climate changes for scenarios PI and RCP8.5. Development of other sequence pattern matching may improve similarity measurement to better identify climate change signatures.

The current time-independent stationary-based risk concepts in multi-dimensional climate change studies should be replaced with the new proposed time-varying multivariate insight of risk analysis in Chapter 4. Thus future work can focus on developing the same concept for different copula families and compare their performances for selecting the best dynamic copula. Using simultaneous estimation of both marginal and copula distributions' parameters in contrast with the two-stage procedure may lead to better understanding of the parameter dependences and also result in better performance of model selection criteria.

Extreme climate phenomena are regional processes and their impacts vary from region to region. The proposed risk concept in this thesis can also be extended to a regional multivariate time-varying framework to assess the risk of multi-dimensional extreme events at a regional scale under non-stationary conditions arising from climate change. In the regional context, multi-dimensional extreme events in different sites in homogeneous regions are spatially inter-dependent in one way or another. To study spatially varying multi-dimensional extreme climate processes or dimensions of two extreme phenomena, the dependence between pairs of sites in a spatial context can thus be taken into account in the time-varying risk framework for future research. The multivariate time-varying risk framework can also be more generalized by fitting Generalized Extreme Value (GEV) distribution to each marginal. According to the extreme value theory, each joint extreme dimension can generally be described by the GEV as the most frequently used distribution for extreme value analysis. Further research should also be dedicated to apply and develop the proposed framework for other stochastic multi-dimensional systems that are under the influence of changing environments.

References

AghaKouchak, A., Easterling, D., Hsu, K., Schubert, S., Sorooshian, S., 2012. Extremes in a changing climate: detection, analysis and uncertainty, 65. Springer Science & Business Media.

AghaKouchak A., Feldman D., Hoerling M., Huxman T., Lund J., 2015. Recognize Anthropogenic Drought,. Nature, 524 (7566). DOI:409-4011, doi:10.1038/524409a

Ahmadi, A., Han, D., Lafdani, E.K., Moridi, A., 2014. Input selection for long-lead precipitation prediction using large-scale climate variables: a case study. Journal of Hydroinformatics, 17(1): 114-129.

Ausin, M.C., Lopes, H.F., 2010. Time-varying joint distribution through copulas. Computational Statistics & Data Analysis, 54(11): 2383-2399.

Bai, Y., Wang, P., Li, C., Xie, J., Wang, Y., 2014. A multi-scale relevance vector regression approach for daily urban water demand forecasting. Journal of Hydrology, 517: 236-245.

Ballato, P. et al., 2010. Middle to late Miocene Middle Eastern climate from stable oxygen and carbon isotope data, southern Alborz mountains, N Iran. Earth and Planetary Science Letters, 300(1): 125-138.

Barshan, E., Ghodsi, A., Azimifar, Z., Zolghadri Jahromi, M., 2011. Supervised principal component analysis: Visualization, classification and regression on subspaces and submanifolds. Pattern Recognition, 44(7): 1357-1371. DOI:10.1016/j.patcog.2010.12.015

Bayazit, M., 2015. Nonstationarity of Hydrological Records and Recent Trends in Trend Analysis: A State-of-the-art Review. Environmental Processes, 2(3): 527-542. DOI:10.1007/s40710-015-0081-7

Bender, J., Wahl, T., Jensen, J., 2014. Multivariate design in the presence of non-stationarity. Journal of Hydrology, 514: 123-130.

Bennett, K.E., Werner, A.T., Schnorbus, M., 2012. Uncertainties in Hydrologic and Climate Change Impact Analyses in Headwater Basins of British Columbia. Journal of Climate, 25(17): 5711-5730. DOI:10.1175/jcli-d-11-00417.1

Borgomeo, E. et al., 2014. Risk-based water resources planning: Incorporating probabilistic nonstationary climate uncertainties. Water Resources Research, 50(8): 6850-6873. DOI:10.1002/2014wr015558

Chebana, F., Ouarda, T.B., 2011. Multivariate quantiles in hydrological frequency analysis. Environmetrics, 22(1): 63-78.

Chebana, F., Ouarda, T.B., Duong, T.C., 2013. Testing for multivariate trends in hydrologic frequency analysis. Journal of Hydrology, 486: 519-530.

Chen, H., Xu, C.-Y., Guo, S., 2012. Comparison and evaluation of multiple GCMs, statistical downscaling and hydrological models in the study of climate change impacts on runoff. Journal of Hydrology, 434: 36-45.

Chen, S.T., Yu, P.-S., Tang, Y.-H., 2010. Statistical downscaling of daily precipitation using support vector machines and multivariate analysis. Journal of Hydrology, 385(1-4): 13-22. DOI:10.1016/j.jhydrol.2010.01.021

Cheng, L., AghaKouchak, A., 2014. Nonstationary precipitation intensity-duration-frequency curves for infrastructure design in a changing climate. Scientific reports, 4, 7093. DOI: 10.1038/srep07093.

Corbella, S., Stretch, D.D., 2013. Simulating a multivariate sea storm using Archimedean copulas. Coastal Engineering, 76: 68-78.

Coumou, D., Rahmstorf, S., 2012. A decade of weather extremes. Nature Climate Change, 2(7): 491-496.

Creal, D.D., Tsay, R.S., 2015. High-dimensional dynamic stochastic copula models Journal of Econometrics, 189(2): 335-345.

Cunderlik, J.M., Jourdain, V., Quarda, T.B., Bobée, B., 2007. Local non-stationary flood-duration-frequency modelling. Canadian Water Resources Journal, 32(1): 43-58.

De Michele, C., Salvadori, G., 2003. A generalized Pareto intensity-duration model of storm rainfall exploiting 2-copulas. Journal of Geophysical Research: Atmospheres (1984–2012), 108(D2): 4067. DOI:10.1029/2002JD002534

De Michele, C., Salvadori, G., Vezzoli, R., Pecora, S., 2013. Multivariate assessment of droughts: Frequency analysis and dynamic return period. Water Resources Research, 49(10): 6985-6994.

DeChant, C.M., Moradkhani, H., 2015. On the assessment of reliability in probabilistic hydrometeorological event forecasting. Water Resources Research, 51: 3867–3883. DOI:10.1002/ 2014WR016617.

Dellaportas, P., Smith, A.F., 1993. Bayesian inference for generalized linear and proportional hazards models via Gibbs sampling. Applied Statistics, 42: 443-459.

Dery, S.J., Wood, E.F., 2005. Observed twentieth century land surface air temperature and precipitation covariability. Geophysical Research Letter, 32: L21414. DOI:10.1029/2005GL024234.

Dibike, Y., Coulibaly, P., 2005a. Hydrologic impact of climate change in the Saguenay watershed: comparison of downscaling methods and hydrologic models. Journal of hydrology, 307(1): 145-163.

Dibike, Y., Velickov, S., Solomatine, D., Abbott, M., 2001. Model induction with support vector machines: Introduction and applications. Journal of Computing in Civil Engineering, 15(3): 208–216.

Dibike, Y.B., Coulibaly, P., 2005b. Hydrologic impact of climate change in the Saguenay watershed: comparison of downscaling methods and hydrologic models. Journal of Hydrology, 307(1-4): 145-163. DOI:10.1016/j.jhydrol.2004.10.012

Dingbao Wang, X.C., 2013. Constructing Comprehensive Datasets for Understanding Human and Climate Change Impacts on Hydrologic Cycle. Irrigation & Drainage Systems Engineering, 02(01): 1000106. DOI:10.4172/2168-9768.1000106

Du, T. et al., 2015. Return period and risk analysis of nonstationary low-flow series under climate change. Journal of Hydrology, 527: 234-250. DOI:10.1016/j.jhydrol.2015.04.041

Ehret, U., Zehe, E., Wulfmeyer, V., Warrach-Sagi, K., Liebert, J., 2012. HESS Opinions" Should we apply bias correction to global and regional climate model data?". Hydrology and Earth System Sciences Discussions, 9(4): 5355-5387.

El Adlouni, S., Ouarda, T., Zhang, X., Roy, R., Bobée, B., 2007. Generalized maximum likelihood estimators for the nonstationary generalized extreme value model. Water Resources Research, 43(3): W03410. DOI:10.1029/2005WR004545.

El Adlouni, S., Ouarda, T.B.M.J., 2009. Joint Bayesian model selection and parameter estimation of the generalized extreme value model with covariates using birth-death Markov chain Monte Carlo. Water Resources Research, 45(6): W06403. DOI:10.1029/2007wr006427

Fowler, H.J., Blenkinsop, S., Tebaldi, C., 2007. Linking climate change modelling to impacts studies: recent advances in downscaling techniques for hydrological modelling. International Journal of Climatology, 27(12): 1547-1578. DOI:10.1002/joc.1556

Galelli, S. et al., 2014. An evaluation framework for input variable selection algorithms for environmental data-driven models. Environmental Modelling & Software, 62: 33-51. DOI:10.1016/j.envsoft.2014.08.015

Galloway, G.E., 2011. If Stationarity is Dead, What Do We Do Now?. Journal of the American Water Resources Association, 47(3): 563-570. DOI:10.1111/j.1752-1688.2011.00550.

Geweke, J., 1991. Evaluating the accuracy of sampling-based approaches to the calculation of posterior moments, 196. Federal Reserve Bank of Minneapolis, Research Department Minneapolis, MN, USA.

Ghosh, S., Mujumdar, P., 2008a. Statistical downscaling of GCM simulations to streamflow using relevance vector machine. Advances in Water Resources, 31(1): 132-146.

Ghosh, S., Mujumdar, P.P., 2008b. Statistical downscaling of GCM simulations to streamflow using relevance vector machine. Advances in Water Resources, 31(1): 132-146. DOI:10.1016/j.advwatres.2007.07.005

Gräler, B. et al., 2013. Multivariate return periods in hydrology: a critical and practical review focusing on synthetic design hydrograph estimation. Hydrology and Earth System Sciences, 17(4): 1281-1296.

Haerter, J., Hagemann, S., Moseley, C., Piani, C., 2011. Climate model bias correction and the role of timescales. Hydrology and Earth System Sciences, 15(3): 1065-1079.

Halwatura, D., Lechner, A., Arnold, S., 2015. Drought severity–duration–frequency curves: a foundation for risk assessment and planning tool for ecosystem establishment in post-mining landscapes. Hydrology and Earth System Sciences, 19(2): 1069-1091.

Hammami, D., Lee, T.S., Ouarda, T.B.M.J., Lee, J., 2012. Predictor selection for downscaling GCM data with LASSO. Journal of Geophysical Research: Atmospheres, 117(D17): D17116. DOI:10.1029/2012jd017864

Hao, Z., Singh, V., 2012. Entropy-copula method for single-site monthly streamflow simulation. Water Resources Research, 48(6): W06604. DOI:10.1029/2011WR011419.

Hardoon, D., Szedmak, S., Shawe-taylor, J., 2004. Canonical correlation analysis:an overview with application to learning methods. NeuralComputation, 16(12): 2639–2664.

Hennessy, K.J., Gregory, J.M., Mitchell, J.F.B., 1997. Changes in daily precipitation under enhanced greenhouse conditions. Climate Dynamics, 13: 667–680.

Hessami, M., Gachon, P., Ouarda, T.B.M.J., St-Hilaire, A., 2008. Automated regression-based statistical downscaling tool. Environmental Modelling & Software, 23(6): 813-834. DOI:10.1016/j.envsoft.2007.10.004

Hewitson, B.C., Crane, R.G., 2012. Large-scale atmospheric controls on local precipitation in tropical mexico. Geophysical Research Letters, 19(18): 1835–1838.

Hotelling, H., 1936. Relations between two sets of variates. Biometrika 28(3/4): 312–377.

Hotelling, H., 1993. Analysis of a complex of statistical variables into components. Journal of Educational Psychology 24: 417- 441.

IPCC (Ed.), 2013. Summary for policymakers, in Climate Change 2013: The Physical Science Basis. Contribution of Working Group I to the Fifth Assessment Report of the Intergovernmental Panel on Climate Change, edited by T. Stocker et al., 29 pp., Cambridge Univ. Press, Cambridge, U. K. Cambridge Univ. Press, Cambridge, U. K., and New York.

IPCC, 2014. Summary for policymakers, in Climate Change 2014, Synthesis Report, edited by The Core Writing Team, R. K. Pachauri, and L. Meyer, pp. 6–15, IPCC, Geneva. [Available at http://www.ipcc.ch/pdf/assessment-report/ar5/syr/SYR_AR5_SPMcorr2.pdf].

Jackson, J.E., 1991. A User's Guide to Principal Components. Wiley, Newark, NJ.

Jammazi, R., Tiwari, A.K., Ferrer, R., Moya, P., 2015. Time-varying dependence between stock and government bond returns: International evidence with dynamic copulas. The North American Journal of Economics and Finance, 33: 74-93. DOI:10.1016/j.najef.2015.03.005

Janga Reddy, M., Ganguli, P., 2012. Application of copulas for derivation of drought severity–duration–frequency curves. Hydrological Processes, 26(11): 1672-1685.

Jiang, C., Xiong, L., Xu, C.Y., Guo, S., 2015. Bivariate frequency analysis of nonstationary low-flow series based on the time-varying copula. Hydrological Processes, 29(6): 1521-1534.

Johnson, F., Sharma, A., 2012. A nesting model for bias correction of variability at multiple time scales in general circulation model precipitation simulations. Water Resources Research, 48(1): W01504. DOI:10.1029/2011wr010464.

Johnson, F., Sharma, A., 2015. What are the impacts of bias correction on future drought projections? Journal of Hydrology, 525: 472-485.

Joshi, D., St-Hilaire, A., Daigle, A., Ouarda, T.B.M.J., 2013. Databased comparison of Sparse Bayesian Learning and Multiple Linear Regression for statistical downscaling of low flow indices. Journal of Hydrology, 488: 136-149. DOI:10.1016/j.jhydrol.2013.02.040

Kalnay, E. et al., 1996. The NCEP/NCAR 40-year reanalysis project. Bulletin of the American Meteorological Society, 77: 437–471.

Kannan, S., Ghosh, S., 2013. A nonparametric kernel regression model for downscaling multisite daily precipitation in the Mahanadi basin. Water Resources Research, 49(3): 1360-1385. DOI:10.1002/wrcr.20118

Karl, T.R., Trenberth, K.E., 2003. Modern global climate change. science, 302(5651): 1719-1723.

Katz, R.W., Parlange, M.B., Naveau, P., 2002. Statistics of extremes in hydrology. Advances in Water Resources, 25(8–12): 1287-1304.

Khalil, A., Almasri, M.N., McKee, M., Kaluarachchi, J.J., 2005. Applicability of statistical learning algorithms in groundwater quality modeling. Water Resources Research, 41(5): W05010. DOI:10.1029/2004WR003608.

Khalil, A.F., McKee, M., Kemblowski, M., Asefa, T., Bastidas, L., 2006. Multiobjective analysis of chaotic dynamic systems with sparse learning machines. Advances in Water Resources, 29(1): 72-88.

Khaliq, M.N., Ouarda, T.B.M.J., Ondo, J.C., Gachon, P., Bobée, B., 2006. Frequency analysis of a sequence of dependent and/or non-stationary hydro-meteorological observations: A review. Journal of Hydrology, 329(3-4): 534-552. DOI:10.1016/j.jhydrol.2006.03.004

Langenbrunner, B., Neelin, J.D., 2013. Analyzing ENSO teleconnections in CMIP models as a measure of model fidelity in simulating precipitation. Journal of Climate, 26(13): 4431-4446.

Leclerc, M., Ouarda, T.B.M.J., 2007. Non-stationary regional flood frequency analysis at ungauged sites. Journal of Hydrology, 343(3-4): 254-265. DOI:10.1016/j.jhydrol.2007.06.021.

Lee, T., Modarres, R., Ouarda, T., 2013. Data-based analysis of bivariate copula tail dependence for drought duration and severity. Hydrological Processes, 27(10): 1454-1463.

Lin, J., Cheng, C.T., Chau, K.W., 2006. Using support vector machines for long-term discharge prediction. Hydrological Sciences Journal, 51: 599-612.

Lloyd-Hughes, B., Saunders, M.A., 2002. A drought climatology for Europe. International journal of climatology, 22(13): 1571-1592.

Madadgar, S., Moradkhani, H., 2013. Drought Analysis under Climate Change Using Copula. Journal of Hydrologic Engineering, 18(7): 746-759. DOI:doi:10.1061/(ASCE)HE.1943-5584.0000532

Madadgar, S., Moradkhani, H., 2014. Improved Bayesian multimodeling: Integration of copulas and Bayesian model averaging. Water Resources Research, 50(12): 9586-9603.
Matalas, N.C., 1967. Mathematical assessment of synthetic hydrology. Water Resources Research, 3(4): 937-945. DOI:10.1029/WR003i004p00937
McKee, T.B., Doesken, N.J., Kleist, J., 1993. The relationship of drought frequency and duration to time scales, Proceedings of the 8th Conference on Applied Climatology. American Meteorological Society Boston, MA, USA, pp. 179-183.
Mehrotra, R., Sharma, A., 2012. An improved standardization procedure to remove systematic low frequency variability biases in GCM simulations. Water Resources Research, 48(12): W12601. DOI:10.1029/2012wr012446
Mehrotra, R., Sharma, A., 2015. Correcting for systematic biases in multiple raw GCM variables across a range of timescales. Journal of Hydrology, 520: 214-223. DOI:10.1016/j.jhydrol.2014.11.037
Milly, P.C.D. et al., 2008. Stationarity is dead: Whither water management? Science, 319: 573–574.
Milly, P.C.D. et al., 2015. On Critiques of "Stationarity is Dead: Whither Water Management?". Water Resources Research, 51(9): 7785-7789. DOI:10.1002/2015wr017408.
Mishra, A.K., Singh, V.P., 2010. A review of drought concepts. Journal of Hydrology, 391(1): 202-216.
Mishra, A.K., Singh, V.P., 2011. Drought modeling–A review. Journal of Hydrology, 403(1): 157-175.
Modarres, R., Ouarda, T., 2014. Modeling the relationship between climate oscillations and drought by a multivariate GARCH model. Water Resources Research, 50(1): 601-618.
Molina, J.-L., Pulido-Velázquez, D., García-Aróstegui, J.L., Pulido-Velázquez, M., 2013. Dynamic Bayesian networks as a decision support tool for assessing climate change impacts on highly stressed groundwater systems. Journal of Hydrology, 479: 113-129.
Moradkhani, H., Meier, M., 2010. Long-Lead Water Supply Forecast Using Large-Scale Climate Predictors and Independent Component Analysis. Journal of Hydrologic Engineering, 15(10): 744–762.
Mujumdar, P., Ghosh, S., 2008. Modeling GCM and scenario uncertainty using a possibilistic approach: Application to the Mahanadi River, India. Water Resources Research, 44(6): W06407. DOI: 10.1029/2007WR006137.
Najafi, M., Moradkhani, H., Wherry, S., 2011. Statistical Downscaling of Precipitation Using Machine Learning with Optimal Predictor Selection. Journal of Hydrologic Engineering, 16(8): 650–664.
Najafi, M.R., Moradkhani, H., 2015. Multi-model ensemble analysis of runoff extremes for climate change impact assessments. Journal of Hydrology, 525: 352-361.
Nash, J.E., Sutcliffe, J.V., 1970. River flow forecasting through. part I. A conceptual models discussion of principles. Journal of Hydrology, 10: 282–290.
Nasseri, M., Tavakol-Davani, H., Zahraie, B., 2013. Performance assessment of different data mining methods in statistical downscaling of daily precipitation. Journal of Hydrology, 492: 1-14. DOI:10.1016/j.jhydrol.2013.04.017
Nazemosadat, M., Cordery, I., 2000. On the relationships between ENSO and autumn rainfall in Iran. International Journal of Climatology, 20(1): 47-61.
Nelsen, R.B., 2007. An introduction to copulas. Springer Science & Business Media.

Ojha, R., Nagesh Kumar, D., Sharma, A., Mehrotra, R., 2013. Assessing Severe Drought and Wet Events over India in a Future Climate Using a Nested Bias-Correction Approach. Journal of Hydrologic Engineering, 18(7): 760-772. DOI:10.1061/(asce)he.1943-5584.0000585

Okkan, U., Inan, G., 2014. Statistical downscaling of monthly reservoir inflows for Kemer watershed in Turkey: use of machine learning methods, multiple GCMs and emission scenarios. International Journal of Climatology, 35(11): 3274–3295.

Ouali, D., Chebana, F., Ouarda, T. B. M. J., 2016. Non-linear canonical correlation analysis in regional frequency analysis, Stochastic Environmental Research and Risk Assessment, 30(2): 449–462.

Ouarda, T., El-Adlouni, S., 2011. Bayesian Nonstationary Frequency Analysis of Hydrological Variables. Journal of the American Water Resources Association, 47(3): 496-505.

Patton, A.J., 2006. Modelling asymmetric exchange rate dependence. International Economic Review, 47(2): 527-556.

Raghavendra, N.S., Deka, P.C., 2014. Support vector machine applications in the field of hydrology: A review. Applied Soft Computing, 19: 372-386. DOI:10.1016/j.asoc.2014.02.002

Read, L.K., Vogel, R.M., 2015. Reliability, return periods, and risk under nonstationarity. Water Resources Research, 51(8): 6381-6398. DOI: 10.1002/2015WR017089.

Requena, A., Mediero Orduña, L., Garrote de Marcos, L., 2013. A bivariate return period based on copulas for hydrologic dam design: accounting for reservoir routing in risk estimation. Hydrology and Earth System Sciences, 17(8): 3023-3038.

Rocheta, E., Evans, J., Sharma, A., 2014a. Assessing atmospheric bias correction for dynamical consistency using potential vorticity. Environmental Research Letters, 9(12): 124010. DOI:10.1088/1748-9326/9/12/124010.

Rocheta, E., Sugiyanto, M., Johnson, F., Evans, J., Sharma, A., 2014b. How well do general circulation models represent lowfrequency rainfall variability?. Water Resources Research, 50(3): 2108-2123. DOI:10.1002/2012WR013085

Roghani, R., Soltani, S., Bashari, H., 2015. Influence of southern oscillation on autumn rainfall in Iran (1951–2011). Theoretical and Applied Climatology, 124(1): 411-423.

Rootzén, H., Katz, R.W., 2013. Design Life Level: Quantifying risk in a changing climate. Water Resources Research, 49(9): 5964-5972. DOI:10.1002/wrcr.20425

Rosner, A., Vogel, R.M., Kirshen, P.H., 2014. A risk-based approach to flood management decisions in a nonstationary world. Water Resources Research, 50(3): 1928-1942. DOI:10.1002/2013wr014561

Sadri, S., Burn, D.H., 2012. Copula-based pooled frequency analysis of droughts in the Canadian Prairies. Journal of Hydrologic Engineering, 19(2): 277-289.

Saeys, Y., Inza, I., Larranaga, P., 2007. A review of feature selection techniques in bioinformatics. Bioinformatics, 23(19): 2507-2517. DOI:10.1093/bioinformatics/btm344.

Salas, J.D., 1980. Applied modeling of hydrologic time series. Water Resources Publication.

Salas, J.D., Obeysekera, J., 2013. Revisiting the concepts of return period and risk for nonstationary hydrologic extreme events. Journal of Hydrologic Engineering, 19(3): 554-568.

Salvadori, G., De Michele, C., Kottegoda, N.T., Rosso, R., 2007. Extremes in nature: an approach using copulas, 56. Springer Science & Business Media.

Salvi, K., Ghosh, S., Ganguly, A.R., 2015. Credibility of statistical downscaling under nonstationary climate. Climate Dynamics, 46(5): 1991-2023.

Santhosh, D., Srinivas, V., 2013. Bivariate frequency analysis of floods using a diffusion based kernel density estimator. Water Resources Research, 49(12): 8328-8343.

Sarhadi, A., Ausín, M., Wiper, P., 2016a. A New Time-varying Concept of Risk in a Changing Climate. Scientific Reports, Submitted.
Sarhadi, A., Burn, D.H., Concepción Ausín, M., Wiper, M.P., 2016b. Time varying nonstationary multivariate risk analysis using a dynamic Bayesian copula. Water Resources Research, 52(3): 2327-2349.
Sarhadi, A., Burn, D.H., Johnson, F., Mehrotra, R., Sharma, A., 2016c. Water resources climate change projections using supervised nonlinear and multivariate soft computing techniques. Journal of Hydrology, 536: 119-132.
Sarhadi, A., Burn, D.H., Yang, G., Ghodsi, A., 2016d. Advances in projection of climate change impacts using supervised nonlinear dimensionality reduction techniques. Climate Dynamics, DOI: 10.1007/s00382-016-3145-0. DOI:10.1007/s00382-016-3145-0.
Schölkopf, B., Smola, A., Muller, K., 1998. Nonlinear Component Analysis as a Kernel Eigenvalue Problem. Neural Computation, 10: 1299–1319.
Shashikanth, K. et al., 2014. Comparing statistically downscaled simulations of Indian monsoon at different spatial resolutions. Journal of Hydrology, 519: 3163-3177. DOI:10.1016/j.jhydrol.2014.10.042
Shiau, J.-T., 2006. Fitting drought duration and severity with two-dimensional copulas. Water Resources Management, 20(5): 795-815.
Shiau, J.-T., Modarres, R., 2009. Copula-based drought severity-duration-frequency analysis in Iran. Meteorological Applications, 16(4): 481-489.
Sklar, M., 1959. Fonctions de répartition à n dimensions et leurs marges. Université Paris 8.
Smith, M.S., 2013. Bayesian Approaches to Copula Modelling. In Hierarchical Models and MCMC: A Tribute to Adrian Smith, P. Damien, P. Dellaportas, N. Polson, and D. Stephen (Eds), Bayesian Statistics, pages 395–402. Oxford University Press, Oxford (UK).
Song, S., Singh, V.P., 2010. Frequency analysis of droughts using the Plackett copula and parameter estimation by genetic algorithm. Stochastic Environmental Research and Risk Assessment, 24(5): 783-805.
Spak, S., Holloway, T., Lynn, B., Goldberg, R., 2007. A comparison of statistical and dynamical downscaling for surface temperature in North America. Journal of Geophysical Research, 112(D8): D08101. DOI:10.1029/2005jd006712.
Spiegelhalter, D.J., Best, N.G., Carlin, B.P., Van Der Linde, A., 2002. Bayesian measures of model complexity and fit. Journal of the Royal Statistical Society: Series B (Statistical Methodology), 64(4): 583-639.
Srikanthan, R., Pegram, G.G.S., 2009. A Nested Multisite Daily Rainfall Stochastic Generation Model. Journal of Hydrology, 371(1): 142-153. DOI:10.1016/j.jhydrol.2009.03.025.
Tallaksen, L.M., van Lanen, H.A., 2004. Hydrological drought: processes and estimation methods for streamflow and groundwater, 48. Elsevier.
Tareghian, R., Rasmussen, P.F., 2013. Statistical downscaling of precipitation using quantile regression. Journal of Hydrology, 487: 122-135. DOI:10.1016/j.jhydrol.2013.02.029
Taylor, K.E., Stouffer, R.J., Meehl, G.A., 2012a. An overview of CMIP5 and the experiment design. Bulletin of the American Meteorological Society, 93(4): 485–498.
Taylor, K.E., Stouffer, R.J., Meehl, G.A., 2012b. An overview of CMIP5 and the experiment design. Bulletin of the American Meteorological Society, 93(4): 485-498.
Tipping, M.E., 2001. Sparse bayesian learning and the relevance vector. Journal of Machine Learning Research, 1: 211– 244.

Tisseuil, C., Vrac, M., Lek, S., Wade, A.J., 2010. Statistical downscaling of river flows. Journal of Hydrology, 385(1-4): 279-291. DOI:10.1016/j.jhydrol.2010.02.030

Tofiq, F.A., Guven, A., 2014. Prediction of design flood discharge by statistical downscaling and General Circulation Models. Journal of Hydrology, 517: 1145-1153. DOI:10.1016/j.jhydrol.2014.06.028

Tripathi, S., Srinivas, V., Nanjundiah, R.S., 2006a. Downscaling of precipitation for climate change scenarios: a support vector machine approach. Journal of Hydrology, 330(3): 621-640.

Tripathi, S., Srinivas, V.V., Nanjundiah, R.S., 2006b. Downscaling of precipitation for climate change scenarios: A support vector machine approach. Journal of Hydrology, 330(3-4): 621-640. DOI:10.1016/j.jhydrol.2006.04.030

Vapnik, V.N., 1998. Statistical learning theory. new yourk. Wiley.

Vogel, R.M., Yaindl, C., Walter, M., 2011. Nonstationarity: Flood Magnification and Recurrence Reduction Factors in the United States1. JAWRA Journal of the American Water Resources Association, 47(3): 464-474. DOI:10.1111/j.1752-1688.2011.00541.

Wahl, T., Jain, S., Bender, J., Meyers, S.D., Luther, M.E., 2015. Increasing risk of compound flooding from storm surge and rainfall for major US cities. Nature Climate Change, 5(12): 1093-1097.

Westra, S., Thyer, M., Leonard, M., Kavetski, D., Lambert, M., 2014. A strategy for diagnosing and interpreting hydrological model nonstationarity. Water Resources Research, 50(6): 5090-5113.

Wilby, R.L. et al., 2004. Guidelines for use of climate scenarios developed from statistical downscaling methods. DDC of IPCC TGCIA, 27 pp. IPCC-DDC:<http://Www.ipcc-data.org/>.

Wilby, R.L., Wigley, T.M.L., 2000. Precipitation predictors for downscaling: Observed and general circulation model relationships,. International Journal of Climatology, 20: 641–661.

Wilhite, D.A., 2000. Drought as a natural hazard: concepts and definitions. Chap. 18, pp. 245–255. (London: Routledge, 2000).

Wójcik, R., 2015. Reliability of CMIP5 GCM simulations in reproducing atmospheric circulation over Europe and the North Atlantic: a statistical downscaling perspective. International Journal of Climatology, 35(5): 714-732. DOI:10.1002/joc.4015

Glossary

ACC	Average Climate Condition
ACF	Auto-Correlation Function
AIC	Akaike Information Criterion
ANN	Artificial Neural Network
ASD	Automated Statistical Downscaling
BMA	Bayesian Model Averaging
CA	Correlation Analysis
CCA	Canonical Correlation Analysis
CDF	Cumulative Distribution Function
CMIP5	Coupled Model Intercomparison Project Phase 5
CML	Canonical Maximum Likelihood
DIC	Deviance Information Criterion
DOE	Design-Of-Experiment
ENSO	El Niño-Southern Oscillation
FML	Full Maximum Likelihood
GCM	General Circulation Model
GEV	Generalized Extreme Value
GT	Gamma Test
HGT	Geopotential Height
HSIC	Hilbert-Schmidt Independence Criterion
ICA	Independent Component Analysis
IFM	Inference Functions for Marginals
IPCC	Intergovernmental Panel on Climate Change
IRIMO	Iran Meteorological Organization
JRP	Joint Return Period
K-S	Kolmogorov-Smirnov
LASSO	Least Absolute Shrinkage and Selection Operator
MAE	Mean Absolute Error
MAR1	Multivariate Autoregressive order 1
MBC	Monthly Bias Correction
MCMC	Markov Chain Monte Carlo
MRNBC	Multivariate Recursive Nesting Bias Correction
NBC	Nested Bias Correction
NCEP/NCAR	National Center for Environmental Prediction/National Center for Atmospheric Research
PCA	Principal Component Analysis
PDF	Probability Density Function

RCM	Regional Climate Model
RCP	Representative Concentration Pathways
RHUM	Relative Humidity
RKHS	Reproducing Kernel Hilbert Spaces
RMSE	Root Mean Squared Error
RNBC	Recursive Nesting Bias Correction
RVM	Relevance Vector Machine
SBL	Sparse Bayesian Learning
SHUM	Specific Humidity
SLP	Sea Level Pressure
SPI	Standardized Precipitation Index
SRM	Structural Risk Minimization
SST	Sea Surface Temperature
SVR	Support Vector Regression
WCRP	World Climate Research Program